AN EXPERIMENTAL INVESTIGATION OF LEAD ZIRCONATE TITANATE - EPOXY – MULTI-WALLED CARBON NANOTUBE BULK AND FLEXIBLE THICK FILM COMPOSITES

By

SANKHA BANERJEE

A Dissertation submitted to the

Graduate School-New Brunswick

Rutgers, The State University of New Jersey

in partial fulfillment of the requirements

for the degree of

Doctor of Philosophy

Graduate Program in Mechanical and Aerospace Engineering

written under the direction of

Kimberly A. Cook-Chennault

and approved by

_____

_____

_____

_____

New Brunswick, New Jersey

May 2014

ABSTRACT OF THE DISSERTATION

AN EXPERIMENTAL INVESTIGATION OF LEAD ZIRCONATE TITANATE - EPOXY – MULTI-WALLED CARBON NANOTUBE BULK AND FLEXIBLE THICK FILM COMPOSITES

By SANKHA BANERJEE

Dissertation Director:

Kimberly A. Cook-Chennault

Piezoelectric sensors and actuators are needed for a wide range of applications from physiological measurement to industrial monitoring systems. Sensors that can be easily integrated with the host, while maintaining high sensitivity and reliability over a wide range of frequencies are not readily feasible and economical with homogenous piezoelectric materials. It is well known that two-phase piezoelectric-epoxy composites offer several benefits over their single phase counterparts, as the properties of the constituent phases combine to improve the range of applicability. However, the piezoelectric properties of these materials suffer from the electrically insulating properties of the epoxy matrix. The electrical properties of the matrix may be enhanced by including electrically conducting inclusions however, less is known about the mechanisms that drive the changes in these properties. Hence, this experimental investigation of sensor materials builds on the previous work in two-phase piezoelectric composites, where the aims are to understand the roles that specific fabrication parameters and inclusion composition play in determining the piezoelectric and

dielectric performance the aforementioned composites. The materials under investigation will be comprised of Lead Zirconate Titanate, Epofix Cold-Setting Embedding Resin and multi-walled carbon nanotubes, i.e. the piezoelectric, epoxy and electrical inclusions respectively. Our work suggests that inclusion of MWCNTs enhances the piezoelectric and dielectric properties with increasing volume fraction below the percolation threshold. This work seeks to understand how the processing parameters: poling temperature, poling type and particle distribution influence the contact resistance, space charge double layer at the piezoelectric and conductor interfaces and electric field intensity at the piezoelectric boundary, which all ultimately dictate the piezoelectric and dielectric performance of the composite materials. Conventional solid oxide mixing, spin coating and deposition techniques will be used to fabricate the bulk and thick films. The piezoelectric and dielectric performance will be determined from the measurement of the piezoelectric strain coefficients, d33 and d31, dielectric constant, impedance and dielectric spectrum, dielectric loss tangent, and capacitance. These measurements will be correlated with inclusion size, shape, distribution, and surface morphology observations obtained from the scanning electron microscope (SEM) and transmission electron microscope (TEM).

Acknowledgements

First of all I would like to acknowledge my advisor Prof. Kimberly Cook-Chennault for her continuous support in my research and her meticulous effort in the development of my intellectual ability towards becoming a better researcher and moreover a better person and becoming a valuable member in the society. Her enthusiasm, patience and inspiration have been motivational for me towards improving my intellectual ability and analyzing skills.

Besides my advisor I would like to thank my committee members, Prof. George Weng, Prof. Assimina Peligri and Prof. Jackie Jie Li for their encouragement, time and helpful insight towards my research work. The members of the Hybrid Energy Systems Laboratory have been an important part of my research and personal life. Without their collaboration and support this thesis would not have been possible.

I would like to thank and show my appreciation to the former and present graduate students, Lei Wang, Sean De Gennaro, Udhay Sundar, Wan Lin, Andrew Tang, Eric Bickford, and undergraduates James Palmer and Eric Refour (summer intern). Lastly I would like to thank my family, specially my parents who have been an inspiration all my life and have motivated me to achieve new heights in my career. I would also like to thank and show great appreciation to my lovely and beautiful wife Debaki, who has been with me through all the ups and downs, the happy and sad times through all these years that we have been together. In spite of being a Biologist she has shown great appreciation and excitement towards my research and has motivated me throughout my professional and academic life to achieve higher standards. Without my parents blessings and my wife’s love and emotional support through some of the tough times in my life this

dissertation would not have been possible.

Sankha Banerjee

Rutgers University

May 2014

Table of Contents

List of Figures

List of Tables

Nomenclature

S	Mechanical Strain
s	Elastic compliance
E	Electric Field
d_{ij}	Piezoelectric strain coefficient (i= 1, 2, 3, j = 1, 2,…, 6)
T	Mechanical Stress
D	Electric charge displacement
ε	Relative Permittivity (Complex dielectric constant)
ε′	Dielectric constant
ε′′	Dielectric loss
δ	Dielectric loss angle
Z	Impedance
R	Resistance
X	Reactance
θ	Phase angle

Chapter 1

Introduction

Piezoelectric materials are ubiquitously used as sensors, actuators and transducers over a wide range of applications spanning across quality assurance [1], process control [2], industrial and automotive monitoring systems [3], medical diagnostics [4], aviation and aerospace structural health monitoring [5], embedded passive devices in consumer electronics applications and as resonators and filters in telecommunications [6]. However, the brittle nature of homogenous ceramic piezoelectric materials limits their operational strains (~0.2 % for homogenous Lead Zirconate Titanate, PZT [7]), cycle life, and ability to be integrated into complex shapes and structures [8] while maintaining high sensitivity and reliability over a wide range of frequencies. Two-phase polymer matrix based composites such as PZT-Epoxy [9], comprised of piezoelectric particles embedded within a continuous polymer matrix, have attracted much attention due to their flexibility, ease of processing and use in embedded passive devices. However, two-phase piezoelectric-epoxy composites suffer from poor electrical and piezoelectric properties due to the insulating epoxy matrix, which decreases the polarization of the piezoelectric phase. Several researchers have demonstrated that the inclusion of electrically conductive particles within the matrix of the aforementioned two-phase composite [10, 11] will address this problem by enhancing the polarization of the composite, thereby enhancing their electrical properties [12-14]. However, less is known about interrelationship between the composite processing technique and the morphology and properties of the electrically conductive particles, which dictate the piezoelectric and dielectric properties

of the materials. [3, 15]. In the following work the mechanisms that influence the piezoelectric and dielectric properties of the three phase composites has been investigated by varying the volume fraction of the conductive phase. The material properties of these piezoelectric composites have been quantified by means of dielectric, piezoelectric and impedance characterization. The distribution of the phases in the matrix, phase interaction, and preprocessing of MWCNTs and PZT have been studied with the aid of a Scanning Electron Microscopy (SEM) and Transmission Electron Microscopy (TEM) to ascertain the degree of separation of particles, particle morphology, composite porosity and agglomeration.

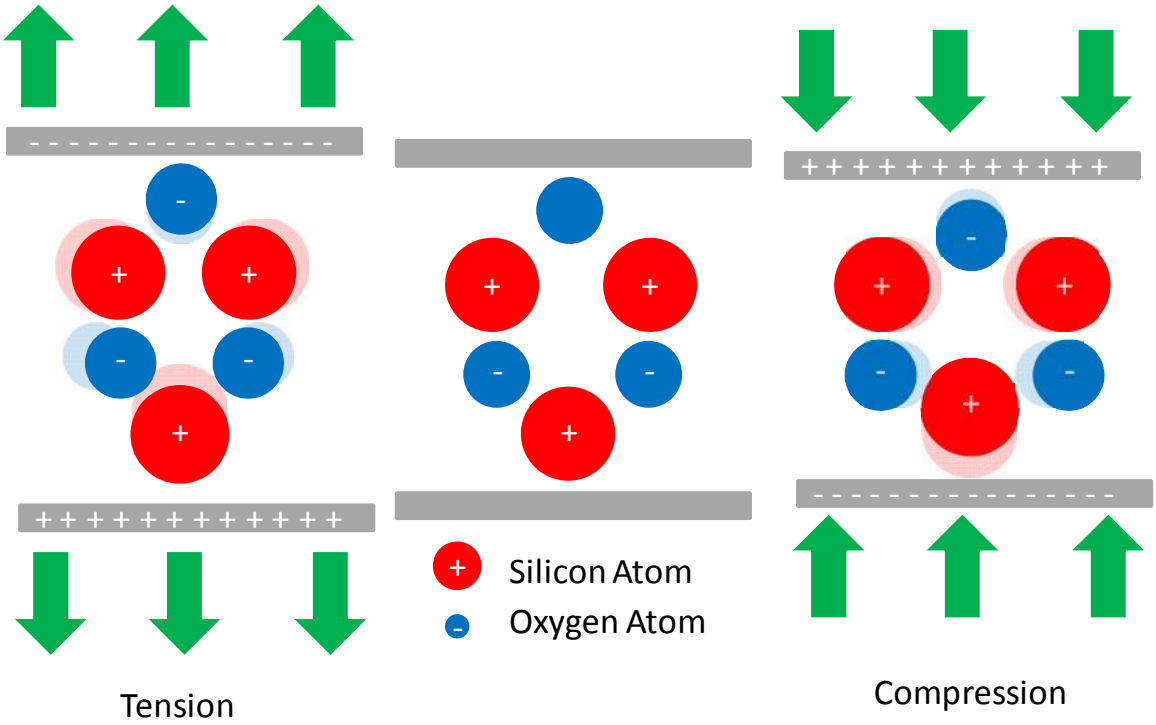

Figure 1.1 Displacement of charges in a quartz crystal when an external tensile or compressive strain is applied. This effect is called the piezoelectric effect.

Piezoelectricity can be defined as a electromechanical interaction between the mechanical and electrical energy states, that is governed by the microscopic lattice

structure of a material; with a unit cell that has no inversion of symmetry [16]. Under application of mechanical strain certain materials become electrically polarized. This linear and reversible phenomenon is called the direct piezoelectric effect. In switching or alternating electric fields the response of these materials are not instantaneous and depends on the characteristic time (or relaxation time) the orientation polarization (or the average dipole moment) takes to adjust to the changing direction of the electric field [17, 18]. The displacement of ionic charges within a crystal structure is responsible for this effect. In the absence of an external strain, the charge distribution within the crystal is symmetric and the net electric dipole moment is zero. However, when an external stress is applied, the charges are displaced and the charge distribution is no longer symmetric as shown in Figure 1.1 (piezoelectric effect in a quartz crystal). A net polarization develops and results in an internal electric field.

The Curie Brothers discovered piezoelectric behavior in Quartz, tourmaline, and Rochelle salt [16] in the early 1880s. The discovery of new piezoelectric materials in the early 1940s was spurred by the pressing need for high dielectric constant (ε) capacitors. During the mid-1940s, $BaTiO_3$ was established as a new type of ceramic capacitor with high dielectric constant values of $\varepsilon>1100$ [2]. Around the same time is was established that the domain within the grains of the material can be oriented by means of an application of an external field [1, 2], which is known as the “poling “ process. The process of poling aligned the asymmetric dipoles of polycrystalline piezo-ceramics in the desired direction producing an electromechanically active ceramic material that behaved similar to a single crystal and possessed piezoelectric properties. Lead Zirconate Titanate (Pb[ZrxTi1-x]O3 $0\leq x\leq 1$)) was reported as a useful piezo-ceramic in the 1950s [2] due to

its enhanced piezoelectric (piezoelectric strain coefficients > 600 pC/N, [19]) and dielectric properties (dielectric constant > 3000, [19]). PZT has been studied extensively in the last few decades and has been one of the most widely used piezoelectric materials for sensor/actuator applications [1, 2, 16, 20].

Single phase and homogenous piezoelectric ceramics such as Lead Zirconate Titanate (PZT, Pb[ZrxTi1-x]O3 $0 \leq x \leq 1$)) and Barium Titanate ($BaTiO_3$), face challenges that limit their applications as industrial sensors and in energy harvesting deices. Piezoelectric ceramics exhibit poor mechanical properties and are prone to premature failure [21, 22] when subjected to static or frequency dependent mechanical loading and/or mechanical shock [3, 8]. Moreover, single phase ceramics posses high stiffness constants and densities which make them less mechanically stable [4]. Also, piezoelectric ceramics encounter problems in impedance match [23, 24] and compatibility of mechanical properties with the host material that limits their application as health monitoring sensors [25, 26]. Composite materials increase the number of design degrees of freedom, which enable these materials to be tailored to address some of the aforementioned challenges [3, 27].

Several researchers have investigated two phase piezoelectric-epoxy composite to address the aforementioned mechanical limitations of homogenous piezoelectric materials [20, 21] listed above. The properties of the constituent phases combine to improve the mechanical properties and range of applicability of the composite [28, 29]. Two phase composites with randomly distributed ferroelectric fillers in a polymer matrix have been investigated towards the development of high stiffness and mechanical strength materials for devices in energy harvesting [30] and structural health monitoring

sensors [31]. Though these composites exhibit an improvement in mechanical properties the electrical characteristics are degraded in comparison to the single phase piezoelectric ceramics due to the insulating characteristics of the polymer matrix [10]. The effective piezoelectric and dielectric properties of the two phase composites also suffer due to the insulating nature and lower dielectric constants and piezoelectric coefficients of the polymer matrix [32, 33]. The non-uniform distribution of the ferroelectric phase in the polymer matrix causes clustering and agglomerations in the microstructure [3, 34] and also contributes towards the insulating nature of the composite. The electrical properties of the matrix may be enhanced by including spherical electrically conducting metallic inclusions [12, 21] and high aspect ratio conductive inclusions such as Carbon Nanotubes (CNTs) [15, 35]; however, less is known about the mechanisms that drive the changes in these properties, such as electron hopping, electron tunneling [36], matrix cracking and interfacial properties [37] between the matrix and the inclusions. Also, more work needs to be done in understanding the effects of the physical relationships between different phases and the measured properties by studying the microstructure of the material. The purpose of this work is to investigate the role of Multiwalled Carbon Nanotubes (MWCNTs) as conductive fillers; on the dielectric and piezoelectric properties of three phase PZT-Epoxy-MWCNT piezoelectric composites.

1.1 Definition of Terms and Abbreviations

Most of the piezoelectric ceramics such as $BaTiO_3$ and PZT, have a perovskite structure (Figure 1.3 A, B and C). The perovskite structure (ABO3) is a simple arrangement, where the corner sharing oxygen octahedral are linked together with smaller cations (Ti, Zr) occupying the center B site in a regular cubic array [38]. The larger

cations (Pb, Ba) fill the interstices in the octahedral at the A site [39]. In polycrystalline piezoelectric materials the dipole is aligned in the desired direction by the application of an external electric field as shown in Figure 1.3 C.

Because of the anisotropic nature of PZT ceramics, piezoelectric effects depend on direction. To identify directions, the axes 1, 2, and 3 will be introduced (corresponding to X, Y, Z of the classical right-hand orthogonal axis set). The axes 4, 5 and 6 identify rotations (shear), θX, θY, θZ (also known as U, V, W.) The axes and polarization are shown in Figure 1.3 C.

Several properties can be used to examine the performance of piezoelectric materials. One of this is the relative permittivity or the dielectric constant of the material [40]. The permittivity of a material is the ability of a material to polarize in response to an electric field.

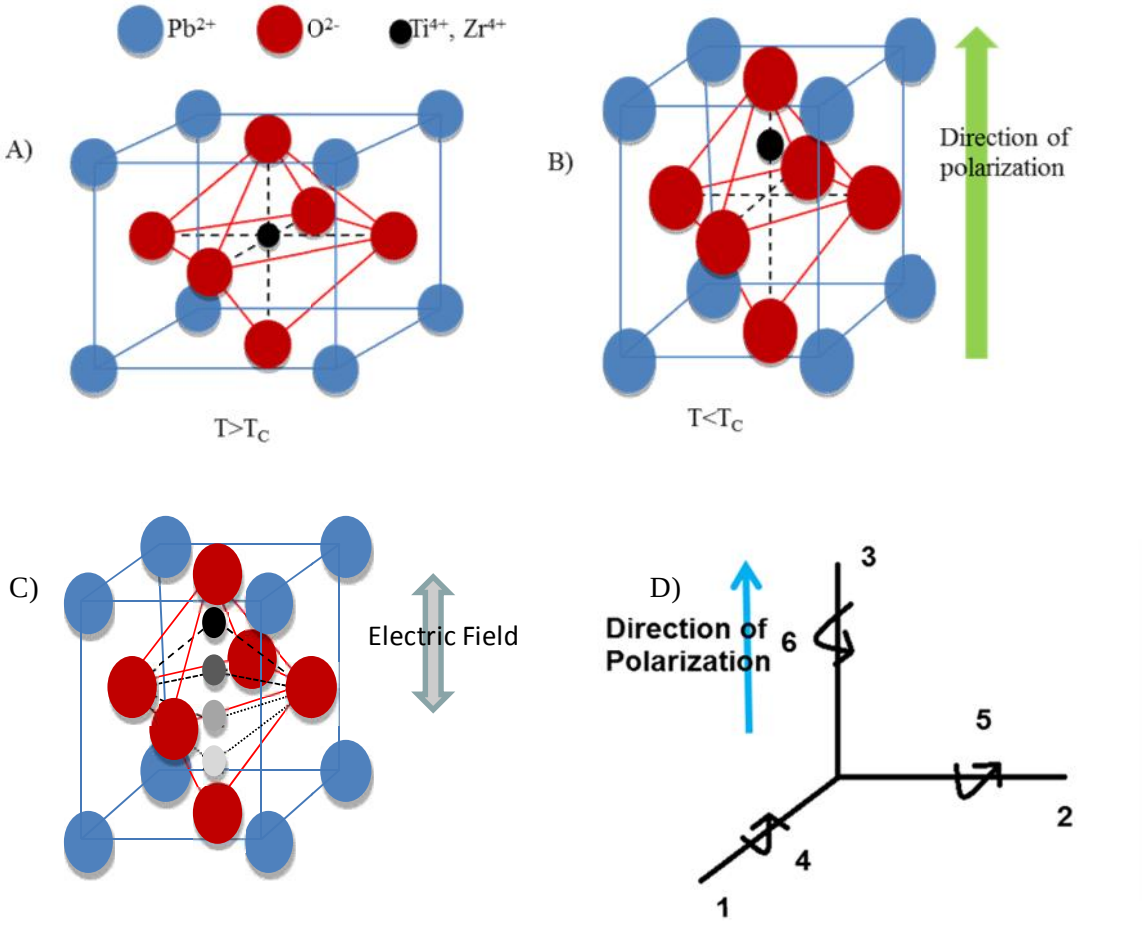

Figure 1.2 A), B) Crystalline structure of PZT (perovskite structure, ABO3), B) In polycrystalline piezo-ceramics the dipole is aligned by the application of an external electric field, an D) Orthogonal system describing the properties of a poled piezoelectric ceramic. Axis 3 is the poling direction.

The absolute complex permittivity of a material can be represented by the equation [41]

$$\varepsilon = \varepsilon' + i\varepsilon'' \quad (1)$$

where ε' and ε'' are the real and imaginary parts of the complex permittivity. ε' represents the dielectric constant and ε'' represents the dielectric loss of the material. The dielectric constant or the relative permittivity of a material can be defined by the extent to which it concentrates electrostatic lines of flux [42]. In other words it is the amount of

charge that the material can store, relative to the absolute dielectric constant i.e. the charge that can be stored by the same electrodes when separated by a vacuum at equal voltage (8.85 x 10-12 farad / meter) [43]. The complex permittivity is often represented in the Argand plane with £'as the abscissa and the £" as the ordinate, showing a curve with the frequency as the parameter as represented in Figure 1.4. When any point of this curve is joined with the origin this represents the complex conjugate or the complex dielectric constant, £ . The complex conjugate makes an angle δ with the abscissa, such that tan (δ) = £"/£'. When an external electric field is applied across a dielectric material the polar molecules orient themselves in a certain direction such that the positive and negative charges are accumulated on either end of the material. When an alternating electric field is applied it has a power dissipation, W/unit volume at each point, resulting from an applied voltage, an electric field of frequency *f*, a root mean square value of the electric field, E. This occurs due to the inability of the molecules in the dielectric material to reorient themselves with the alternating electric field. This is dependent on the composition of the dielectric, size and orientation of polarity of the molecules, the frequency of the alternating field, and relative orientation of the different phases in a composite dielectric material [44]. The power dissipation can then be defined by [45, 46]

$$W = 2\pi f E^2 \varepsilon'' = 2\pi f E^2 \varepsilon \tan(\phi) \quad (2)$$

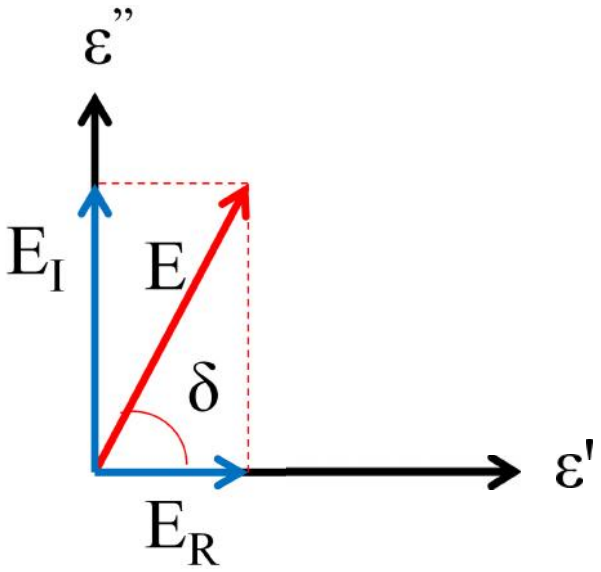

Figure 1.3 Representation of complex permittivity in the Argand plane where E_R and E_I are the two components in the real and imaginary directions, of the permittivity E.

Thus ε'' measures the energy dissipation per period and is known as the loss factor and δ is known as the loss angle. Also, $\tan(\phi)$ is known as the tangent loss of the dielectric material as shown in Figure 1.4.

Relationships between applied forces and the resultant responses depend upon the piezoelectric properties of the ceramic, the size and the shape of the material, and the direction of the electrical and mechanical excitation. These relationships can be quantified by the use of electromechanical coefficients. The linear constitutive equations for a piezoelectric material can be expressed as

$$\{S\} = [[s^E]\{T\} + [d^t]\{E\}] \quad (3)$$

$$\{D\} = [[d]\{T\} + [\varepsilon^T]\{E\}] \quad (4)$$

where S is the strain, T is the stress, s^E is the elastic compliance at constant electric field, E is the electric field, D is the electric charge displacement, ε^T is the dielectric constant at a constant stress, and d is the piezoelectric strain constant. In homogenous piezo-ceramics and composite materials the response to alternating electric fields is not instantaneous and shows frequency dependence due to the relaxation time for the piezoelectric dipoles [17, 18]. This result in a deviation from the linear behavior described above by the equations 3 and 4. Electromechanical coefficients such as; s, d and ε, relate both to the direction of the applied mechanical or electrical excitation, and the direction of the response. Each of the coefficients has two subscripts that relate to the directions of the two related quantities. The piezoelectric strain coefficient, d_{ij} (i= 1, 2, 3, j = 1, 2,…, 6) can be defined as the polarization generated per unit mechanical stress applied to the piezoelectric material or alternatively; the mechanical strain induced per unit electric field applied to the material. As shown in Figure 1 C the direction of positive polarization (direction of the effective dipole moment after poling of a piezoelectric material) coincides with the Z axis. The directions X, Y, Z are represented by the numbers 1, 2 and 3 and the shear around these axes is represented by 4, 5, and 6. The first subscript indicates the direction of polarization induced in the material and the second subscript indicates the direction of applied stress or induced strain. It an important indicator of the efficiency of the material in polarization dependent (energy harvesting) and strain dependent (actuating) applications.

Electrical Impedance describes a measure of opposition to the alternating current. It extends the concept of resistance in the AC circuits. Impedance is represented by Z,

$$Z=Ze^{i\theta} \quad (5)$$

where the magnitude of the complex impedance, Z can be defined as the ratio of the voltage and the current amplitude and θ is the phase shift by which the current is ahead of the voltage, as shown in Figure 1.5.

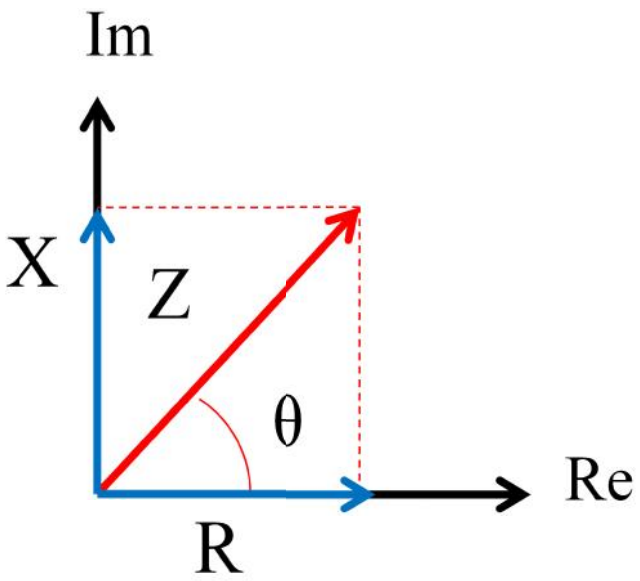

Figure 1.4 Representation of the electrical impedance as resistance and reactance in the real and imaginary axes.

In composite piezoelectric materials; the piezoelectric and dielectric coefficients, provide a measure of the influence of the individual phases on the effective properties [47, 48]. They also relate the microstructural characteristics such as agglomeration, contact resistance, percolation and particle distribution of the composite material to the effective properties [15, 21].

1.2 Literature Review

The material properties of piezoelectric composites are governed by the arrangement of the phases within the composite. This is referred to as connectivity. The concept of connectivity was first developed by Skinner et al. [43] and later enhanced by Pilgrim et al. [49]. In general, 10 connectivity patterns can be used for a diphasic system, which refers to the manner in which individual phases are self-connected. The ten connectivity patterns are (0-0), (0-1), (0-2), (0-3), (1-1), (1-2), (2-2), (1-3), (2-3) and (3-3), where the first digit within the parenthesis refers to the number of dimensions of connectivity for the piezoelectric active phase and the second digit is used for the polymer phase. This convention can also be extended to include a third phase by adding a third number within the parenthesis [10]. Two phase composites have been an active area of research. The addition of a piezoelectric ceramic to a matrix material (which acts as the second phase) retains the mechanical properties of the matrix and utilizes the piezoelectric properties of the first phase.

1.2.1 Piezoelectric Composites

Two-phase composite piezoelectric materials, so-called 0-3 composites comprised of piezoelectric particles embedded within a continuous polymer matrix, have attracted much attention due to their flexibility, ease of processing and use in embedded passive devices [50, 51], such as capacitors. Integration of embedded passive components into printed circuit boards generally results in enhanced electrical performance of the device, improved reliability, reduction of device size, faster switching speed, and lower

production costs [34, 35, 40]. Two-phase composites: metal-polymer [52, 53] and ceramic-polymer have been extensively studied [27, 54, 55] for application in coupling or by-pass capacitor technology, wherein emphasis has been placed on achievement of high effective dielectric constants via analysis based on percolation theory and mixing rules. Piezo-polymer composites are promising materials because of their excellent tailored properties [3, 56]. These materials have many advantages including high electromechancial coupling factors [46, 57, 58], low acoustic impedance [13, 59], mechanical flexibility [60, 61], a broad bandwidth [62, 63] in combination with a low mechanical quality factor [64, 65]. The mechanical, electrical and acoustic properties of these materials can also be tailored according to the nature of application of the composite material [54, 66-68]. Inclusions of electrically conductive fillers within polymer matrixes have been demonstrated by several researchers [69-72]. All researchers have reported that the polymer matrix conductivity was enhanced by the electrically conductive fillers [73, 74]. Recently Carbon Nanotubes (CNTs) has emerged as an attractive filler material [11, 15] due to its electrically conductive nature and high aspect ratio [71, 75].

1.2.2 Carbon Nanotube Composites

Carbon nanotubes consist of a single graphite sheet wrapped into a cylindrical tube as shown in Figure 1.2 A. An array of these nanotubes that are concentrically nested together form MWCNTs [76] as seen in Figure 1.2 B. MWCNTs' has been extensively studied due to their unique electrical and mechanical properties as shown in Table 1.1 [64, 69]. MWCNTs have high electrical conductivity due to the due to a unidirectional structure and the ballistic transport of electrons over long nanotube lengths. This enables

the MWCNTs' to transport currents with negligible joule heating [77, 78]. Carbon nanotubes also have high young's modulus i.e. they have high stiffness and tensile strength. The young's modulus for an individual nanotube has been reported to be around ~ 0.64 TPa [79], which is similar to high stiffness silicon carbide nanowires [77, 78]. MWCNTs' has been investigated towards commercial applications in polymer matrix based composite materials that enhance both electron transport and mechanical strength of the composite structure [79, 80].

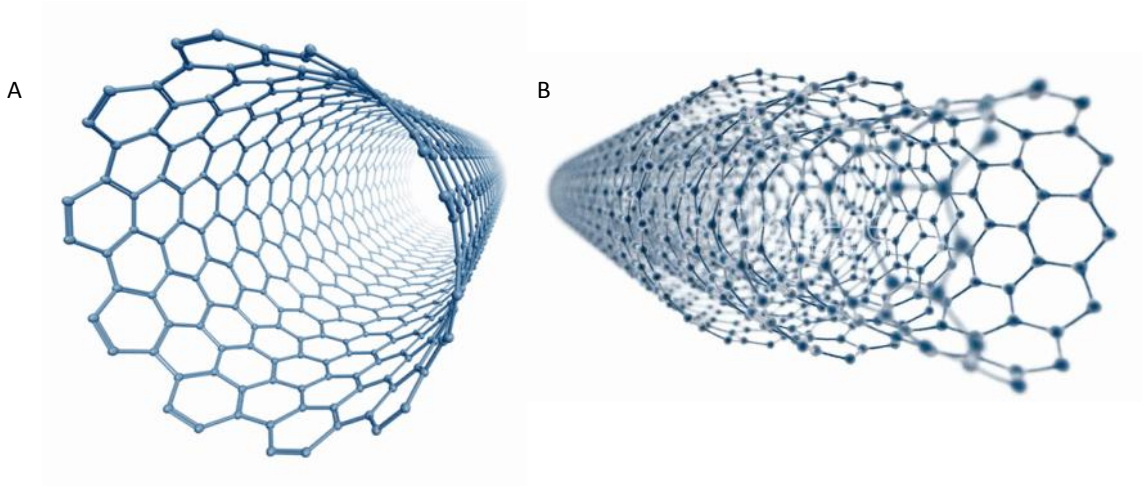

Figure 1.5 Structure of A) Carbon nanotubes with a single graphite sheet wrapped into a tube and B)Multiwalled Carbon Nanotubes with concentric tubes of carbon nanotubes [81].

Table 1.1 Unique mechanical and electrical properties of carbon nanotubes as compared to other electrically conductive materials [77, 82].

Material	Specific Density	Young's Modulus (TPa)	Strength (GPa)	Electrical Conductivity (S/m)
Carbon Nanotube	1.3 - 2	1	10 - 60	10^6-10^7

Silver	10.4	0.083	0.054	$6.3x10^7$
Copper	8.9	0.125	0.069	$5.96x10^7$
Stainless Steel	7.8	0.2	4.1	$2\text{-}8.5x10^6$
Carbon Fiber	1.7 - 2	0.2 - 0.6	1.7 - 5	$1.45x10^6$

Composites with carbon nanotubes embedded in a polymer matrix have been studied by researchers [13, 34, 36, 55, 59, 71, 83-85]. The dielectric properties of these composites are enhanced due to the increase in charge carriers from the carbon nanotubes. However beyond a certain volume fraction of the CNTs, the composite reaches percolation threshold due to the formation of electrically conductive pathways in the composite, and there is a sharp rise in the conductivity [86].

Ma and Wang [55] compared the microstructure and dielectric properties of epoxy-based damping composites that contained carbon nanotubes (CNTs) and PMN PZT piezoceramics. They concluded that the composites exhibited a percolation threshold in the range of 1.0–1.5 g CNTs per 100 g epoxy. They also concluded that in the region of the percolation threshold, a continuous electro-conductive network was formed, and that beyond the percolation threshold, these materials demonstrated dynamic mechanical loss factors that were superior to those below the percolation threshold, and those without semiconductive inclusions. Tian and Wang [87] also examined the performance of epoxy-multiwalled carbon nanotube-piezoelectric ceramic composites as rigid damping materials. Their results were similar to Ma and Wang [55], where the percolation threshold was found to be in the range of 1.0–1.5 g CNTs per 100 g epoxy. They too concluded that loss factors were improved with the incorporation of CNT and

(PZT), where the amount of CNT was above the critical electrical percolation loading. Researchers have predicted that the increase in the volume fraction of the electrically conductive inclusion phase in composite can also lead to an increase in conductivity [88, 89]. The conductivity can also increase due to the effect of tunneling resistance in Carbon Nanotube nanocomposites [36]. A change in percolation threshold by variation in the aspect ratio of the conductive inclusions has also been demonstrated [90, 91]. The percolation threshold of multiphasic piezoelectric composite materials with Carbon Nanotube (CNT) inclusions and its variation in with the aspect ratio of the CNTs is shown in Table 1.2. Due to their enhanced dielectric and piezoelectric properties [11, 15] and multifunctional nature [88], multphasic piezoelectric composite have a high potential for applications as sensors transducers and energy harvesting devices.

Table 1.2 Variation of percolation threshold with the variation in aspect ratio of the electrically conductive inclusion (CNTs).

Electrically Conductive Filler	Composite/Fabrication Method	Percolation (%, Volume fraction)
MWCNT (aspect ratio = 400) [34]	MWCNT-PVDF/Sol-gel and hot molding	1%
MWCNT(aspect ratio ~ 100) [91]	MWCNT-PMMMA/ Compression Moulding	2.4%
SWCNT (aspect ratio ~ 100) [91]	SWCNT-PMMA/Compression Moulding	3.4%
SWCNT (aspect ratio ~ 1000) [75]	SWCNT-PZT-PMMA/ Solution Casting	0.8%
CNT (aspect ratio ~ 100) [92]	CNT-Alumina/ Colloidal Processing	1.2%
MWCNT (aspect ratio ~ 100) [87]	MWCNT-Epoxy/ Sol-gel Sintering	1-1.5 %
Double Walled CNTs (aspect ratio >1000) [85]	CNT-Epoxy/ Vacuum Sintering	0.25%

MWCNT (aspect ratio >100) [82]	MWCNT-Epoxy/ Sol-gel Sintering	3.2%
CNT (aspect ratio = 200-1000) [89]	CNT-Epoxy/ Sol-gel Sintering	0.5-1.5%

In multiphasic piezoelectric composite sensors and transducers the piezoelectric properties can be controlled by polarization of the polycrystalline piezoelectric phase in the composite [50]. Initially the dipoles of the piezoelectric phase are aligned in random directions. The alignment of the dipoles determines the effective electromechanical properties [93] of the composite. The dipoles are aligned at a high temperature along with the application of high voltage static electric field. Traditionally the contact or parallel plate poling method has been used to pole piezoelectric materials and composites [50, 93]. Recently many researchers have also been using the corona discharge poling method where higher poling voltages can be achieved [50]. The strength of the poling field and poling temperature have also been identified as important parameters in determining the effectiveness of poling process [14, 94] and also the effective electromechancial properties of the composite.

Researchers have investigated both bulk [3] and thick/thin film[15] composite piezoelectric materials, geared towards applications at different length scales [95]. In thin/thick films interfacial characteristics [96, 97] play a bigger role in determining the effective dielectric and piezoelectric properties as compared to bulk materials. The electrode material of the piezoelectric film plays a very important role in the device sensitivity and the effectiveness of energy conversion [98, 99]. Ideal electrodes have a good lattice match [15, 100] between the piezoelectric material and the electrode, which

reduces contact resistance between the two mating materials, and enhances the electron mobility between the surface of the film and the piezoelectric material [100, 101]. Traditionally, metals such as silver, gold, copper, carbon or aluminum have been used as electrode materials acting as ceramic to metal contacts for these flexible piezoelectric devices [97, 102].

1.3 Poling Process

The piezoelectric phase in the composite material has to be oriented in a certain direction by means of application of an external electric field to align the piezoelectric dipoles; to ensure required working characteristics of the material [50, 94]. This process is called the poling process and is an important step in obtaining the desired properties of the material. In polymer matrix based composites, this procedure, called poling is carried out by heating the material close to its glass transition temperature and exposing it to a strong static electric field [14, 93]. The poling temperature and strength of the poling field are important parameters that determines the effective dipole moments in the poling direction and dictates the piezoelectric and dielectric properties of the materials [50, 94]. Multiphasic piezoelectric composite materials has been traditionally poled using the contact poling or the parallel plate poling method where the material is in contact with the poling electrodes [14, 93]. The contact poling method can cause dielectric breakdown in the piezoelectric composite specifically in the presence of conductive inclusions in the material [93, 103]. To overcome this drawback researchers have developed the corona discharge poling process where a high poling voltage is applied to two asymmetric electrodes such as a point and a plate [93]. Researchers have shown that higher voltages can also be achieved by the corona poling process in comparison to the contact poling

method [14, 103]. The poling process and poling parameters play a major role in determining the piezoelectric and dielectric properties of the composites.

This work seeks to understand the relationship that material processing, conductive filler shape and volume fraction [28]; electrode material, and poling method, temperature and voltage, play in determining the electromechanical properties of bulk and thick film composites [3, 29]. The materials that will be studied comprises of PZT (piezoelectric), Epoxy (polymer matrix) and Multiwalled Carbon Nanotubes (electrically conductive inclusions). The following work deals with the investigation of the role of Multiwalled Carbon Nanotubes (MWCNTs) as a conductive filler [8, 15, 21] and the effect of contact and corona discharge poling in polymer based three phase PZT-Epoxy-MWCNT flexible thick films [15] and bulk composites.

1.4 Research Motivation

Composite piezoelectric materials have been investigated due to their multifunctional nature that provides high sensitivity [31, 104] as well as high mechanical strength and flexibility [30, 102]. Two-phase piezoelectric composites have been investigated for smart materials in applications such as structural health monitoring of civil structures [105, 106] magnetoelectric sensors [104], and transducer applications [2, 20] . However, the piezoelectric properties of these materials suffer from the electrically insulating nature of the epoxy matrix [15, 96]. Though the effective mechanical properties of the composite is enhanced due to the flexible nature of the polymer matrix (for example, the maximum strain is >10% before failure of epoxy, [33]) , the effect piezoelectric and dielectric properties are lower than that of their single phase

counterparts (epoxy has strain coefficients <1/10th of PZT and dielectric constant values <10, [32]). In the last few years many researchers have looked into three phase composite materials with two different phases (ceramic and conductive filler) embedded inside a polymer matrix [12, 107]. The dielectric constant of three-phase composites can be increased by the combination of the piezoelectric and the conductive phase embedded and distributed in an uniform matrix material [11, 15]. Also in the presence of ceramic particles and the polymer matrix the leakage current and the dielectric loss of the composite can be controlled due to the separation of the conductive inclusions from each other [35, 107].

Two phase composites with randomly distributed electrically conductive fillers have drawn a lot of attention in the past few years due to their scalability and the ease of processing techniques and their flexibility [76, 108]. Towards the direction of fabrication of embedded passive components, two phase metal-polymer and metal-ceramic composites has been studied to obtain high dielectric constants of >500 [35, 107]. Among these materials two-phase composites with MWCNT as conductive inclusions randomly distributed in a relaxor ferroelectric matrix, PMMA show improvements in electrical properties with increased volume fraction of the conductive inclusion [83, 84] and exhibit a dramatic increase in electrical properties around the critical concentration around 0.1% of MWCNT by weight, known as the percolation threshold [3, 12]. One drawback in these kinds of composites is the high variation of the electrical properties as the concentration reaches close to the percolation threshold which occurs due to the formation of conductive pathways in the composite by direct contact or electron tunneling between the conductive inclusions. This causes a sharp increase in conductivity

in the composite which leads to high dielectric loss [11, 32]. This can be largely attributed to increasing values of the dielectric loss that renders the composite non-desirable in practical applications. For example in the case of PZT-Epoxy composites researchers have shown a decrease in the dielectric constant from >1000 for the single phase PZT to values <50 [9] for two phase PZT-Epoxy composites. Even the values of the piezoelectric strain coefficients decrease from ~ 20pC/N for the single phase to values < 5pC/N for the di-phasic ferroelectric-polymer composites [32, 51]. This decline in the piezoelectric and dielectric properties is due to the decrease in the number of charge carriers in the insulating polymer matrix [86]. As a solution for the above problems researchers have started to investigate three phase composites that consist of ferroelectric and conductive inclusions that are randomly distributed in an uniform polymer matrix [10, 12] . The conductive filler with variation in size, shape and concentration plays a vital role in determining the electromechanical properties of the three phase composites.

1.5 Research Objectives

Polymer matrix composites with piezoelectric inclusions have shown a lot of promise in applications as sensors and actuators. An addition of conductive inclusions enhance the piezoelectric and dielectric properties of these composites due to the increase in polarization of the charge carriers. This enhancement in material properties is directly proportional to the increase in volume fraction (or weight %) of the conductive inclusions below the percolation threshold. The composites reach the percolation due to the development of percolation pathways indicated by a sharp decrease in the impedance or a sharp increase in conductivity of the composite. In addition to the influence of the conductive inclusions in the polymer matrix, interfacial interaction plays a major role in

determining the material properties of the thick film composites [63]. The piezoelectric and dielectric properties of the composite piezoelectric thick films are influenced by the nature of the electrode on the surface of the thick film. This is due to an increase in charge carriers and the number of contact points between the film surface and the electrode [99]. Micro-structural interactions between the conductive inclusions, the matrix material and the piezoelectric phase [13, 15] also play a major role in influencing the effective properties of the composite.

The process of poling is an important step in the fabrication of bulk and micron sized thick film composites. Compared to traditional contact poling which causes dielectric breakdown at high voltages, corona discharge poling, [68, 74] which involves the ionization of the air near the surface of the composite material is an effective technique to align the dipoles of the piezoelectric phase; and can achieve poling at higher voltages. .

The objective of this work is the fabrication of three phase PZT-Epoxy-MWCNT bulk and micron sized flexible composite thick films as a function of the MWCNT volume fraction by a combination of solvent and spin coating techniques. The effect of the change in MWCNT volume fraction on the piezoelectric and dielectric properties of the composite is studied by measuring the composite for the dielectric and piezoelectric properties such as the dielectric constant, tangent of the dielectric loss angle (tan δ) and the piezoelectric strain coefficients namely the d33 and the d31 coefficients. The influence of two different poling techniques, namely contact and corona poling methods on the dielectric and piezoelectric characteristics of the material are also investigated. In

addition to the above, the composites are characterized by impedance analysis to understand the change in resistance of the composite around the percolation threshold.

The effect of micro-structural properties and interactions such as surface roughness, particle contact resistance, aspect ratio of inclusions and particle clustering/agglomerations on the electromechancial properties are investigated by Scanning Electron Microscopy (SEM), Energy Dispersive X-Ray Spectroscopy (EDS) and Transmission Electron Microscopy (TEM) [6, 7, 24, 26, 27].

1.6 Outline of the Dissertation

The dissertation consists of eight chapters. Chapter 1 introduces the background and literature review related to the present work. It also talks about the objectives of the following work.

Chapter 2 describes the characterization of the Multiwalled Carbon Nanotubes (MWCNTs), PZT and the composite sol-gel. It presents the design of experiments that will be used to determine the best experimental method to obtain desired properties. It demonstrates the time study and the SEM and TEM characterization of dispersion of MWCNTs and the sol-gel to observe the size, shape and morphology of the specific species and to determine the optimal parameters of the experimental methods.

Chapter 3 talks about the methodology and procedure for fabrication of the PZT-Epoxy-MWCNT composites. It gives an overview of the fabrication procedures of the composite bulk and flexible thick films.

Chapter 4 and 5 presents the poling temperature and poling voltage study of the three phase PZT-Epoxy-MWCNT bulk and flexible thick film composites respectively. The electromechancial properties are shown as a function of the MWCNT volume fraction. A comparison of piezoelectric, dielectric and impedance characteristics obtained through the contact poling and corona discharge poling is also demonstrated. The identification of the percolation threshold for both the bulk and thick films composites are also presented. SEM and TEM characterization of the composites are also presented to identify the effect of the micro structural interactions and morphology on the effective properties of the composites.

Chapter 6 talks about the variation in piezoelectric and dielectric properties of the three phase flexible thick films with the use of a metallic coating on the top surface.

Finally conclusions and suggestions for future work are provided in Chapter 7.

Chapter 2

Characterization of MWCNTs and PZT- Design of Experiments

The piezoelectric composites under investigation are comprised of a cold-setting resin that is based on two fluid epoxy components: a Bisphenol-A-Diglycidylether-based resin and a Triethylenetetramine-based hardener, PZT piezoelectric and MWCNT particles. It is well known that the distribution of particles and interface between particle and the matrix influence the mechanical and electrical properties of the composite [10, 109, 110]. Prior to sample preparation, PZT and MWCNT particles must be pre-processed and examined with the aid of SEM and TEM to understand their morphology and separation. Hence, the amount of time required to separate the MWCNTs (which arrive agglomerated and attached to the cathode) is described in Section 2.1 of this thesis.

A general overview of the fabrication process is provided in Figure XX. A design of experiments approach was used to determine the best parameters for the fabrication of the PZT Epoxy-MWCNT sol-gel prior to investigation of the roles of poling on the sample. In particular, the dispersion of particles within the matrix is a function of the sonication time of the sol-gel. Hence, the sonication time is optimized by relating the sonication time to the distribution of particles using SEM and Energy Dispersive Spectroscopy (EDS) images (Section 2.2). Furthermore, composites exhibiting high porosity are known to have poor piezoelectric and dielectric properties. Hence, the porosity of the composites were examined using SEM and EDS analyses as a function of dessication time (2.3).

2.1 Characterization of dispersion of MWCNTs in ethanol

The MWCNTs used in the experiments are cathode deposited and are in the form of pellets. First the dispersion of MWCNTs is characterized by SEM and TEM micrographs to determine the best time for maximum dispersion, formation of the least number of agglomerated MWCNTs and the morphology of the dispersed MWCNTs. In transmission electron microscopy (TEM) a beam of electrons are passed through a material and an image is formed due to the interaction between the electrons and the sample. On the other hand scanning electron microscopy (SEM) is a microscopy technique where a focused beam of electrons are used to scan the material by detection of either the secondary or the backscattered electrons (most common methods of detection) from the sample surface. In general the TEM is used for high resolution imaging of the microstructure and/or for material phase detection. On the other hand the SEM is used to scan the topography and the microstructure of the material.

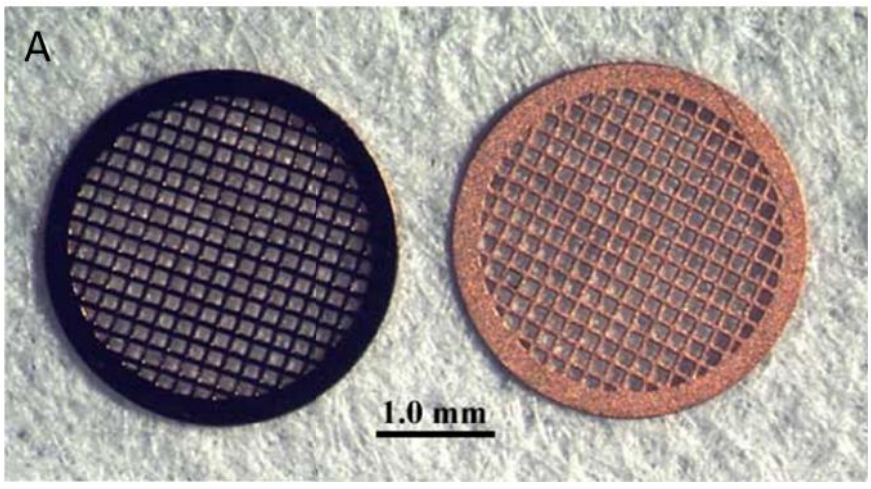

Figure 2.1 A) Structure of a TEM Grid, B) A SEM stub

Figure 2.1 A and B shows the shape and structure of the SEM stubs and the TEM grids. The high resolution TEM imaging and the grid structure of the TEM sample grids enables us to look at the size, shape and structure of the MWCNTs when dispersed in ethanol. On the other hand the micro structural properties of the MWCNT dispersion such as the extent of dispersion of the nanotubes in ethanol and the formation of agglomerations can be investigated by utilizing the planar surface of the SEM stubs.

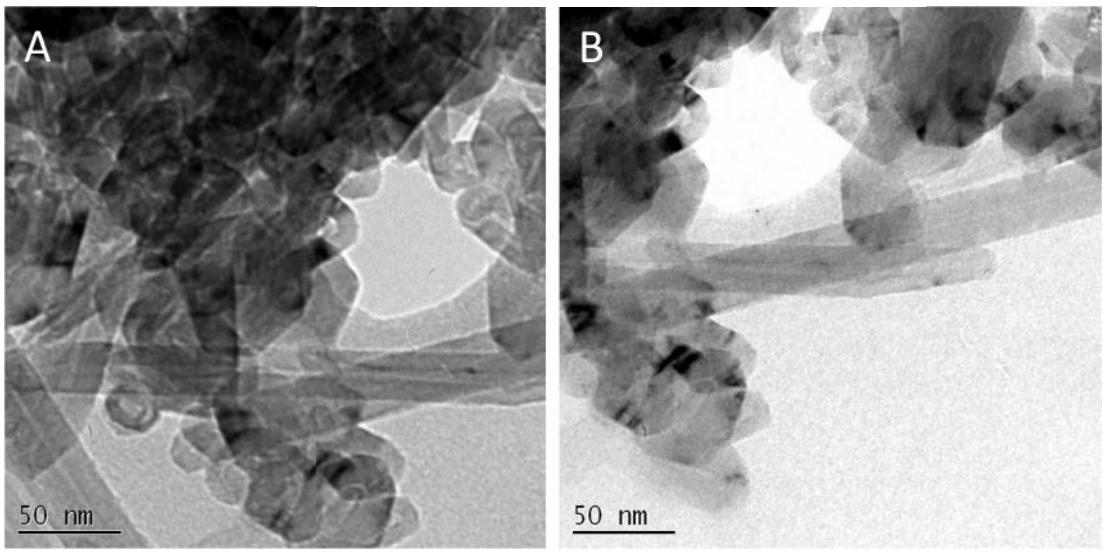

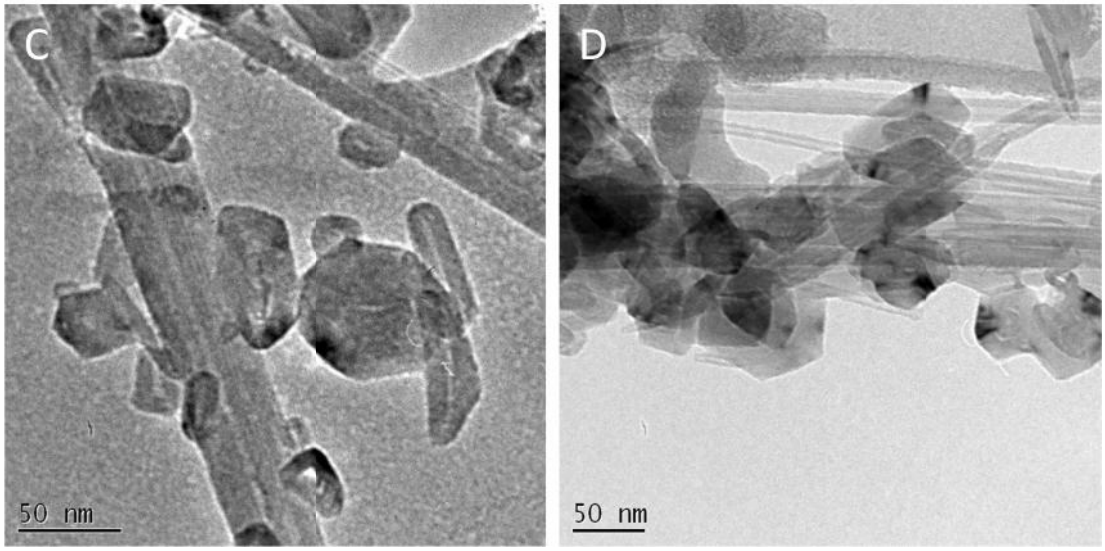

Figure 2.2 A), B) C) and D) shows the morphology of the MWCNTs dispersed in ethanol (for 4 hours). The rod shaped structures are the individual MWCNTs and the spherical particles are the clusters of MWCNTs.

The MWCNTs are dispersed in ethanol and then put on the TEM grids. The nanotubes stick to the grids for imaging after the ethanol evaporates. In the case of the SEM samples the ethanol evaporates on the stub and the MWCNTs get sufficient time to stick together due to the Van der Wall's forces of attraction to form clusters and clouds of MWCNTs. So the SEM micrographs are used to look at the dispersion of these MWCNT clusters and analyze the larger agglomerations of the clusters of MWCNTs. The appropriate sonication time is determined by examining the average particle size and separation of particles by analysis of the SEM images.

Figure 2.2 shows the TEM micrographs of the MWCNTs in ethanol. The rods like structures are the individual MWCNTs. Some of the multiple rings in the MWCNTs are visible in Figure 2.2 D. Some of the MWCNTs come close to each other and stick to

form clusters of MWCNTs as seen by the curled up MWCNTs and the agglomerations. These are the spherical shaped particles seen in the micrographs.

A single pellet of undispersed MWCNTs produced by arc discharge cathode deposition (from Stream Chemicals Inc.), is shown in Figure 2.3 A. Figure 2.3 B, C and D shows the dispersion of MWCNTs in 40 ml of ethanol for a sonication time of 30 mins in an ultrasonicator. The samples for obtaining the SEM micrographs are obtained by dropping 1 ml of the suspension of MWCNTs in ethanol onto a SEM stub with a pipette and with the subsequent evaporation of the ethanol.

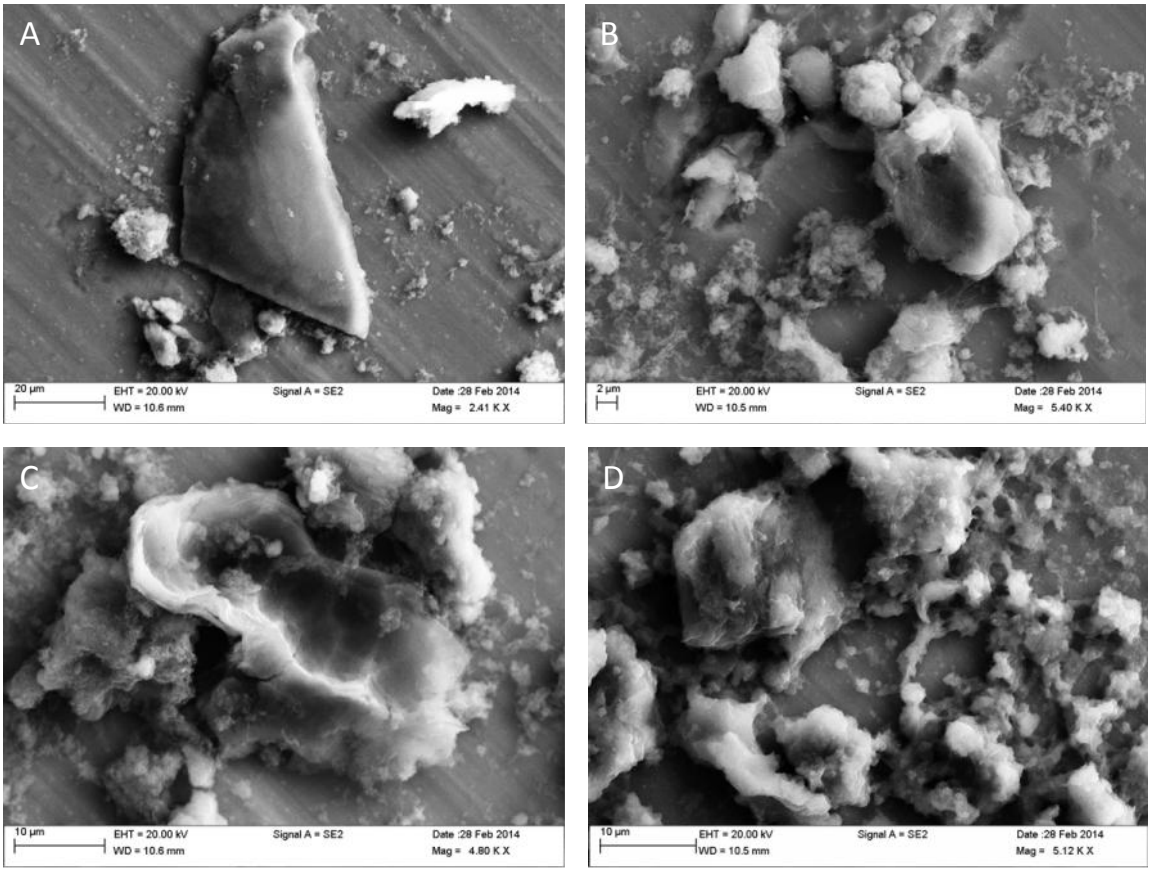

Figure 2.3 A) A pellet of undispersed MWCNT. Dispersion of MWCNTs in ethanol for 30 mins with B) MWCNT = 36.4 mg (3% in volume of the final PZT-Epoxy-MWCNT mixture), C) MWCNT = 72.9 mg (6% in volume of the composite PZT-Epoxy-MWCNT

mixture), D) MWCNT = 109.35 (9% in volume of the final composite mixture) shows huge agglomerations of MWCNT clusters.

The figure shows three different amounts of MWCNTs, namely 36.4 mg (MWCNT 1), 72.9 mg (MWCNT 2) and 109.35 mg (MWCNT 3) dispersed in 40 ml volume of ethanol. These amounts of MWCNTs correspond to 3%, 6% and 9% volume fractions in the PZT-Epoxy-MWCNT composite mixture respectively. The SEM micrographs show huge agglomerations of the MWCNT clusters. An analysis using Image analysis software ImageJ show that the agglomeration size varies from 5-50μm , 6-60 μm and 8-65 μm for MWCNT 1,2 and 3 respectively.

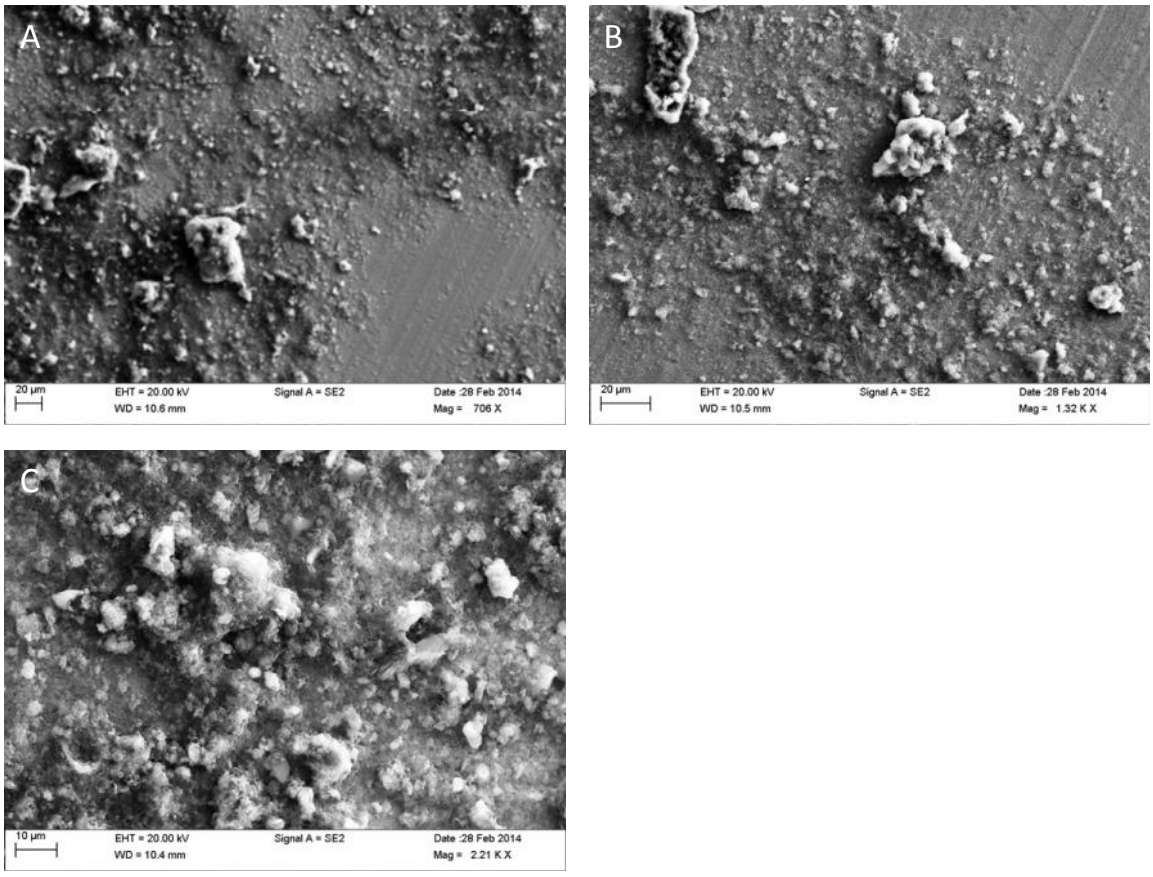

Figure 2.4 Dispersion of MWCNTs in ethanol for 2 hours at A) MWCNT = 36.4 mg (MWCNT 1), B) MWCNT = 72.9 mg (MWCNT 2) and C) MWCNT = 109.35 (MWCNT 3), shows smaller agglomerations of MWCNT clusters.

Figure 2.4 A, B and C shows the dispersion of the MWCNT pellets in ethanol for 2 hours. An image analysis shows that for (MWCNT 1) the average particle size is around 15μm with a standard deviation of 14.25μm. For (MWCNT 2 and 3) the average particle size / standard deviations are 17.5/16.25 μm and 13.25/15.73 μm respectively. The average particle size and standard deviation indicates that a sonication time of 2 hours improves the dispersion the MWCNT clusters as compared to a sonication for 30 mins.

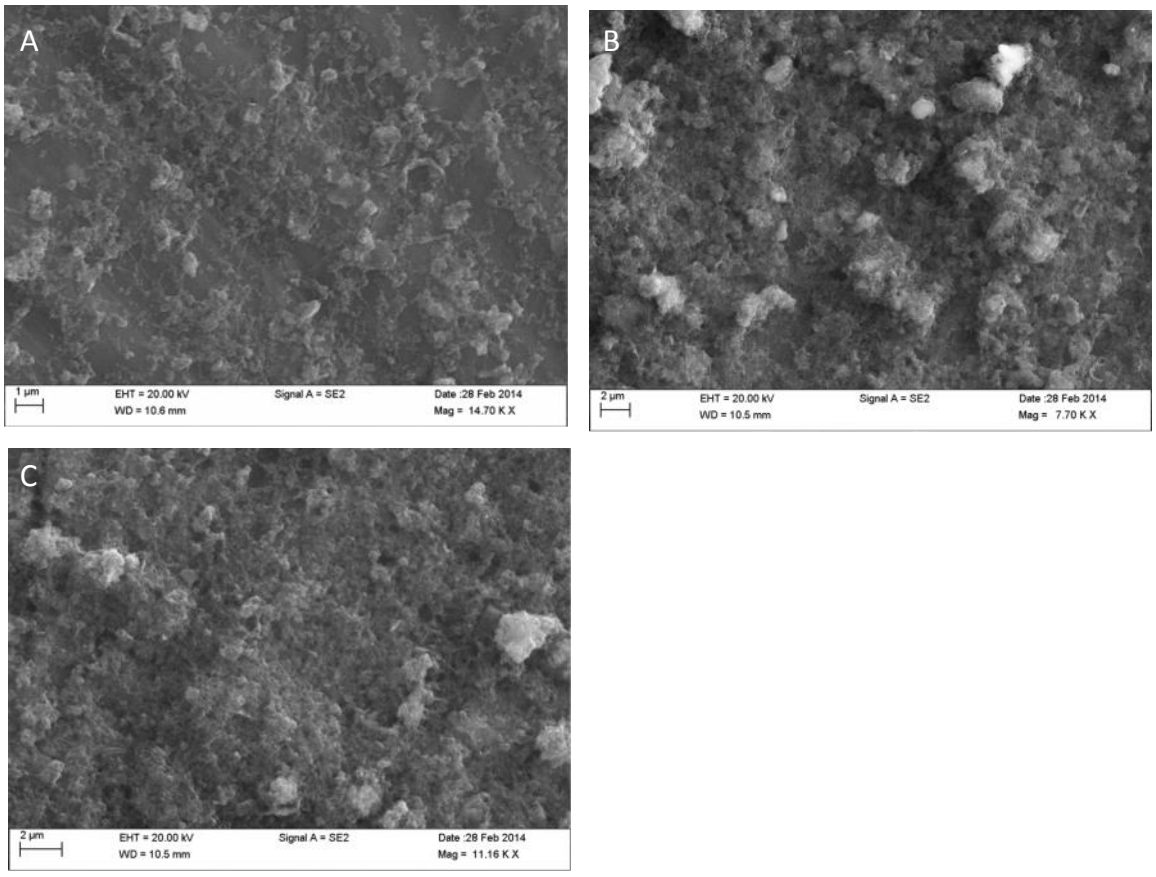

Figure 2.5 Dispersion of MWCNTs in ethanol for 3 hours at A) MWCNT = 36.4 mg (MWCNT 1), B) MWCNT = 72.9 mg (MWCNT 2) and C) MWCNT = 109.35 (MWCNT 3), shows clouds of MWCNT clustered together.

Figure 2.5 A, B and C shows the dispersion of the MWCNT pellets in ethanol for 3 hours. In the images the MWCNTs inclusions disperse from their clusters which lead to the formation of clouds of the individual MWCNTs on the SEM stub with the evaporation of ethanol. The average particle size for (MWCNT 1,2 and 3) was found to be 0.8/0.84/0.85 μm from image analysis by the ImageJ software. The standard deviations for the three different amounts of MWCNTs are 1.25/1.44/1.36 μm respectively. A few agglomerations of MWCNT clusters are still visible specifically for the higher weight/volume % of MWCNTs. A further improvement is dispersion is observed from a sonication time of 2 hours.

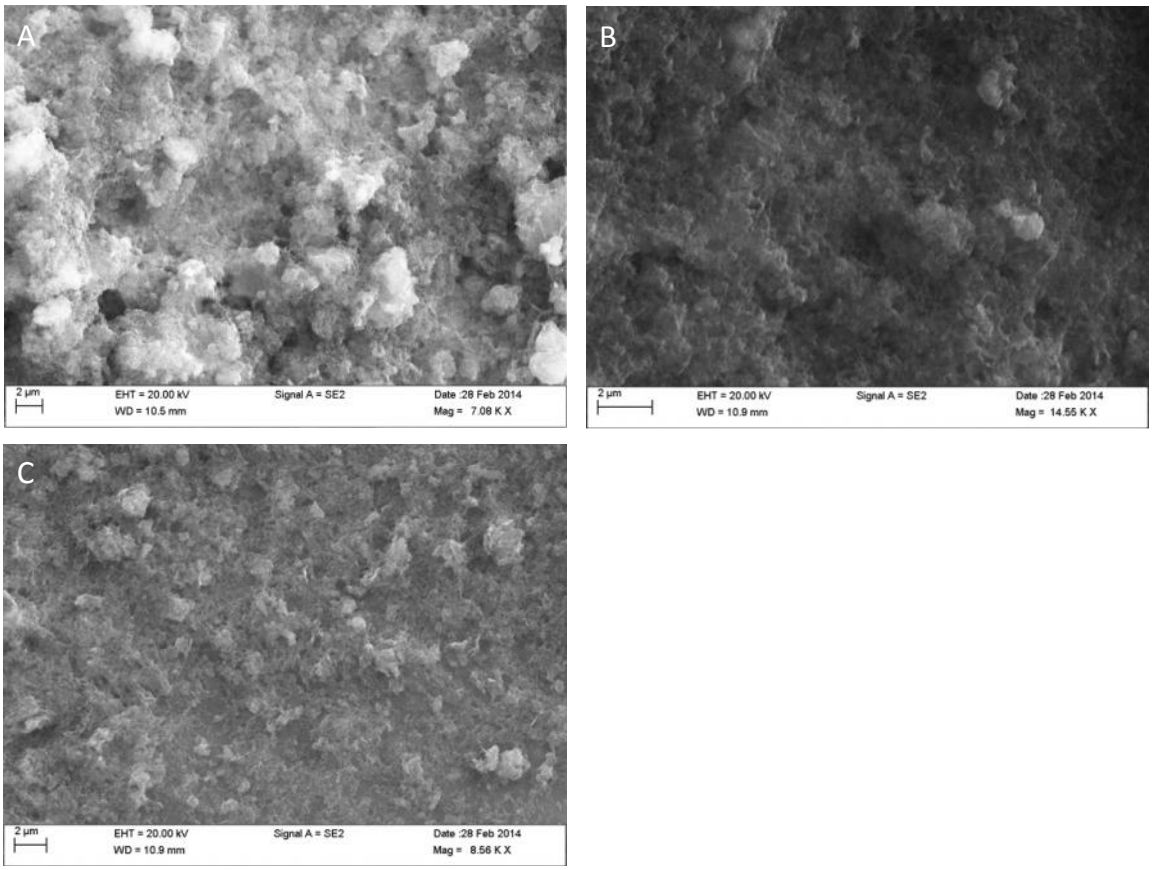

Figure 2.6 Dispersion of MWCNTs in ethanol for 4 hours at A) MWCNT = 36.4 mg (MWCNT 1), B) MWCNT = 72.9 mg (MWCNT 2) and C) MWCNT = 109.35 (MWCNT 3), shows smaller agglomerations of MWCNT clusters.

Figure 2.6 A, B and C shows the dispersion of the MWCNT pellets in ethanol for 4 hours. The average particle size reduces to 340/345/326 nm and the standard deviation is calculated as 55/63/53 nm for MWCNT 1, 2 and 3 respectively. A considerable decrease in the particle size is observed for all volume fractions of MWCNT. From the TEM images it is seen that average length of the MWCNTs are around 350 nm which suggests that at a sonication time of 4 hours the clusters of MWCNT consist of about 1-3 MWCNT strands, as some of the MWCNTs might we wound around in coils decreasing the effective length.

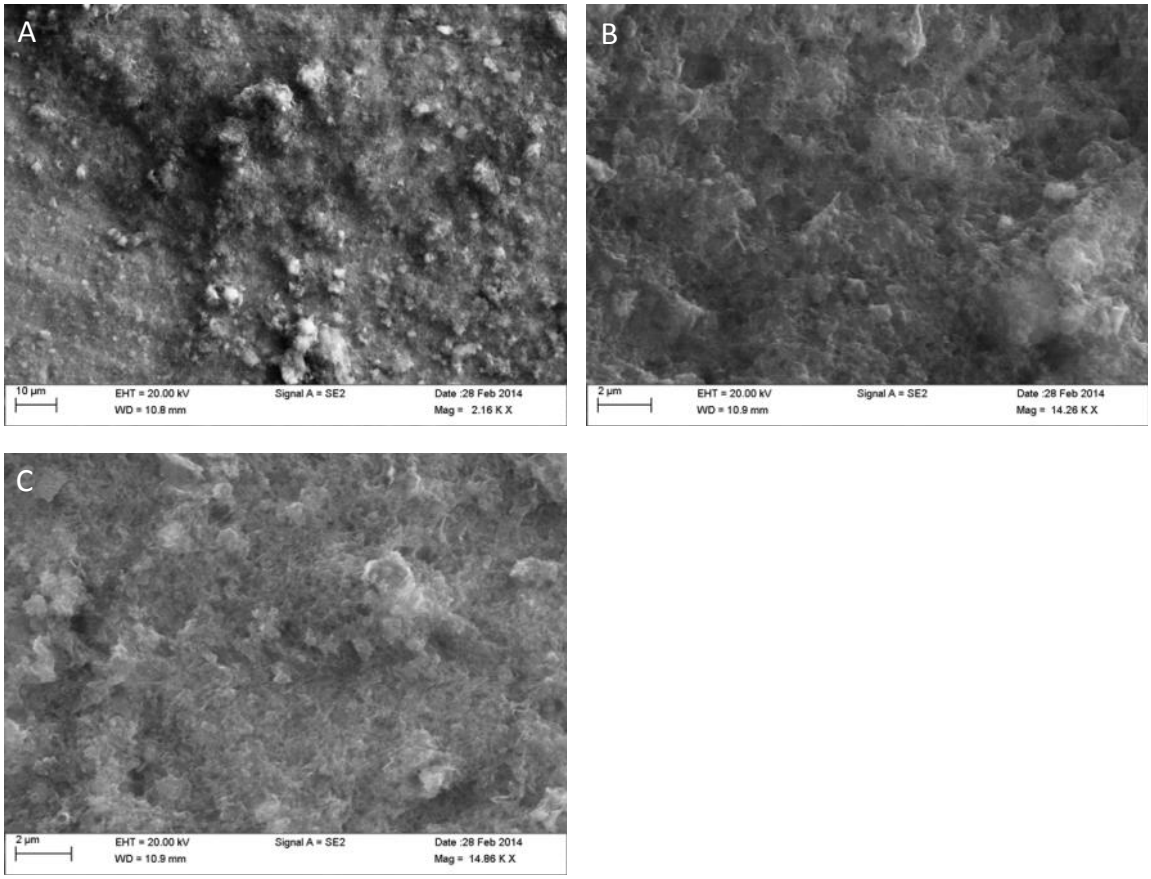

Figure 2.7 Dispersion of MWCNTs in ethanol for 8 hours at A) MWCNT = 36.4 mg (MWCNT 1), B) MWCNT = 72.9 mg (MWCNT 2) and C) MWCNT = 109.35 (MWCNT 3) shows similar MWCNT cluster size as observed for a sonication time of 4 hours.

An analysis of the SEM micrographs in Figure 2.7 at a sonication time of 8 hours show the average particles size at MWCNT 1,2 and 3 are 338/347/331 nm respectively. The standard deviation is 53/61/57 respectively. The average size and deviation of particle size suggests that the clusters of MWCNTs are similar to the ones observed at a sonication time of 4 hours. It is observed from the SEM micrograph analysis that the dispersion observed at a sonication time of 4 hours seems to be the best choice for

fabrication of PZT-Epoxy-MWCNT sol-gel at MWCNT volume fractions from 0.1% to 10%.

2.2 Optimization of Sonication Time for Well Distributed Particles

After dispersion of the MWCNTs in ethanol for 4 hours, ball milled PZT (particle size around 1.5 +/- 0.3) and Epoxy is added to form a sol-gel. This sol-gel is sonicated for proper mixing and to break up agglomerations in the PZT-Epoxy-MWCNT sol-gel mixture in ethanol. The sol-gel is characterized by Energy Dispersive Spectroscopy (EDS) performed by dispersion of 1 ml of the sol-gel over an SEM stub and the subsequent evaporation of ethanol; over variable sonication times to obtain the desired mixing of the three different phases in the sol-gel.

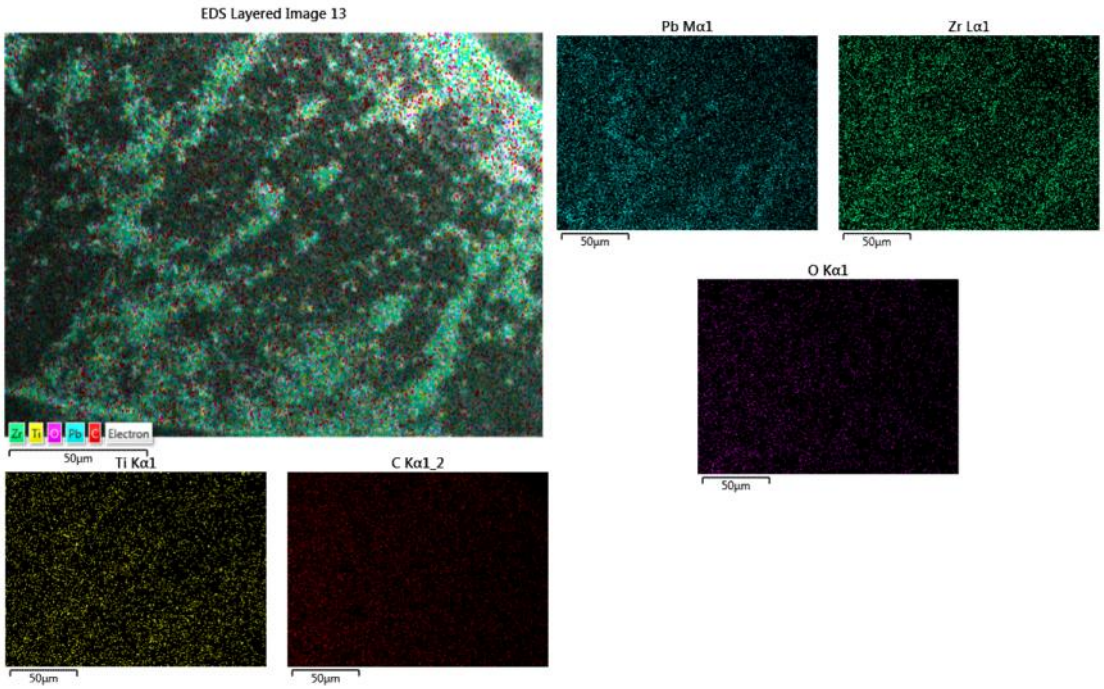

Figure 2.8 EDS layered image with the SEM micrograph and elemental analysis of the sol-gel of PZT-Epoxy-MWCNT at a sonication time of 30 minutes and PZT and MWCNT volume fractions of 30% and 6%.

Figures 2.8 – 2.12 shows the EDS spectroscopy of the PZT-Epoxy-MWCNT sol-gel over sonication times of 30 mins, 2 hours, 3 hours, 4 hours and 8 hours respectively; with a PZT volume fraction of 0.3 (30%) and a MWCNT volume fraction of 0.06 (6%). An image analysis of the EDS layered image in Figure 2.8 shows that the average size of agglomerations is around 35 μm with a standard deviation of 25 μm. The average size of the agglomerations decrease with an increase in the sonication time. The average size / standard deviation of the agglomerations of the sol-gel for sonication times of 2 hours, 3 hours and 4 hours are 15.5/7.4 μm, 7.6/4.7 μm and 3.5/2.7 μm. The average size / standard deviation of the agglomerations for a sonication time of 8 hours is calculated to be 3.4/2.75 μm.

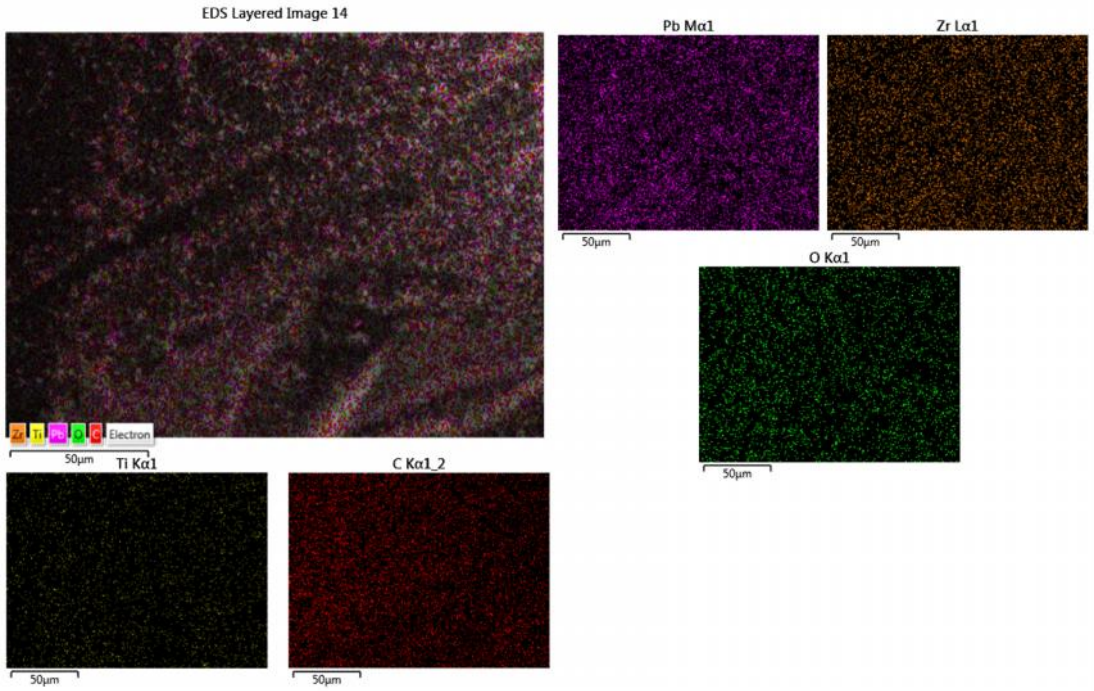

Figure 2.9 EDS layered image with the SEM micrograph and elemental analysis of the sol-gel of PZT-Epoxy-MWCNT at a sonication time of 2 hours and PZT and MWCNT volume fractions of 30% and 6%.

All the average and standard deviation were calculated over three different sample regions for each SEM stub. The elemental analysis of Pb, Zr, Ti, O (from Lead Zirconate Titanate) and Carbon (from Epoxy and MWCNTs) also show that the distribution of the individual phases become more uniform with increasing sonication times from 30 mins to 4 hours. It is observed from the above EDS spectroscopic analysis that a sonication time of 4 hours of the PZT-Epoxy-MWCNT sol-gel is the best time for fabrication of the bulk and thick film composite materials.

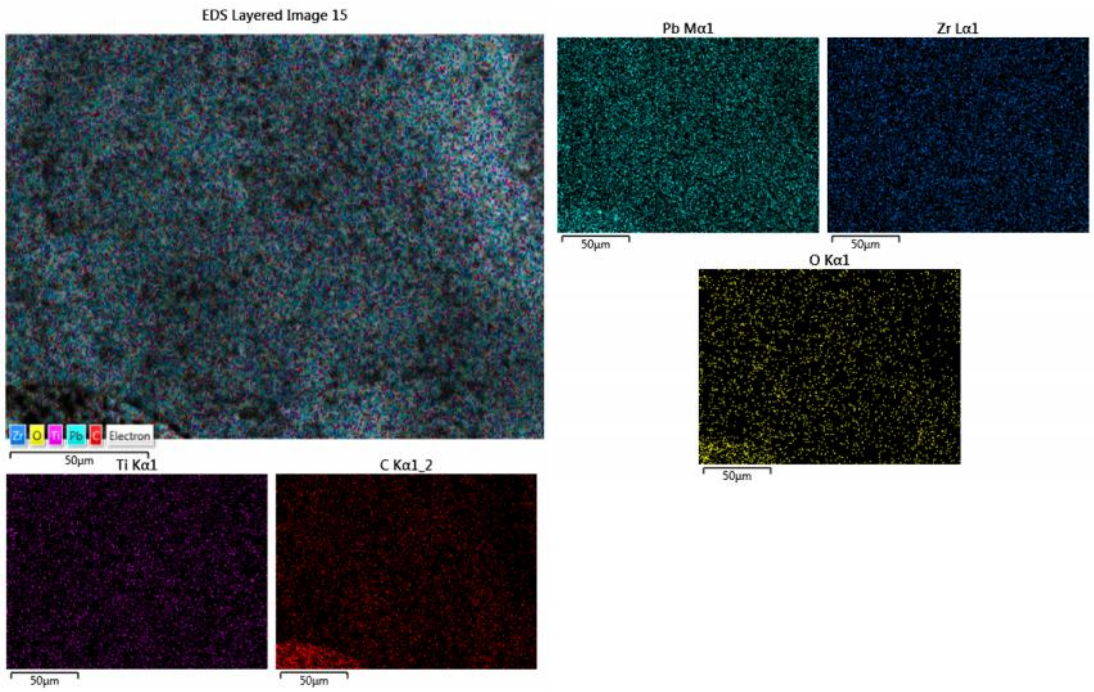

Figure 2.10 EDS layered image with the SEM micrograph and elemental analysis of the sol-gel of PZT-Epoxy-MWCNT at a sonication time of 3hours and PZT and MWCNT volume fractions of 30% and 6%.

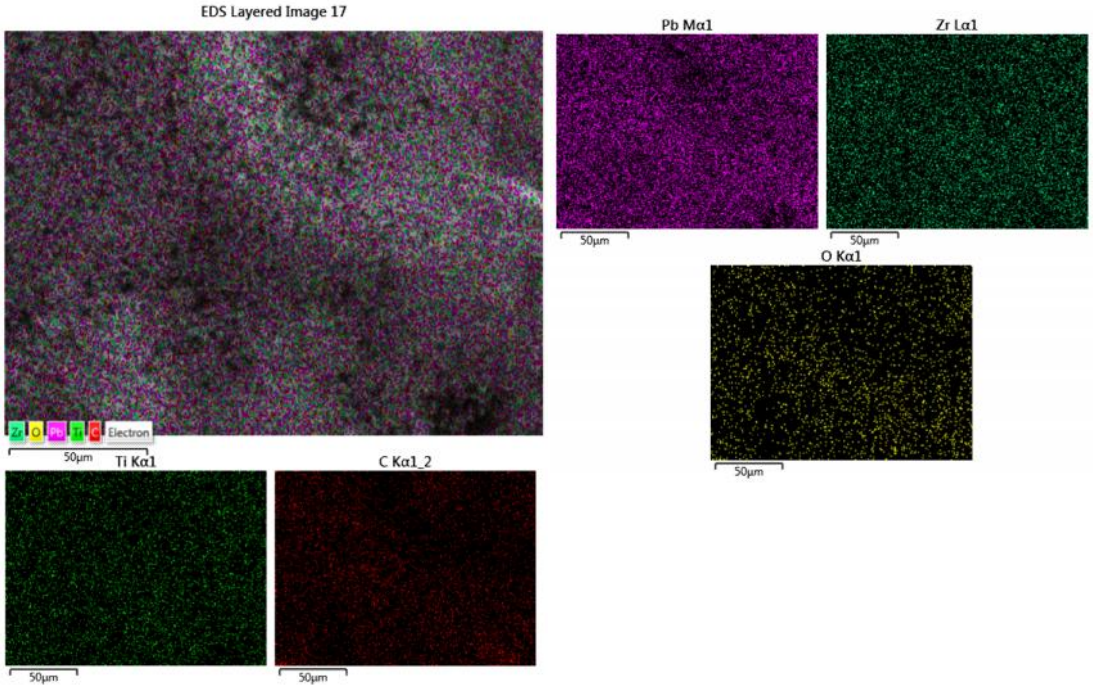

Figure 2.11 EDS layered image with the SEM micrograph and elemental analysis of the sol-gel of PZT-Epoxy-MWCNT at a sonication time of 4hours and PZT and MWCNT volume fractions of 30% and 6%.

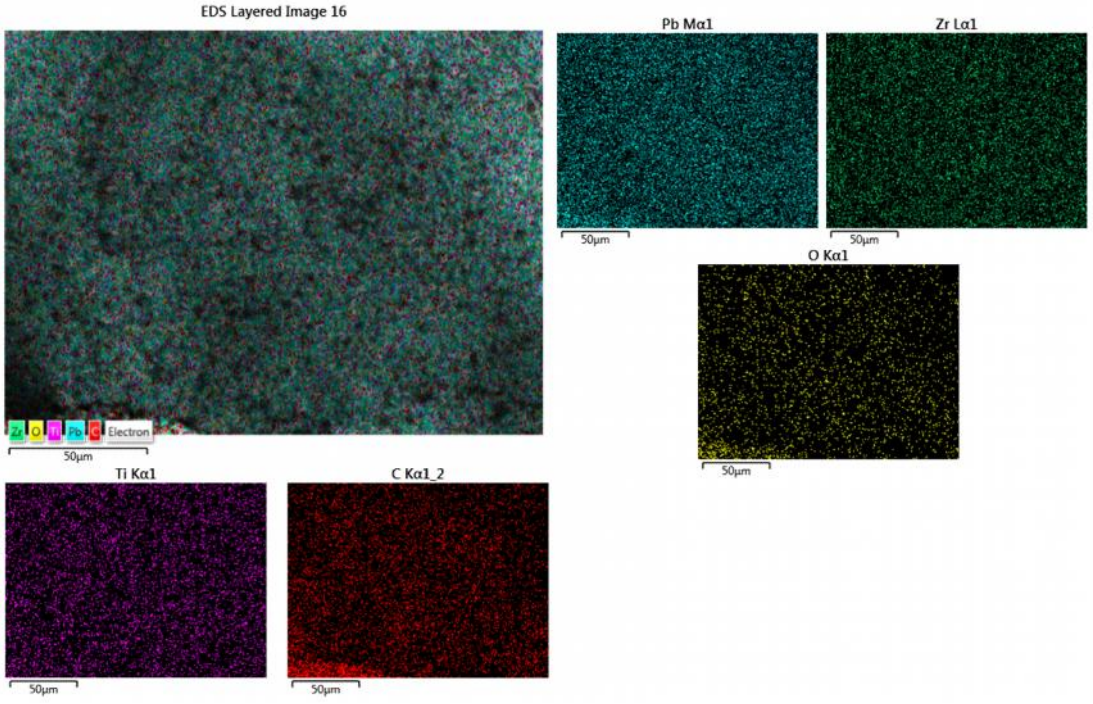

Figure 2.12 EDS layered image with the SEM micrograph and elemental analysis of the sol-gel of PZT-Epoxy-MWCNT at a sonication time of 8hours and PZT and MWCNT volume fractions of 30% and 6%.

2.3 Desiccation time study to minimize sample porosity

After sonication of the composite PZT-Epoxy-MWCNT sol-gel for 4 hours is it subjected to a desiccation process to get rid of the air pores in the microstructure. The SEM micrographs of the composite sol-gel at sonications times of 30 mins, 2hours, 3 hours 4 hours and 8 hours are shown in Figure 2.13 A, B, C, D and E respectively. Photoshop CS5.1 is used to analyze the SEM micrographs and calculate the area of the pore sizes. From Figure 2.13 A it is calculated that the pore area is ~ 25.6 % of the total area of the SEM micrograph. A decrease in the pore areas is observed with increase in desiccation times. For example for a desiccation time of 2 hours the pore area is ~ 4.6% in Figure 2.13 B. The pore area further decreases to ~ 1.9% and 1.7% for desiccation times of 3 and 4 hours respectively. The pore area for desiccation time of 8 hours is calculated as ~ 1.7 %. The air pores does not seem to decrease above a desiccation time of 4 hours. It is observed from the SEM micrographs and Photoshop CS5.1 image analysis that a desiccation time of 4 hours is the best time for fabrication of the PZT-Epoxy-MWCNT composites. The viscosity of the sol-gel measured at this point is ~ 200-210 Pa-s. The epoxy hardener (from the Epofix resin kit, EMS) is then added to the composite sol-gel and the mixture is sonicated for an additional 30 minutes for proper mixing of the hardener and the sol-gel. The composite bulk material is then fabricated by casting the composite sol-gel in a cylindrical mould. For fabrication of the flexible thick films, the sol-gel is then spin coated over a flexible stainless substrate of thickness 20 μm. The spin coating speed is increased in steps of 100 rpm to a 1000 rpm for uniform distribution of the sol-gel over the substrate. The spin coating speed was chosen to maintain uniform distribution (quantified by thickness of the coating) of the spin coated

composite thick film over the stainless steel substrate. A deviation from the chosen spin coating parameters and the given viscosity of the sol-gel produces non uniform thickness of the composite layer.

The composites are then sintered at a temperature of 75^0 C for 8 hours (as directed in the Epofix kit from EMS to cure the epoxy), which is the glass transition temperature of the epoxy matrix. After curing the samples are poled using either the contact or the corona discharge poling methods. The poling parameters of temperature and voltage are varied to investigate their influence on the electromechancial properties of the

composites.

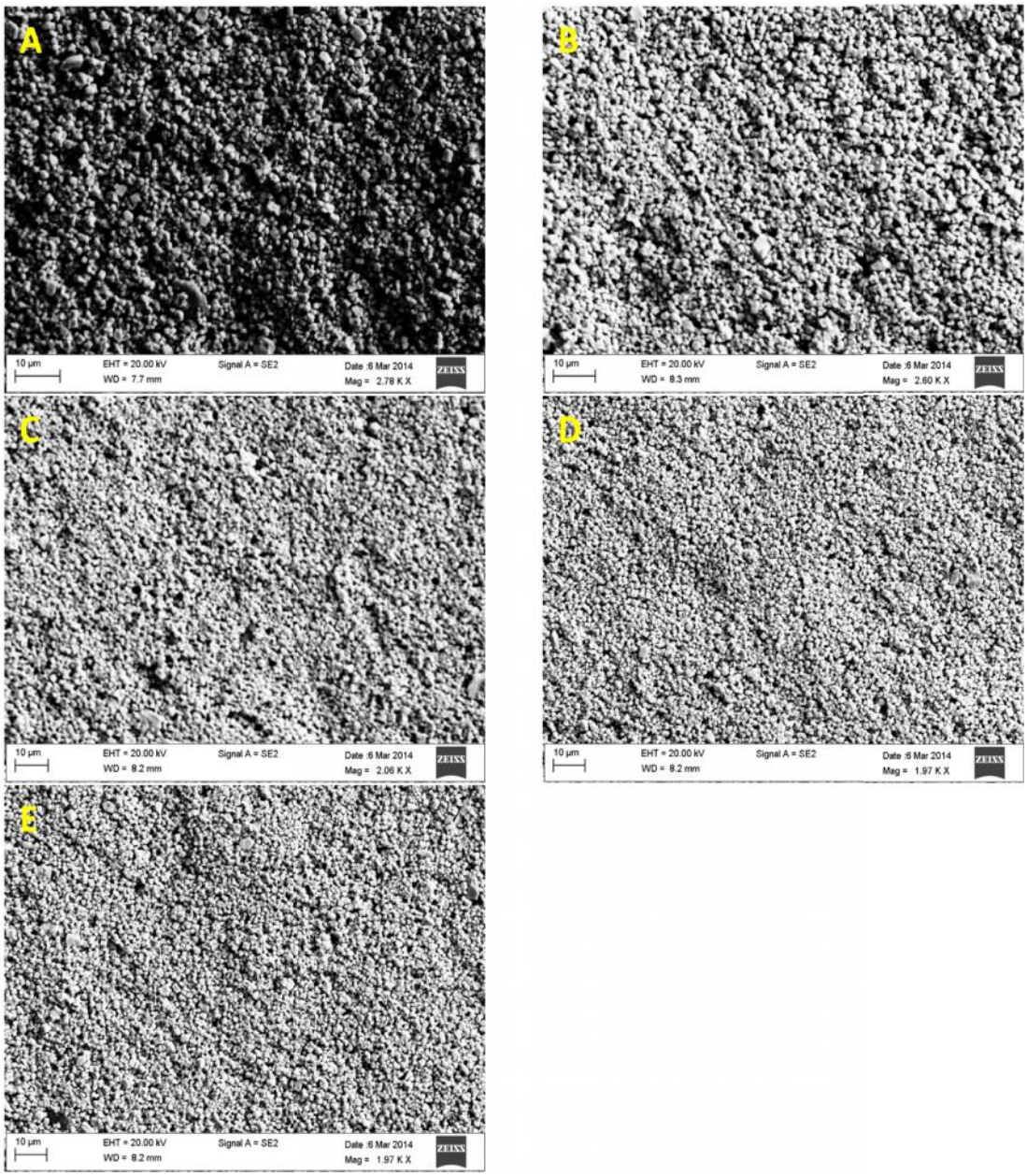

Figure 2.13 The above figure shows the SEM micrographs of the PZT-Epoxy-MWCNT composite sol-gel with desiccation times of A) 30 mins, B) 2 hours, C) 3 hours, D) 4 hours and D) 8 hours. The pore size in the microstructure decreases with increasing desiccation times from 30 mins to 4 hours and varies from ~25.6 % , 4.6%, 1.9% and 1.7% and remains almost constant after that.

Chapter 3

Methodology and Procedure

3.1 Preparation of composite sol-gel

The composite sol-gel consists of the Multiwalled Carbon Nanotubes (MWCNTs), Lead Zirconate Titanate (PZT, APC International 855, Navy VI) and Epoxy resin which act as different phases in the composite. The mixture has both the components of a sol (non-macroscopic particles in solution) and a gel (bushy structures as clusters and agglomeration pockets of PZT epoxy and MWCNTs). The organic residues left behind by the gradual evaporation of the ethanol from the sol-gel bind the different phases in the mixture forming the gel-like structures. The volume fraction of PZT is kept constant at 30% and the volume fraction of MWCNTs are varied from 0.1% - 10% to optimize the piezoelectric and dielectric properties in this region and to identify the percolation threshold. The MWCNT (MWCNT from Stream Chemicals, CAS - 1333-86-4) is dispersed in ethanol (200 proof, Sigma-Aldrich) and subsequently sonicated for four hours in an ultrasonicator. The Transmission Electron Microscope (TEM) images in Figure 3.1 A and B show MWCNTs sonicated in ethanol. Single and multiple MWCNTs surrounded by agglomerations and clusters of nanotubes are seen in the TEM micrographs in Figure 3.1 A and B. The diffraction patterns in the figure shows the presence of multiple rings namely 4 rings; which can be attributed to the different 2D graphite sheets rolled up in the form MWCNTs. The structure of the MWCNTs with the rings in the diffraction pattern and their morphology in the TEM micrographs are consistent with the literature [111, 112].

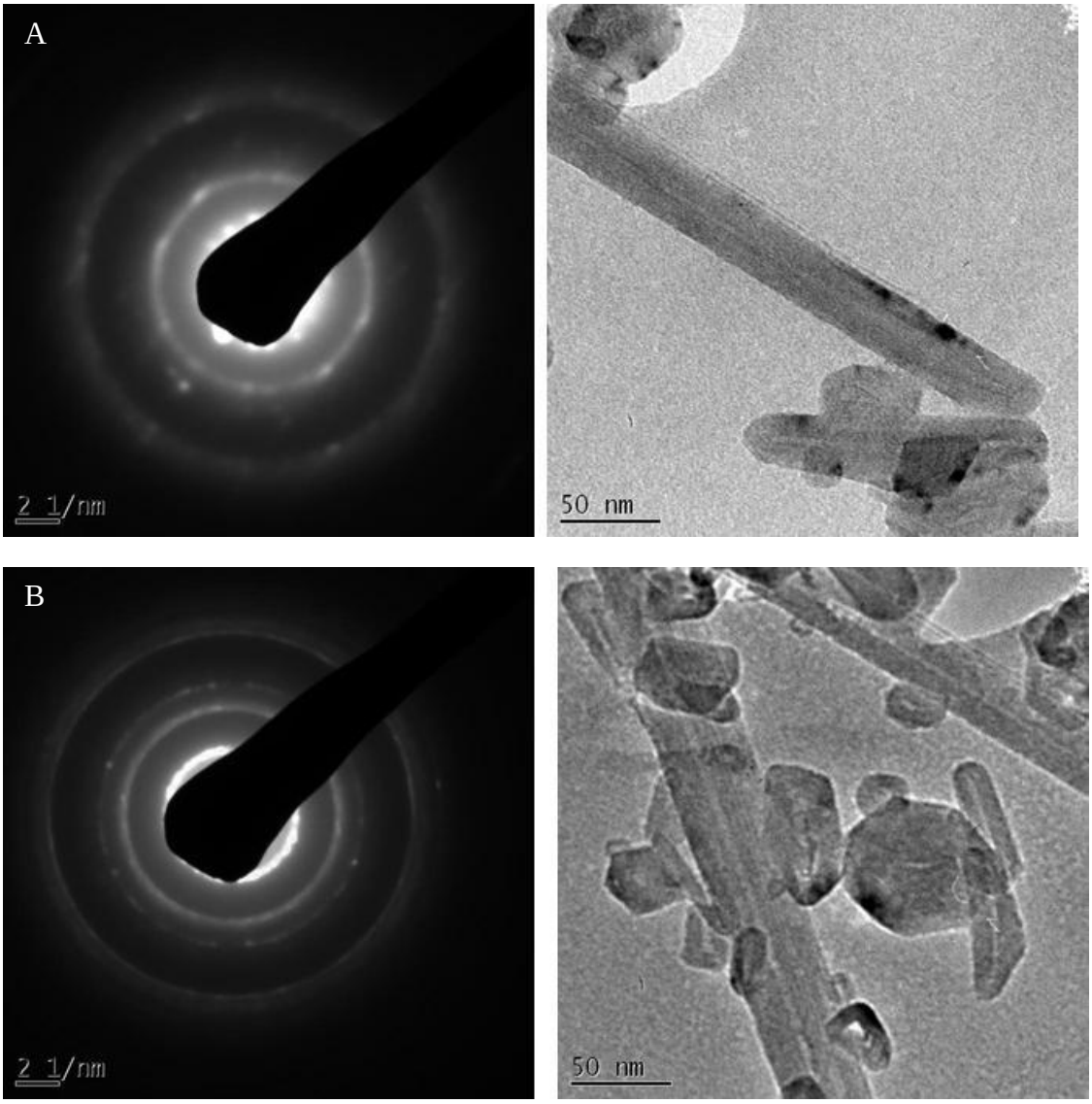

Figure 3.1 A) and B) Diffraction pattern and TEM images of MWCNTs dispersed in ethanol after a sonication time of 4 hours which was selected from the design of experiments in Chapter 2. It shows the cylindrical ring like structures of the MWCNTs. Even after sonication in ethanol the TEM images can show agglomerations of MWCNTs. This is due to the fact that the sonicated MWCNTs are dropped on the TEM grid and some of the MWCNTs can come close to each other due to the Van der Wall's forces even if they are dispersed in the suspension.

A mixture of PZT (from APC International, 855, Navy VI) and Epoxy resin (DGEBA, EMS 1232) were added to the MWCNT suspension in ethanol and the mixture

was sonicated for an additional four hours. The dielectric and piezoelectric properties of PZT are listed in Table 3.1.

Table 3.1 Dielectric and piezoelectric properties of PZT

Material	Dielectric Constant	Piezoelectric Strain Coefficient, d33 (pC/N)	Piezoelectric Strain Coefficient, d31 (pC/N)	Dielectric Loss (tan δ)
PZT (APC International, 855, Navy VI)	3300	400	175	≤ 2.50

Before mixing, the PZT powder is sintered at 500^0 C for evaporation of the PVA (Poly Vinyl Alcohol) coating and is then ball milled for 24 hours. Figure 3.2 A and B show the SEM micrographs of the PZT particles with and without PVA coating and Figure 3.2 C shows ball milled PZT particles. The average particle size of the PZT was determined by use of SEM micrograph image analysis by software packages ImageJ and Photoshop CS5.1. The particles coated with PVA had an average particle size of ~ (4.6+/- 1.5 µm) with a standard deviation of ~ 10 µm. After evaporation of the PVA coating the particle size reduces to 3 +/- 0.5 µm with a standard deviation of 15 µm. The SEM micrograph analysis of the ball milled PZT particles show that that mean particle size reduces to 1.5 +/- 0.3 µm with a standard deviation of 1.5 µm. The uniformity of the particle size increases and the standard deviation decreases with ball milling. The particle size distribution from the SEM micrograph analysis of the sintered PZT and the ball milled PZT are shown in Figures 3.3 A and B with a sample size of 1330 and 400 particles respectively. The particle size was averaged over three different sample regions.

The suspension of the three-phase mixture was desiccated for 4 hours to eliminate air pockets from the microstructure. The resulting mixture was then sonicated again for a half an hour after the epoxy binder (Epofix hardener, EMS 1232) was added to produce the PZT-MWCNT-epoxy mixture.

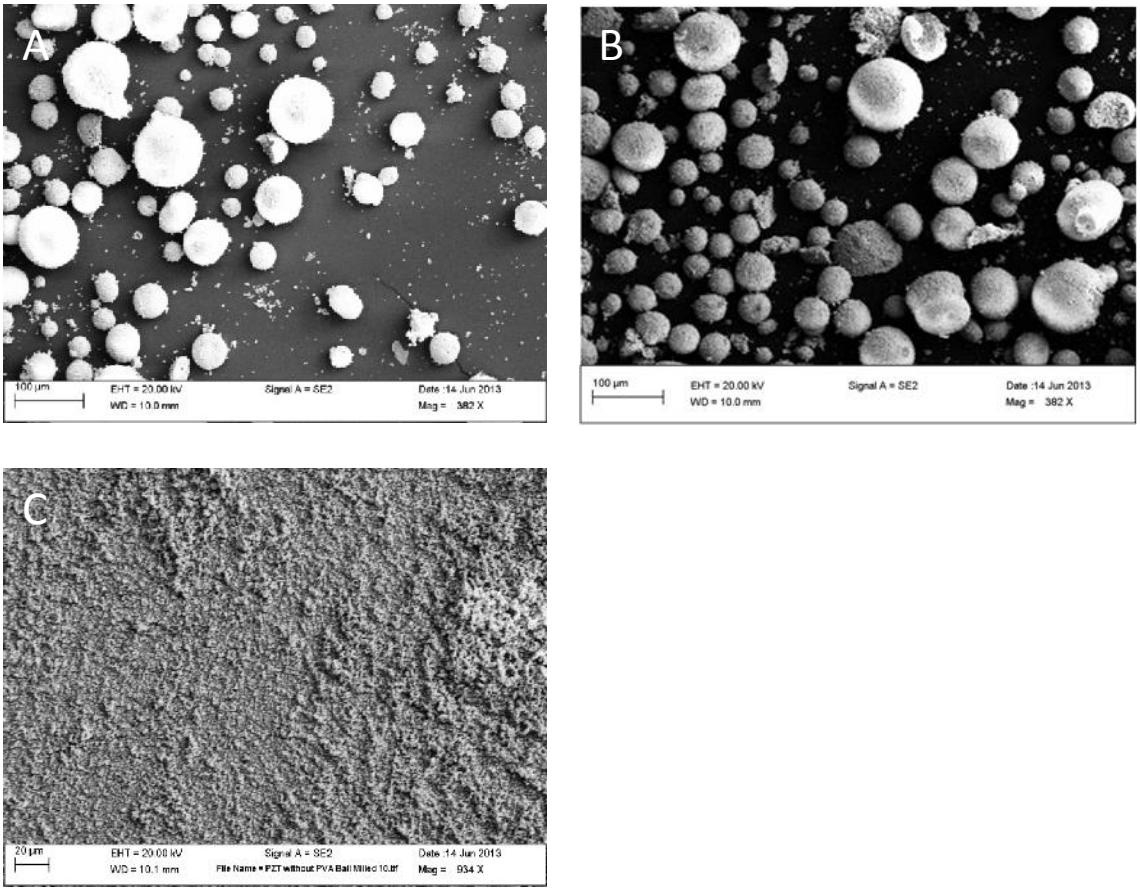

Figure 3.2 SEM micrographs of distribution of A) PZT particles with PVA coating at a magnification of ~ 300X , B) PZT particles without PVA coating at a magnification of ~ 300X and C) Ball milled PZT particles at a magnification of ~ 900X. The images show an increase in the uniformity of particle size due to ball milling.

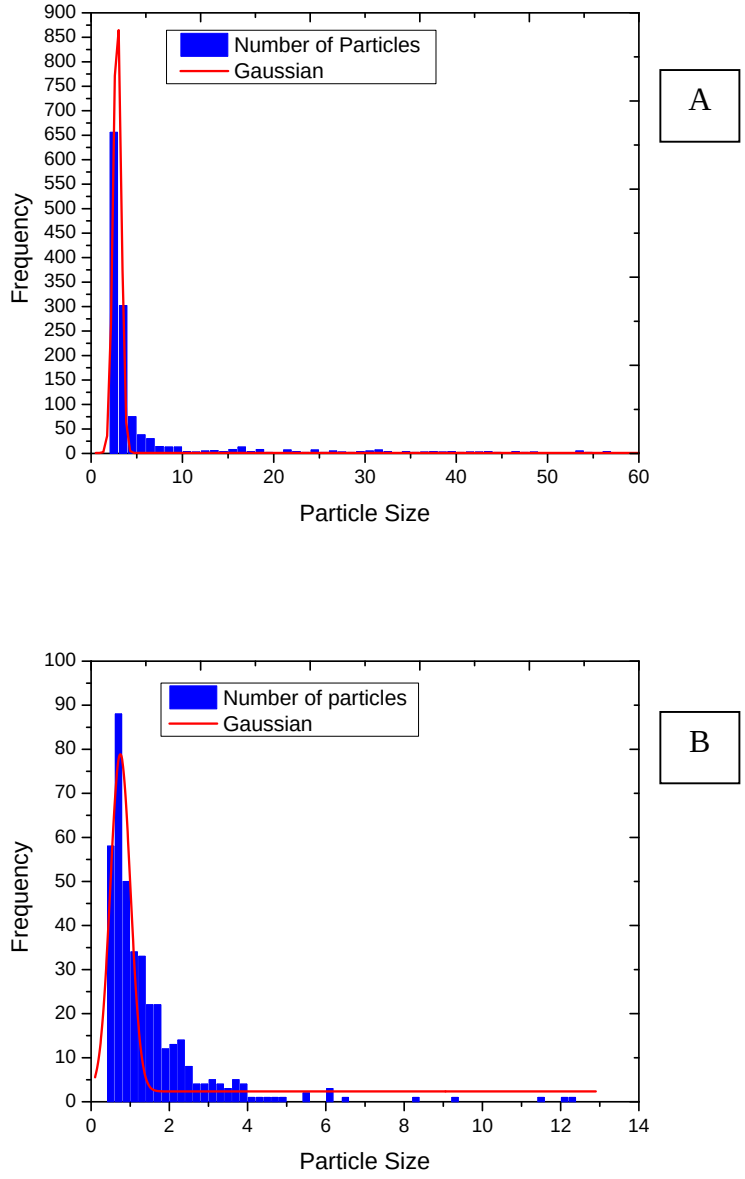

Figure 3.3 Particle size distributions of A) PZT particles without the PVA coating with a sample size of 1300 particles and averaged over three sample regions , B) PZT particles ball milled for 24 hours with a sample size of 400 particles and averaged over three sample regions.

The three phase mixture is then used to fabricate two different kinds of samples: bulk and flexible thick film composites. The bulk samples are cylindrical in shape and have a thickness of 6mm and a diameter of 7mm. The thick film composites have a flexible stainless substrate and a combined thickness of ~ 200 μm. The next two sections will describe the fabrication procedure of the bulk and flexible thick film composites.

3.2 Bulk three-phase PZT-Epoxy-MWCNT piezoelectric composites

The Epo-fix curing agent was then added and the composite mixture is then sonicated for an additional 30 minutes to ensure proper mixing of the curing agent in the mixture. The three phase PZT-Epoxy-MWCNT mixture was cast in a mould 6 mm thick with a radius equal to 7 mm and was then cured at 75^0 C for 8 hours. After curing the samples are polished using a 2000 grit sand paper and colloidal silver electrodes are painted on both the surfaces of the material. The bulk composites are then poled at a high potential using a Spellman SL Series high voltage generator to align the Ti / Zr dipoles of the PZT phase in the composite. The samples were poled using two different techniques; contact or the parallel plate poling method and the corona discharge poling method.

The contact poling method is achieved by placing the composite material in between the top electrode and the ground base plate in a dielectric medium (silicone oil) as shown in Figure 3.4 A. The composite is heated to the glass transition temperature of the matrix phase and an electric field is applied at the electrodes. This method might also lead to the formation of small localized currents owing to the presence of conductive MWCNTs in the composite [113]. When a sufficiently high electric field is reached the dipoles of the PZT phase start aligning along the poling direction.

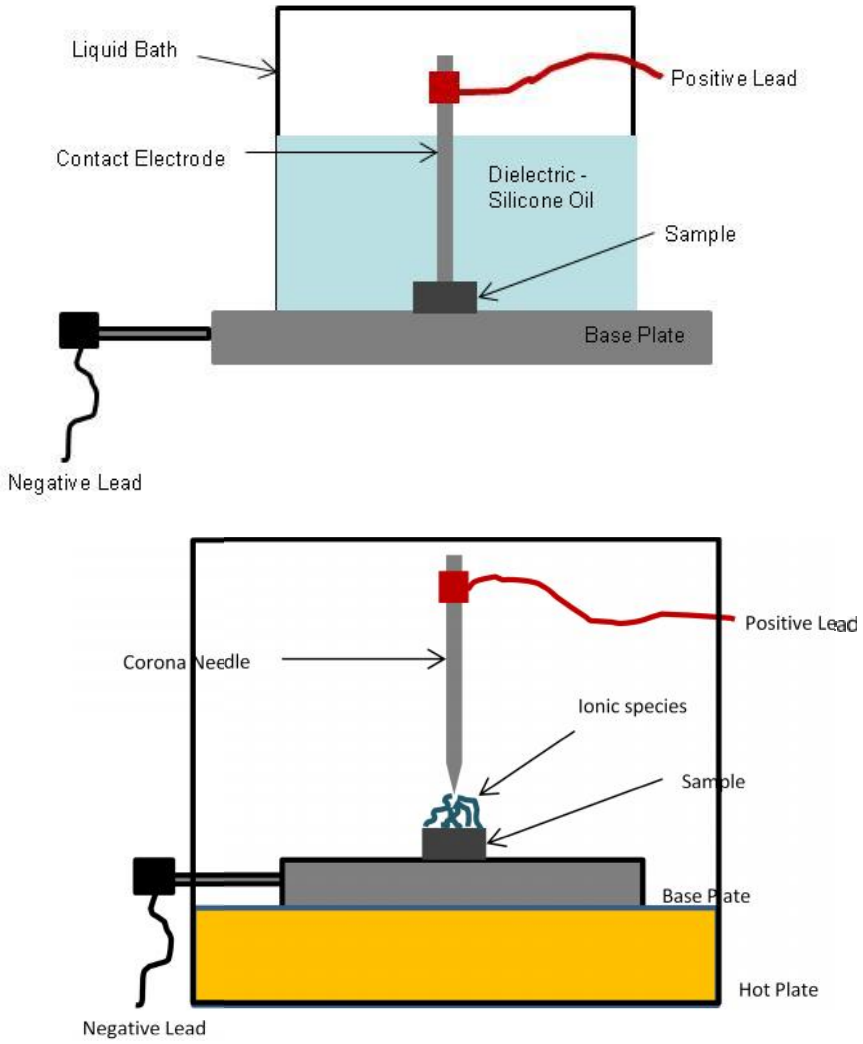

Figure 3.4 A) The figure shows the contact or the parallel plate poling method with both the electrodes in contact with both the surfaces of the composite material. B) The corona discharge poling method is shown where the needle ionizes the volume of air surrounding it. The ions on the top surface of the composite material are attracted towards the ground base plate.

The corona discharge poling method which is shown in Figure 3.4 B; is performed by applying a high electric field to a needle which is maintained at a certain distance with the composite material, which is heated to its glass transition temperature [43, 46]. When the needle reaches the ionizing potential of the surrounding air, ionic species are generated. These ionic species are attracted towards the ground base plate.

When a sufficient surface charge density is reached, the ions flow towards the base plate through the thickness of the composite material and align the dipoles of the PZT phase.

The samples are poled for 60 minutes at a varying poling voltage from 2.2 kV/mm to 0.7 kV/mm. The poling temperature is varied from the glass transition temperature of epoxy at 75^0 C to 45^0 C.

3.3 Flexible thick film three-phase PZT-Epoxy-MWCNT piezoelectric composites

The three phase PZT-Epoxy-MWCNT sol-gel is spin coated by using the Laurell WS-650-23NPP spin coater onto a stainless steel substrate that was 1.5 cm x 2.5 cm and 20 μm thick. The spin coat process included incremental increases by 100 rpm, until a final speed of 1000 rpm was achieved. The spin coat process is depicted in Figure 5. The substrate is coated with a three phase PZT-Epoxy-MWNCT composite material of thickness ~ 150 μm, and subsequently sintered at a temperature of 75^0 C for 8 hours. After sintering the samples were poled using the contact poling or the corona discharge poling techniques at varying temperatures and voltages. Poling enables the unidirectional alignment of the PZT dipoles within the matrix.

3.4 Testing and Characterization

After poling, the samples are wrapped in aluminum foil for 24 hours to remove any residual charges on either surface. A Piezometer is used to measure the dielectric constant, dielectric loss tangent and the piezoelectric strain coefficients (d33 and d31) at a frequency of 110Hz. Impedance spectroscopy and dielectric spectroscopy of the bulk and

thick film composites are performed by using the HP4194A Impedance Analyzer at varying frequencies from 100Hz-20MHz. The fractured surface morphology and Electron Dispersion Spectroscopy (EDS) of the samples are studied with the help of the Scanning Electron Microscope (FESEM ZEISS 982) and the Field Emission Transmission Electron Microscope (TEM JEOL 2010F).

Chapter 4

Piezoelectric, dielectric and micro structural characterization of PZT-Epoxy-MWCNT bulk and thick film composites

The following chapter deals with the characterization of the microstructure, dielectric and piezoelectric properties of the three phase PZT-Epoxy-MWCNT composites. The morphology and the distribution of the constituent phases in the three phase PZT Epoxy-MWCNT bulk and thick films were studied with the help of SEM, TEM imaging and EDS spectroscopy. The piezoelectric and dielectric properties are characterized by testing the piezoelectric strain coefficients, the dielectric constant (ε′) and the tangent of the loss angle (tan (δ)) of the composites.

4.1 SEM and TEM micrograph analysis of three phase PZT-Epoxy-MWCNT bulk composites

Several SEM, TEM micrographs and EDS spectrum were analyzed for the different volume fractions of MWCNTs in the bulk composites. The TEM images show the morphology and the structure of the MWCNTs embedded in the three phase composite. Whereas, the SEM micrographs show the morphology of the fractured surface with the PZT and MWCNT inclusions embedded in the epoxy matrix of the composite material. An EDS spectrum shows the distribution of the different phases in the epoxy matrix by use of selective elemental analysis.

The TEM micrographs with MWCNT volume fraction of 0.06 (6%) and 0.02 (2%) are studied in this section. A higher and a lower volume fraction of MWCNT are chosen to compare the distribution of MWCNTs and the formation of clusters and

agglomerations in the epoxy matrix. Figure 4.1 A shows the selective area diffraction pattern of the three phase bulk composite with a MWCNT volume fraction of 0.06 (6%). The white spots correspond to the polycrystalline PZT and the rings correspond to the cylindrical tubes of the MWCNTs in the epoxy matrix. The TEM micrograph in Figure 4.1 B shows three MWCNTs embedded in the Epoxy matrix. The PZT particle clusters are not visible in the TEM due to their average particle size (~1.5 μm +/- 0.3 μm) being much larger than the scope of the micrograph. An analysis of the PZT-Epoxy-MWCNT composite with a MWCNT volume fraction of 0.02 (2%) shows a similar diffraction pattern with the PZT polycrystalline phase and the MWCNT inclusions and the Epoxy matrix as shown in Figure 4.2 A. Figure 4.2 B shows a single MWCNT embedded in the epoxy matrix for the region of the composite under observation.

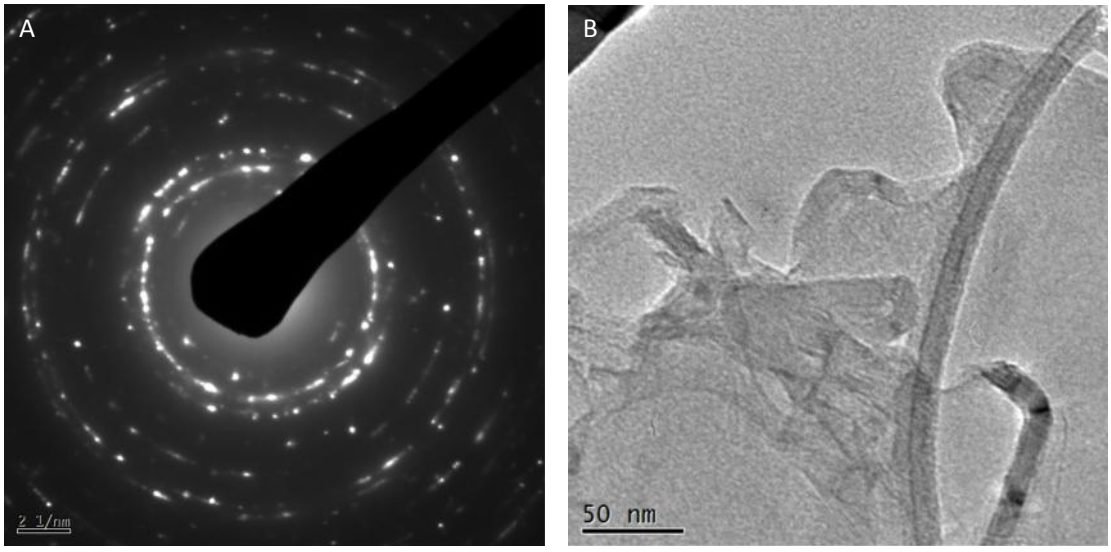

Figure 4.1 A) Diffraction pattern of the bulk PZT-Epoxy-MWCNT composite with a MWCNT volume fraction of 0.06 (6%) showing rings and spots. The rings correspond to the MWCNTs and the spots correspond to the pollycrstalline structure of the PZT phase. B) TEM micrograph of the three phase composite shows MWCNTs embedded in the Epoxy matrix.

In both the figures it is observed that the MWCNTs embedded in the epoxy matrix and shown in the TEM micrographs and are curled and twisted. This might have formed due to stresses developed during the mixing process of the sol-gel.

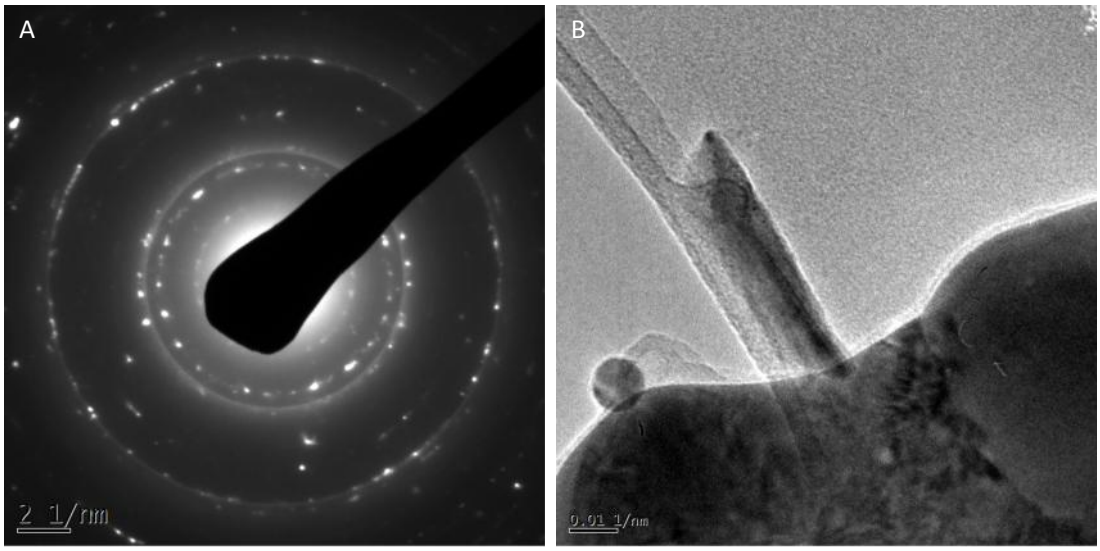

Figure 4.2 A) Diffraction pattern of the bulk PZT-Epoxy-MWCNT composite with a MWCNT volume fraction of 0.02 (2%) showing rings and spots similar to Figure 4.1. B) TEM micrograph of the three phase composite shows a MWCNT embedded in the Epoxy matrix.

Figure 4.3 shows the SEM micrograph along with the EDS spectrum, layered image and selective elemental analysis of the fractured surface of bulk PZT-Epoxy-MWCNT composite with a MWCNT volume fraction of 0.01 (1%). The larger particle clusters in the SEM micrograph are that of PZT particles which can also be seen in the layered image and from elemental analysis. The smaller clusters are that of the MWCNT agglomerations distributed in the epoxy matrix (representated by the background in the SEM image). The carbon element in the elemental analysis represents both the MWCNT and the epoxy matrix.

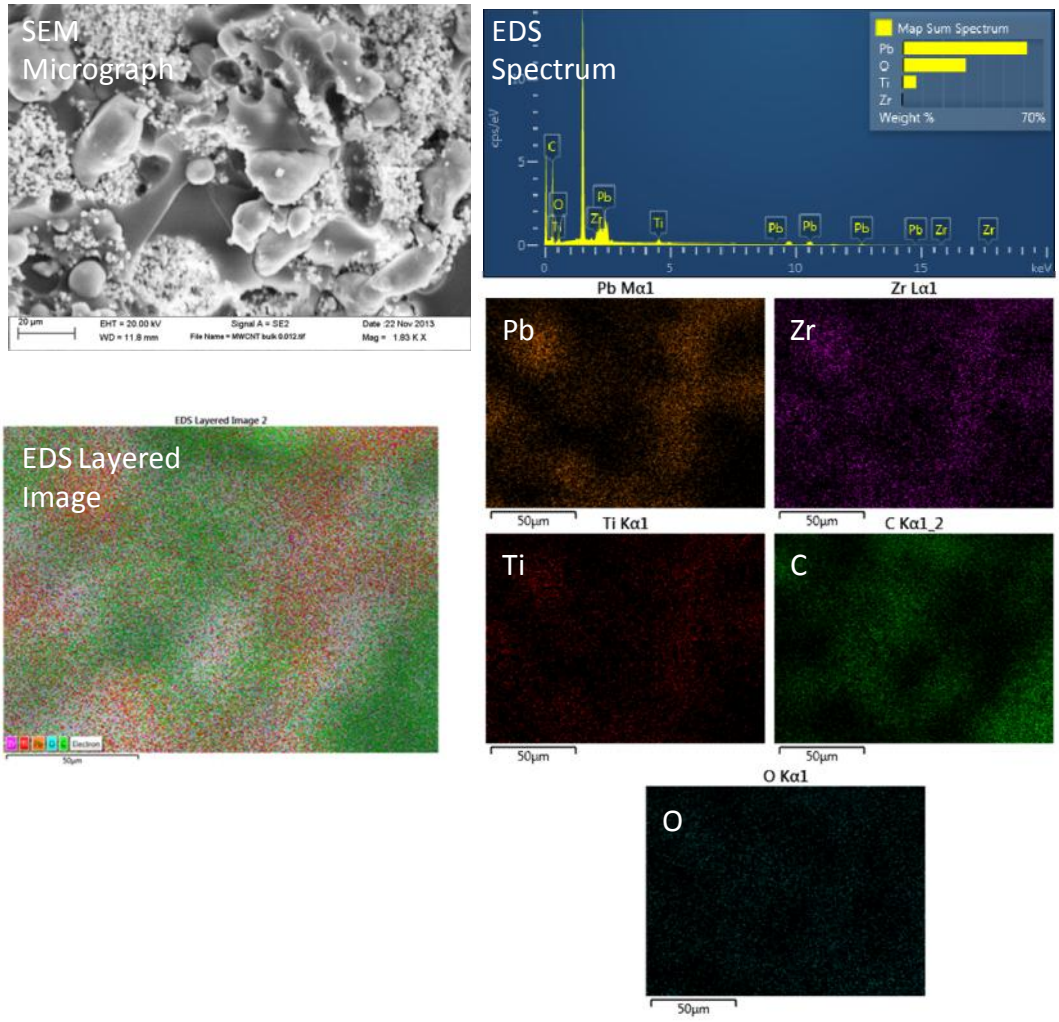

Figure 4.3 The SEM micrograph of the fractured surface of a bulk composite, shows the distribution of PZT clusters and MWCNT agglomerations embedded in the epoxy matrix with a MWCNT volume fraction of 0.01 (1%). The larger clusters comprise of the PZT particles and the smaller clusters are the MWCNT agglomerations. The dispersion is also shown by the EDS layered image that combines the elemental analysis of Pb, Zr, Ti, O (in PZT) and C (in MWCNTs and epoxy). The EDS spectrum also shows the peaks for the selective elemental analysis. (Note – The unmarked peak in the EDS spectrum is that of gold that is coated over the SEM sample for the purpose of SEM imaging.)

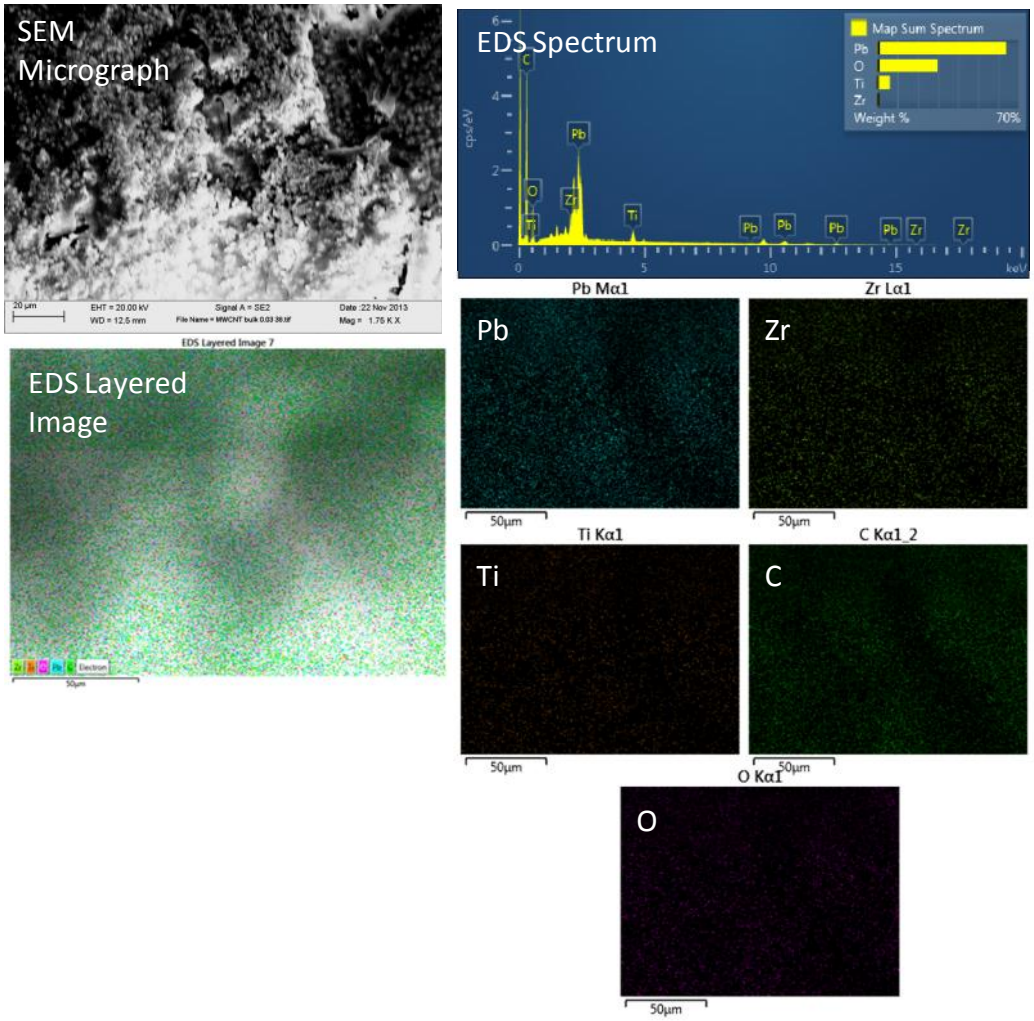

Figure 4.4 The SEM micrograph of the fractured surface of a bulk composite, shows the distribution of PZT clusters and MWCNT agglomerations embedded in the epoxy matrix with a MWCNT volume fraction of 0.03 (3%). The dispersion is also shown by the EDS layered image similar to that of Figure 4.4. The EDS spectrum also shows the peaks for the selective elemental analysis.

A similar distribution of the three different phases is observed in Figures 4.4 and 4.5 where the MWCNT volume fraction in the composite are 0.03 (3%) and 0.06 (6%) respectively. The next section discusses the TEM, SEM micrographs and EDS spectroscopy of three phase PZT-Epoxy-MWCNT thick films.

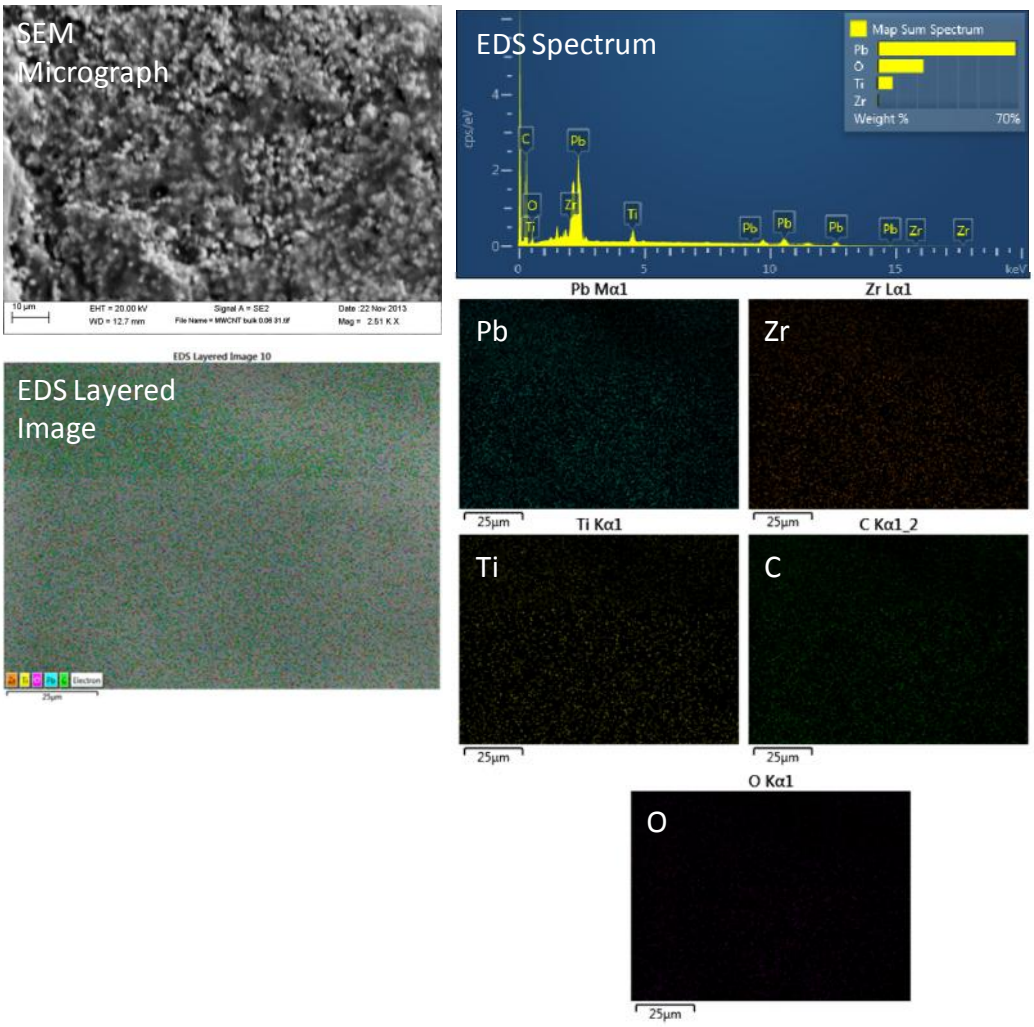

Figure 4.5 The SEM micrograph of the fractured surface of a bulk composite, shows the distribution of PZT clusters and MWCNT agglomerations embedded in the epoxy matrix with a MWCNT volume fraction of 0.06 (6%). The dispersion is also shown by the EDS layered image similar to that of Figures 4.4 and 4.5. The EDS spectrum also shows the peaks for the selective elemental analysis.

4.2 SEM, TEM micrograph and EDS spectrum analysis of three phase PZT-Epoxy-MWCNT flexible thick film composites

A MWCNT volume fraction of 0.06 (6%) is chosen for the TEM micrograph analysis. The morphology of the MWCNT inclusions embedded in the PZT-Epoxy-

MWCNT thick films is observed. A sample region of the three phase thick film with a MWCNT volume fraction of 0.06 (6%) seen in the TEM as shown in Figure 4.6 A and B. The diffraction pattern shows the presence of the polycrystalline PZT inclusions and the MWCNTs embedded in the Epoxy matrix. Similar to the bulk composites the PZT particles are not visible in the micrograph at such high magnifications of the TEM due to their particle size. The MWCNT inclusions also appear to be twisted and curled due the stresses developed during the sol-gel mixing process and the spin coating process.

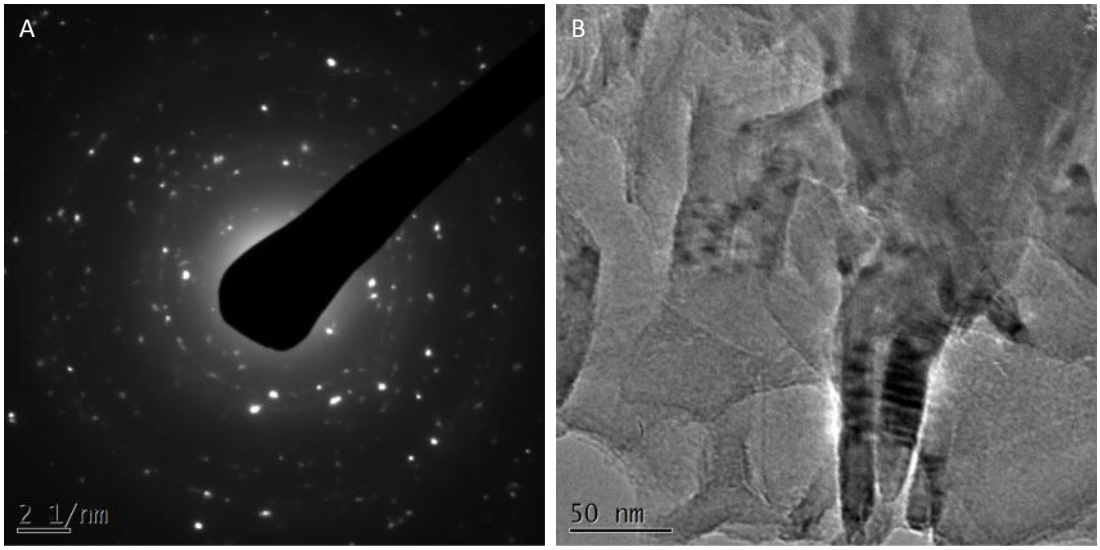

Figure 4.6 A) Diffraction pattern of the PZT-Epoxy-MWCNT thick film composite with a MWCNT volume fraction of 0.06 (6%) showing rings and spots similar to Figures 4.1 and 4.2. B) TEM micrograph of the composite thick film shows three MWCNTs embedded in the Epoxy matrix.

The three phase PZT-Epoxy-MWCNT thick film with MWCNT volume fractions of 4 and 6% are shown Figure 4.7 A and B. The figure shows the composite thick film spin coated over a flexible stainless substrate. SEM micrographs of the fractured surfaces of the composite thick films are shown in Figure 4.7 C and D. The PZT clusters and cloud shaped clusters of MWCNTs are seen distributed in the epoxy matrix. As observed

from the image analysis from ImageJ, the MWCNT clusters range in sizes < 2 μm with an average cluster size of ~ 600 nm. This is consistent with the MWCNT particle cluster size after sonication as seen from Chapter 2 in design of experiments. On the other hand the PZT clusters are > 2 μm with an average cluster of around 12 μm.

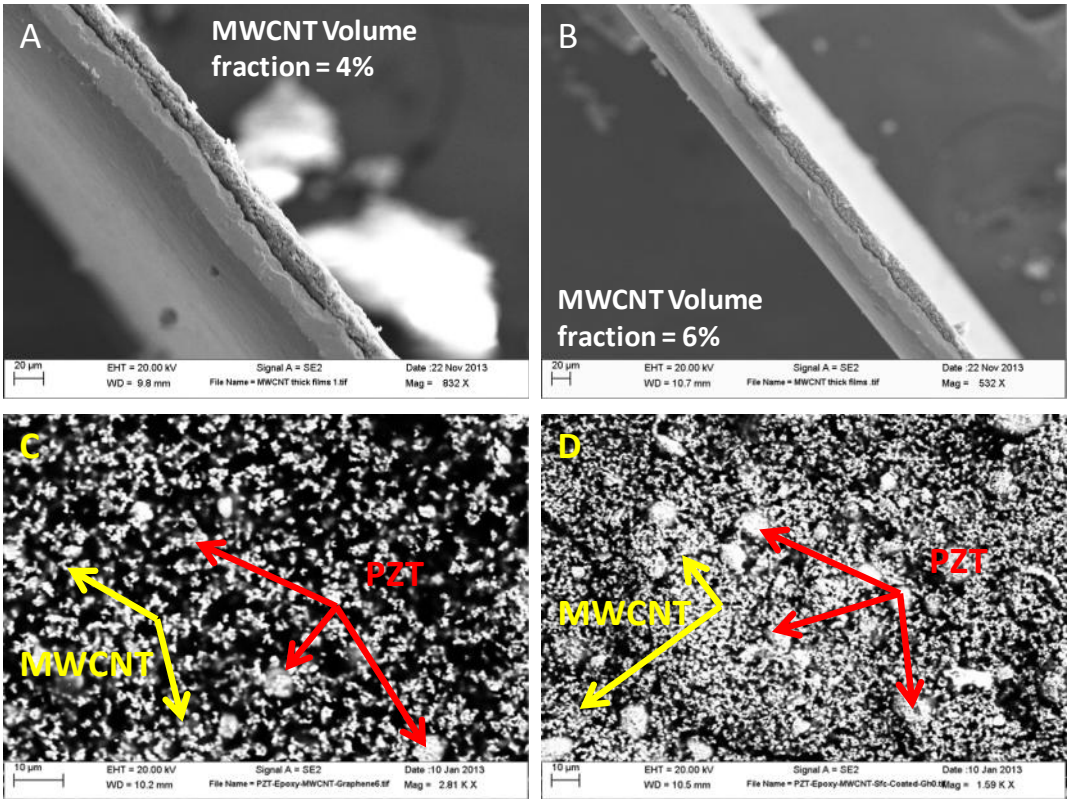

Figure 4.7 Cross-sectional SEM micrograph of a PZT-Epoxy-MWCNT thick film with MWCNT volume fractions of A) 0.04 (4%) and B) 0.06 (6%) showing the thick film of thickness ~ 150 μm spin coated over a flexible stainless substrate of thickness 20 μm. C) and D) shows the SEM micrographs of the fractured surface of the three phase composite with MWCNT volume fractions of 0.04 (4%) and 0.06 (6%). They show the distribution of the PZT clusters and MWCNT clusters in the Epoxy matrix.

Figures 4.8 and 4.9 show the SEM micrograph and EDS spectroscopy of the PZT-Epoxy-MWCNT thick film fractured surface and the top surface respectively. The fractured surface shows the distribution of the PZT and MWCNT clusters in the Epoxy matrix

similar to that of the bulk composites. The EDS elemental analysis and the layered image of the top surface of the thick film shows a uniform distribution of the different phases on the surface. An image analysis in ImageJ shows that the average PZT particle size in the fractured surface and on the top surface are ~ 10 μm and 11 μm respectively. The average MWCNT cluster size is ~ 650 nm at the fractured surface and ~ 550 nm at the top surface of the thick film. This might be due to the presence of a higher viscosity sol-gel (containing larger clusters of MWCNTs) closes to the substrate surface as compared to the top surface of the thick film during the spin coating process. As analyzed by InageJ, the PZT cluster sizes are > 2 μm and that of the MWCNTs are < 2 μm.

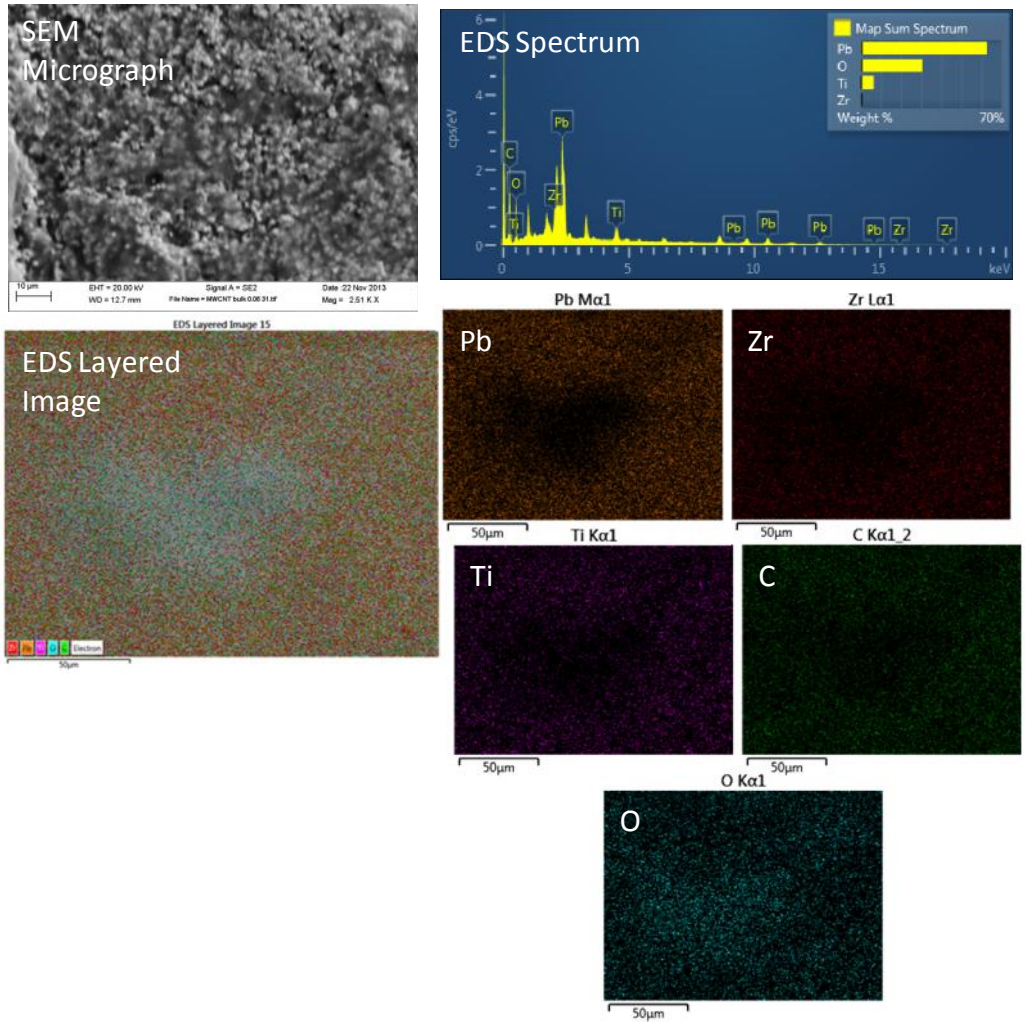

Figure 4.8 The SEM micrograph of the fractured surface of the flexible composite thick film, shows the distribution of PZT clusters and MWCNT agglomerations embedded in the epoxy matrix with a MWCNT volume fraction of 0.06 (6%). The EDS layered image also shows the dispersion of the different elements present in the composite. The peaks for the selective elemental analysis are shown in the EDS spectrum.

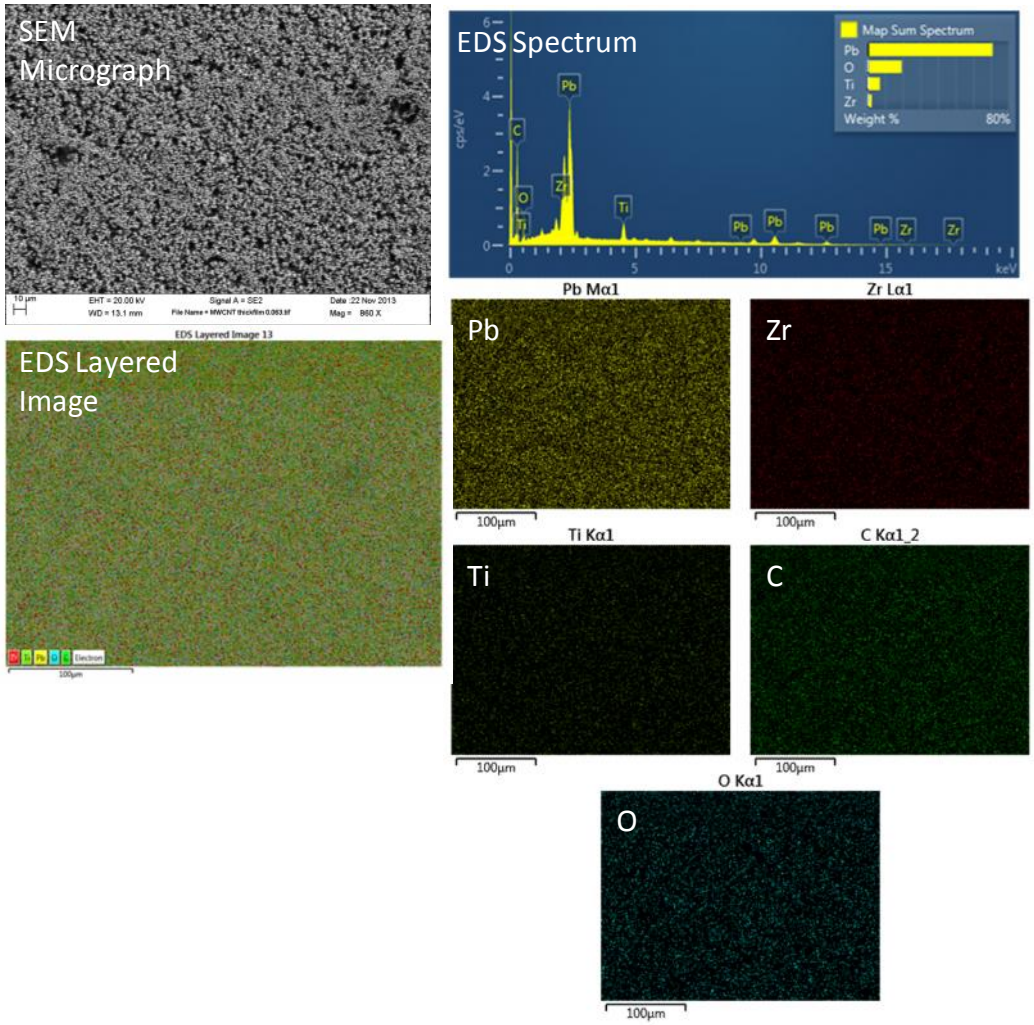

Figure 4.9 The SEM micrograph of the surface of the flexible composite thick film, shows the distribution of PZT particles and MWCNTs in the epoxy matrix with a MWCNT volume fraction of 0.06 (6%). The EDS layered image also shows the dispersion of the different elements present in the composite. The peaks for the selective elemental analysis are shown in the EDS spectrum.

4.3 Piezoelectric and dielectric characteristics of bulk PZT-Epoxy-MWCNT composites

The piezoelectric and dielectric characteristics of the bulk three phase PZT-Epoxy-MWCNT composites are presented in this section. The material properties are tested using a Piezometer and a HP4194A impedance analyzer. The composites are poled by using either the contact or the corona poling methods.

4.3.1 Contact poled bulk PZT-Epoxy-MWCNT composites

The strain coefficient, d33, loss factor, tan (δ) and the dielectric constant ε are measured using a Piezo Meter System manufactured by Piezo Test, Piezoelectric Materials & Device Testing Company and the HP4194 A impedance analysis system. Figure 4.10 shows the variation of the effective dielectric constant (ε′) and the tangent of the loss angle tan (δ) of the PZT-Epoxy-MWCNT bulk composites with varying MWCNT volume fraction of 1% to 6% for contact poling and 0.1% to 10% for corona poling, and a constant PZT volume fraction of 30%, at 110 Hz poled with the contact poling method.

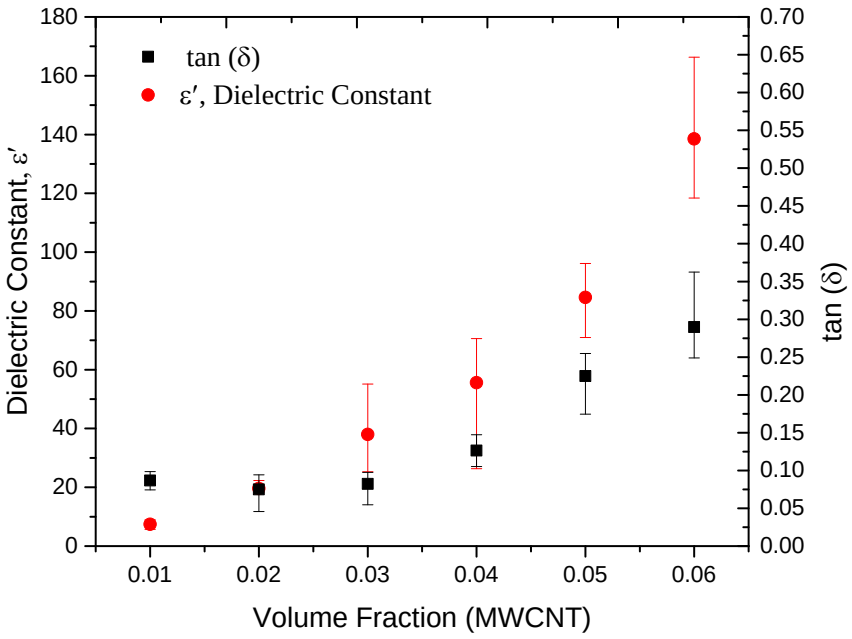

Figure 4.10 Variation of dielectric constant (ε′) and tan (δ) of three phase PZT-Epoxy-MWCNT bulk composites poled with a contact poling method; as a function of the MWCNT volume fraction at 110 Hz. Both the ε and the tan (δ) increase with increasing MWCNT volume fraction.

Both the ε′ and the tan (δ) values of the composite increase with an increase in the volume fraction of the MWCNT inclusions. For example for an increase in MWCNT volume fraction from 2% to 5% the ε increases from ~ 40 to ~70 and the tan (δ) ~ 0.07 to ~ 0.22.

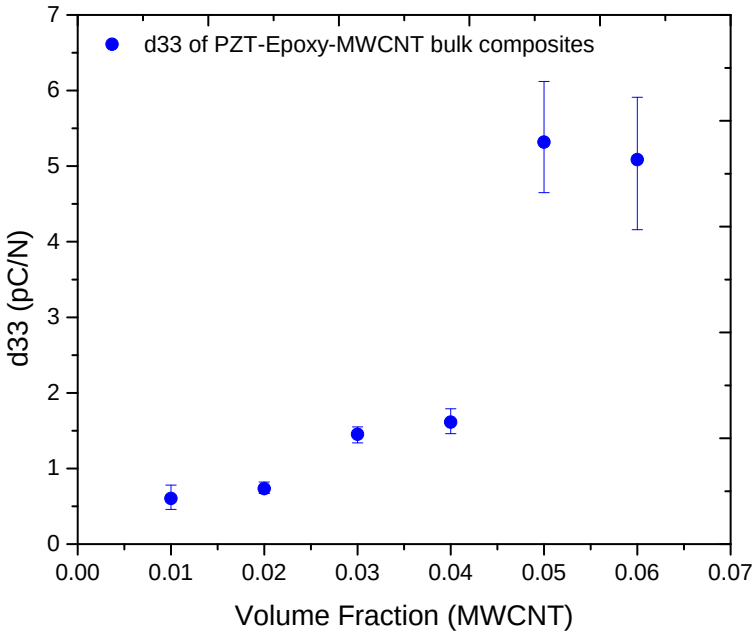

Figure 4.11 Variation of the piezoelectric strain coefficient, d33 of three phase PZT-Epoxy-MWCNT bulk composites with contact poling, as a function of the MWCNT volume fraction measured at a frequency of 110 Hz and an applied force of 0.25N. The d33 coefficient increases with an increase in the MWCNT volume fraction from 1% to 5 %, below the percolation threshold.

A similar trend is observed for the piezoelectric strain coefficient (d33) of the composite as shown in Figure 4.11. The strain coefficient is an important parameter which is a function of the effective dipole moment in the direction of the energy generation under an applied mechanical deformation. For an increase in MWCNT volume fraction from 2% to 5% the d33 increases from ~ 0.7 to ~ 5.3 pC/N. The enhanced d33, ε' and tan (δ) of the three phase PZT-Epoxy-MWCNT with the increase in MWCNT volume fraction can be attributed to the role of MWCNTs in enhanced transport of electrons and the formation of conductive pathways [15] due to electron hopping.

However, a decrease in the d33 value from ~ 5.3 to ~5.08 pC/N is also observed for a change in the MWCNT volume fraction from 5% to 6%. This decrease in the d33 values is coupled with a sharp rise in the ε and tan (δ) values from ~84 and 0.22 to ~138 and 0.28 with a change in the MWCNT volume fraction from 5% to 6%. This can be attributed to the role of MWCNTs in the formation of localized agglomeration clusters leading to the formation of conductive pathways favorable to electrical percolation by means of electron tunneling between the percolation clusters.

Compared to a contact poled PZT-Epoxy two phase composite with ε′ ~ 8.64 all the values of dielectric constant are enhanced for all MWCNT volume fractions of the three phase composite (ε′ ~ 14 for a MWCNT volume fraction of 1%). The tan (δ) values (for MWCNT volume fraction of 1%, tan (δ) ~ 0.08) also increase when compared to the two phase composite (tan (δ) ~ 0.0060). A similar trend is also observed with the d33 coefficient. The d33 for a three phase PZT-Epoxy-MWCNT composite (d33 ~ 0.60 pC/N for a MWCNT volume fraction of 1%) is also enhanced when compared to a two phase composite (d33 ~ 0.2 pC/N). The increase in the ε′ and the d33 values can be attributed to the increase in charge carriers due to the addition of MWCNTs. On the other hand the MWCNT inclusions in the epoxy matrix also increase the conductivity of the composite causing a rise in the dielectric loss [21]. Hence the three phase composite has higher values of tan (δ) as compared to the two phase composite.

4.3.2 Corona discharge poled bulk PZT-Epoxy-MWCNT composites

In Figure 4.12 the ε′ and tan (δ) values of the PZT-Epoxy-MWCNT composite with corona discharge poling are plotted as a function of increasing values of MWCNT

volume fraction. The volume fraction in this case is varied is varied from 0.1% to 10% to locate the region of percolation threshold. The values of ε′ and tan (δ) increases with increasing volume fraction of MWCNTs showing a similar trend to the contact poled samples. For example the ε′ increases from a value of ~ 54 to ~ 249 for a change in MWCNT volume fraction from 2% to 6%. This trend is also visible in MWCNT volume fractions lower than that of 1%. A change in MWCNT volume fraction from 0.1% to 0.9% increases the ε of the composite from ~ 14 to ~46. A similar trend is seen for the tan (δ) values. For example the tan (δ) increases from ~ 0.09 to ~ 0.20 for a change in MWCNT volume fraction from 2% to 5%.

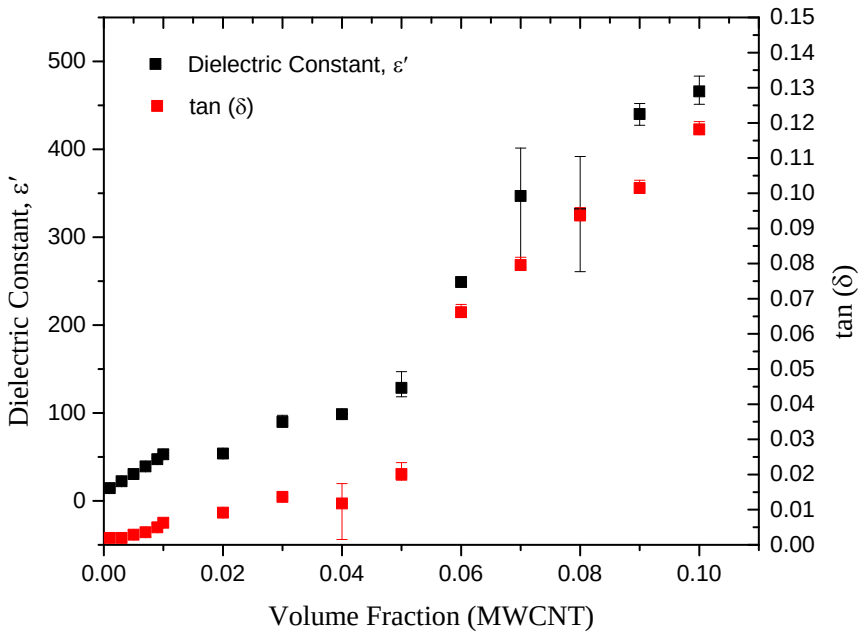

Figure 4.12 Variation of dielectric constant (ε′), and tan (δ) of three phase PZT-Epoxy-MWCNT bulk composites poled with a corona discharge poling method; as a function of the MWCNT volume fraction at 110 Hz. Both the ε and the tan (δ) increase with increasing MWCNT volume fraction from 0.1% to 10%. A sharp jump in both ε and the tan (δ) is observed after a MWCNT volume fraction of 6%.

The d33 values of the three phase composite are plotted as a function of the MWCNT volume fraction as shown in Figure 4.13. For a change in MWCNT volume fraction from 2% to 5% the d33 coefficients increase from ~ 12 to ~ 18 pC/N. Even below MWCNT volume fractions of 1% (the d33 changes from ~ 2 to ~ 10 pC/N for MWCNT volume fractions of 0.1% and 0.9% respectively) the same trend is observed.

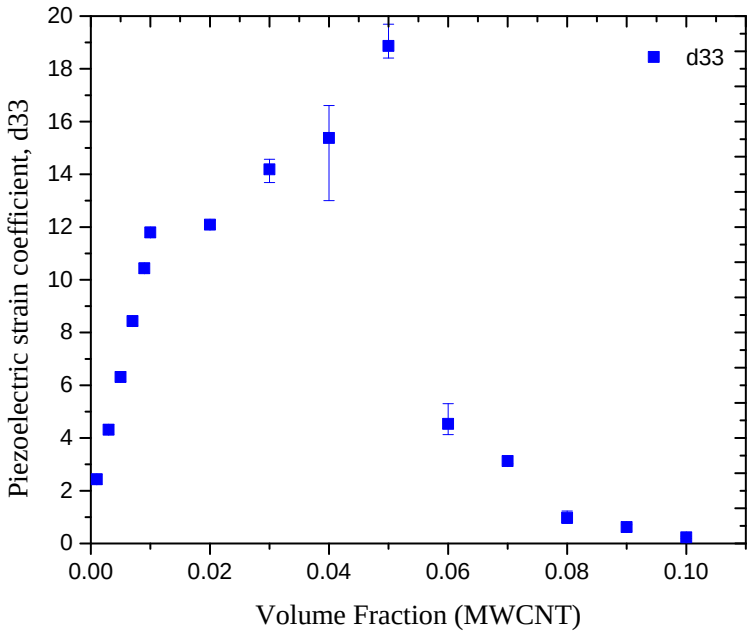

Figure 4.13 Variation of the piezoelectric strain coefficient, d33 of three phase PZT-Epoxy-MWCNT bulk composites with corona discharge poling, as a function of the MWCNT volume fraction measured at a frequency of 110 Hz and an applied force of 0.25N. The d33 coefficient increases with an increase in the MWCNT volume fraction from 1% to 5 %, below the percolation threshold. There is a sharp drop in the d33 value when the MWCNT volume fraction changes from 5% to 6%.

A sharp decrease in the d33 coefficient and a sharp increase in ε′ and tan (δ) values are observed at a MWCNT volume fraction change from 5% to 6%. The d33 values change from ~ 18 pC/N to ~ 4 pC/N and the ε′ and tan (δ) values increase from

~128 and 0.02 to ~ 248 and ~ 0.06 for a MWCNT volume fraction increase from 5% to 6%. The d33 values further decrease to ~ 3, .97 and 0.62 pC/N for MWCNT volume fractions of 7, 8 and 9% respectively. This change in the dielectric and piezoelectric coefficients correspond to the sharp rise in conductivity due to the increase in the number of localized MWCNT percolation clusters which leads to formations of conductive pathways due to electron tunneling and direct contact [36]. This change in the material properties takes place around a MWCNT volume fraction of about 5-6% and the number of these conductive pathways increase with further increase in the MWCNT volume fraction in the composite.

As described in the introduction different aspects of the polarization of three phase composites has been investigated here. Two types of composite polarization methods have been used, namely, the contact poling method and the corona poling methods. Based on the results obtained above for the piezoelectric strain coefficient, d33, the dielectric constant, ε', and the tangent of the loss angle, tan (δ), the corona poling method is seen to be the more effective one. For example for a MWCNT volume fraction of 5% the d33 coefficients for contact and corona poling are ~ 5 and ~ 18 pC/N. The d33 coefficient is enhanced to more than three times by the use of the corona poling method. For volume fractions of the MWCNT inclusions from 1% to 5% the d33 coefficients for the corona poling are 3 to 12 times higher than that of the values from contact poling. In the case of the ε and tan (δ), for a MWCNT volume fraction of 5% the contact poling and corona poling values are (ε' ~ 84, tan (δ) ~ 0.2) and (ε' ~ 128 and tan (δ) ~ 0.02). This trend is similar for all volume fractions of the MWCNTs. The enhanced values of the d33 and ε', and lower values of tan (δ) can be attributed to formation of localized spots and

regions of dielectric breakdown in the three phase composite. These localized regions increase the conductivity of the composites which leads to high dielectric loss as indicated by the higher values of tan (δ) for the contact poled composites [14, 50]. The next section will investigate the effect of variation in MWCNT volume fraction and the effects of contact and corona poling in PZT-Epoxy-MWCNT thick film composites.

4.4 Piezoelectric and dielectric characteristics of flexible composite PZT-Epoxy-MWCNT thick films

The piezoelectric and dielectric characteristics of the three phase PZT-Epoxy-MWCNT thick film composites are presented in this section. The material properties are tested using a Piezometer and a HP4194A impedance analyzer. The thick films are poled by using either the contact or the corona poling methods. The thick films are studied to investigate the effect of the microstructure and the influence of the different phases on the effective properties of the composite at a different length scale as compared to the bulk composites.

4.4.1 Contact poled PZT-Epoxy-MWCNT composite thick films

The capacitance and effective dielectric constant of the three phase PZT-Epoxy-MWCNT micron-sized films with contact poling are plotted as a function of MWCNT volume fraction in Figure 4.14 A, where the volume fraction of PZT is held constant at 30% volume fraction. The capacitance and the dielectric constant of the thick films increase with the increase in the volume fraction of the MWCNT inclusions. For example, the dielectric constant and capacitance are C~ 3pF, $\varepsilon' \sim 39$ and C ~5pF, $\varepsilon' \sim 61$ for MWCNT volume fractions of 1% and 5% respectively. The tan (δ) of the composite

is plotted as a function of increasing MWCNT volume fraction as shown in Figure 4.14 B. The value of tan (δ) increases from ~ 0.02 to ~ 0.03 for an increase in MWCNT volume fraction from 1% to 5%. This increase in Capacitance (C), ε′ and tan (δ) and can be attributed to the higher MWCNT volume fractions which enhance the electron transport due to the formation of conductive pathways within the matrix as is seen for the bulk composites .

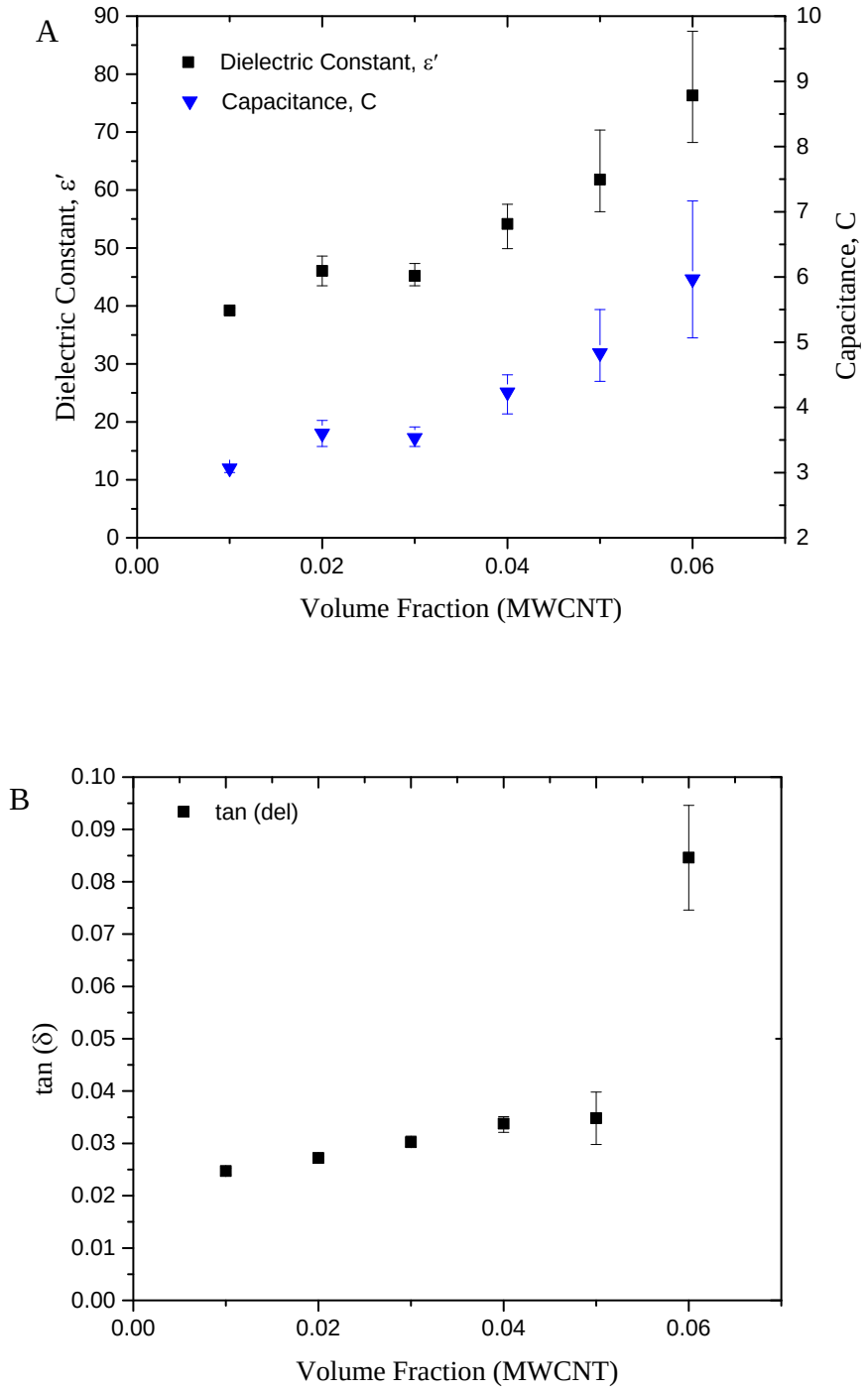

Figure 4.14 A) Capacitance (C) and Dielectric Constant (ε′) of three phase PZT-Epoxy-MWCNT thick films with contact poling, plotted with varying MWCNT volume fraction shows an enhancement in the values with an increase in the volume fraction of MWCNT

at 110 Hz. B) Tangent of the loss angle, tan (δ) of the three phase composite, increases with increasing volume fraction of MWCNTs.

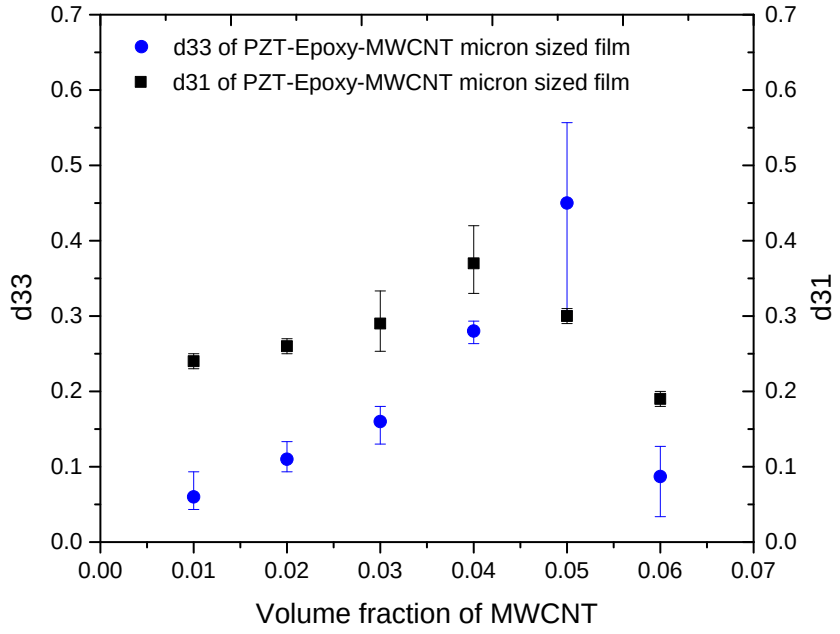

Figure 4.15 Piezoelectric Strain coefficients, d33 and d31 of three phase PZT-Epoxy-MWCNT thick films with contact poling, plotted with varying MWCNT volume fraction, shows an enhancement in the piezoelectric properties with increase in the MWCNT volume fraction at a frequency of 110 Hz and an applied force of 0.25N.

The variation of the piezoelectric strain coefficients of the micron sized composite film is shown in Figure 4.15. The strain coefficient d33 increases from 0.06 to 0.45 pC/N with an increase in MWCNT volume fraction from 1% to 5%. A similar trend is seen with d31 strain coefficient, which increases from ~ 0.24 to ~ 0.3 pC/N with an increase in MWCNT volume fraction from 1% to 4%. The increase in the piezoelectric strain coefficients (d33 and d31) with the increase in the MWCNT volume fraction can be attributed to the increase in polarization of the thick film composite due to the increased conductivity by the MWCNT inclusions.

However, the piezoelectric strain coefficients, d33 and d31 drop to d33 ~ 0.09 pC/N and d31 ~ 0.20 pC/N after the volume fraction of MWCNTs increase 6%. A sharp rise in tan (δ) from ~ 0.03 to ~ 0.08 is also observed for a change in MWCNT volume fraction from 1% to 5%. This is also coupled with a sharp jump in the C and ε′ values from C ~ 5 pF and ε′ ~ 61 to C ~ 6 pF and ε′ ~ 76. This may happen due to electron tunneling along localized conductive pathways formed by MWCNT agglomerations along the thickness of the composite thick film. This phenomenon is observed in the three phase composite micron-sized film around a MWCNT volume fraction of around 5-6%. This is also indicated by the sharp increase in the tan (δ) which is caused by a sharp rise in conductivity due to the MWCNT conductive pathways.

When compared to a contact poled PZT-Epoxy two phase composite with ε′ ~ 19.18 all the values of dielectric constant are enhanced for all MWCNT volume fractions of the three phase composite (ε′ ~ 39 for a MWCNT volume fraction of 1%). A similar trend is also observed with the d33 and d31 coefficients. The d33 and d31 for a three phase PZT-Epoxy-MWCNT composite (d33 ~ 0.03 pC/N, d31 ~ 0.22 pC/N for a MWCNT volume fraction of 1%) is also enhanced when compared to a two phase composite (d33 ~ 0.02 pC/N, d31 0.10 pC/N). Similar to the bulk composites this enhancement in the dielectric constant and piezoelectric strain coefficients are a result of the MWCNT inclusions that increases the electron transfer pathways in the composite.

4.4.2 Corona poled PZT-Epoxy-MWCNT composite thick films

Capacitance, ε′ and tan (δ) values of the PZT-Epoxy-MWCNT composite with corona discharge poling are plotted as a function of increasing values of MWCNT

volume fraction as shown in Figure 4.16 A and B. Similar to the bulk composites the volume fraction in this case is varied is varied from 0.1% to 10% to locate the region of percolation threshold.

The values of C, ε′ and tan (δ) increases with increasing volume fraction of MWCNTs. This trend is similar to the contact poled samples. For example the C and ε increase from C ~ 6 pF and ε′ ~ 70 to C ~ 9 pF and ε′ ~ 115 for a change in MWCNT volume fraction from 1% to 5%. For MWCNT volume fractions lower than that of 1% the same trend is observed. A change in MWCNT volume fraction from 0.1% to 0.9% increases the C and ε′ of the composite from C ~ 3 and ε′ ~ 50 to C ~ 5 pF and ε′ ~68. The tan (δ) values also increase with a increasing MWCNT volume fraction. For example the tan (δ) increases from ~ 0.001 to ~ 0.004 for a change in MWCNT volume fraction from 1% to 5%.

The d33 and d31 values of the corona poled three phase composite is shown in Figure 14.17. Both the strain coefficients increase with an increasing volume fraction of the MWCNTs. For a change in the MWCNT volume fraction from 1% to 5% the d33 and d31 increases from d33 ~ 6 pC/N and d31 ~ 3 pC/N to d33 ~ 11 pC/N and d31 ~ 9pC/N. A similar increase in the strain coefficient values is also observed at MWCNT volume fractions lower than that of 1%. For example an increase in MWCNT volume fraction from 0.1% to 0.9% increases the strain coefficients from d33 ~ 3 pC/N and d31 ~ 1 pC/N to d33 ~ 5 pC/N and d31 ~ 3 pC/N. Similar to the bulk and the contact poled three phase PZT-Epoxy-Composites this increase in the dielectric and piezoelectric properties are due the addition of the MWCNTs.

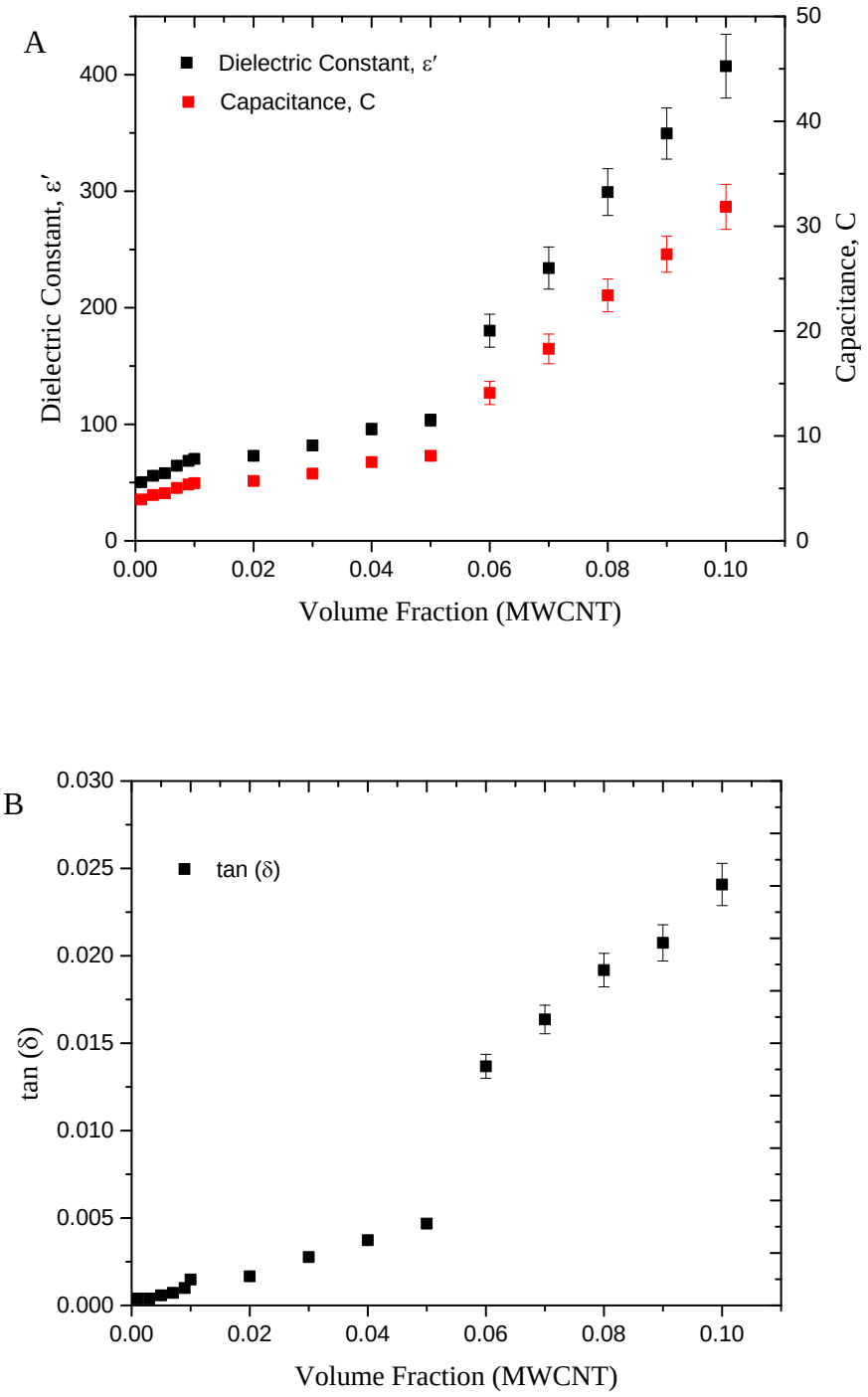

Figure 4.16 A) Capacitance (C) and Dielectric Constant (ε′) of three phase PZT-Epoxy-MWCNT thick films with corona discharge poling, plotted with varying MWCNT volume fraction shows an enhancement in the values with an increase in the volume

fraction of MWCNT at 110 Hz. B) Tangent of the loss angle, tan (δ) of the three phase composite, increases with increasing volume fraction of MWCNTs.

Following the trend from the previous samples the d33 and d31 values decrease sharply at a change of MWCNT volume fraction from 5% to 6% to d33 ~ 8 pC/N and d31 ~ 3 pC/N. The same change in MWCNT volume fraction shows a sharp increase in the C and ε′ values to C ~ 18 pF and ε′ ~ 180. These changes indicate that the location of the percolation threshold is around this region.

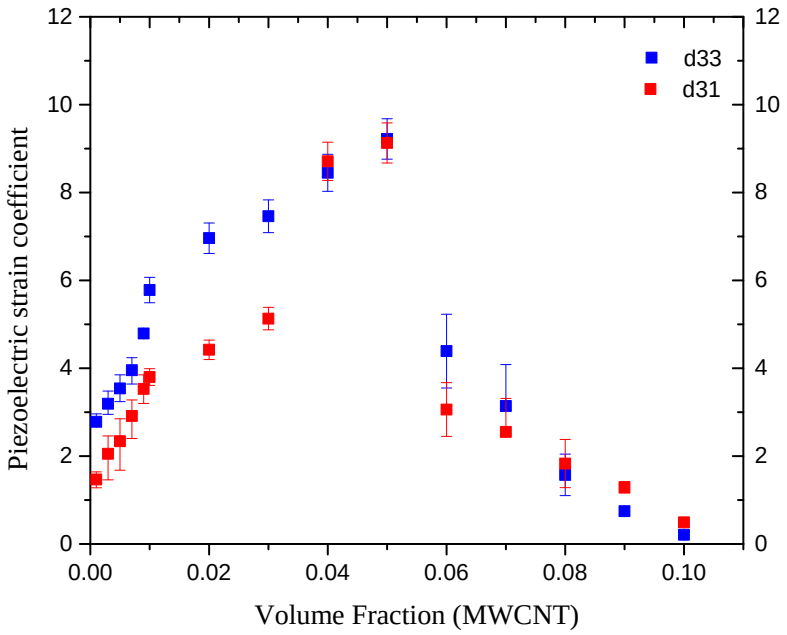

Figure 4.17 Piezoelectric Strain coefficients, d33 and d31 of three phase PZT-Epoxy-MWCNT thick films with corona discharge poling, plotted with varying MWCNT volume fraction, shows an enhancement in the piezoelectric properties with increase in the MWCNT volume fraction at a frequency of 110 Hz and an applied force of 0.25N.

As observed in the bulk composites the corona poling in the composite thick films are more effective than that of the contact poling method. This can be seen by the enhanced

values of ε, and the strain coefficients d33 and d31 for all volume fractions of MWCNT ranging from 1% to 5% (below the percolation threshold). For example for a MWCNT volume fraction of 4% the ε′, d33 and d31 for the corona poling is (ε′ ~ 96, d33 ~ 8 pC/N and d31 ~ 9 pC/N) as compared to (ε′ ~54 , d33 ~ 0.2 pC/N and d31 ~ 0.3 pC/N). The increase in the strain coefficients is due to the increase in effectiveness in poling. The ε which is also measures in the 33 direction is also enhanced due to the increase in the number of the dipoles aligned along the 33 direction. The tan (δ) values also decrease with corona poling as seen for a MWCNT volume fraction of 4% (tan (δ), corona ~ 0.003, tan (δ), contact ~ 0.03). Similar to the bulk composites this increase in the value of tan (δ) is attributed to the defects caused by localized dielectric breakdown by the corona poling.

4.5 Conductivity measurements of corona and contact poled bulk and thick film composites

The conductivity values for the bulk and thick film composites are shown in Figures 4.18 A and B for corona and contact poled composites respectively. The conductivity increases with an increase in the MWCNT volume fraction due to the increase in the formation of conductive pathways in the composite and electron transport through electron tunneling in the composites. In figure 4.18 A for a change in MWCNT volume fraction from 5-6% the conductivity shows a sharp rise in value from 0.17 -0.69 μS/m and from 0.10-0.77 μS/m for the bulk and thick films respectively.

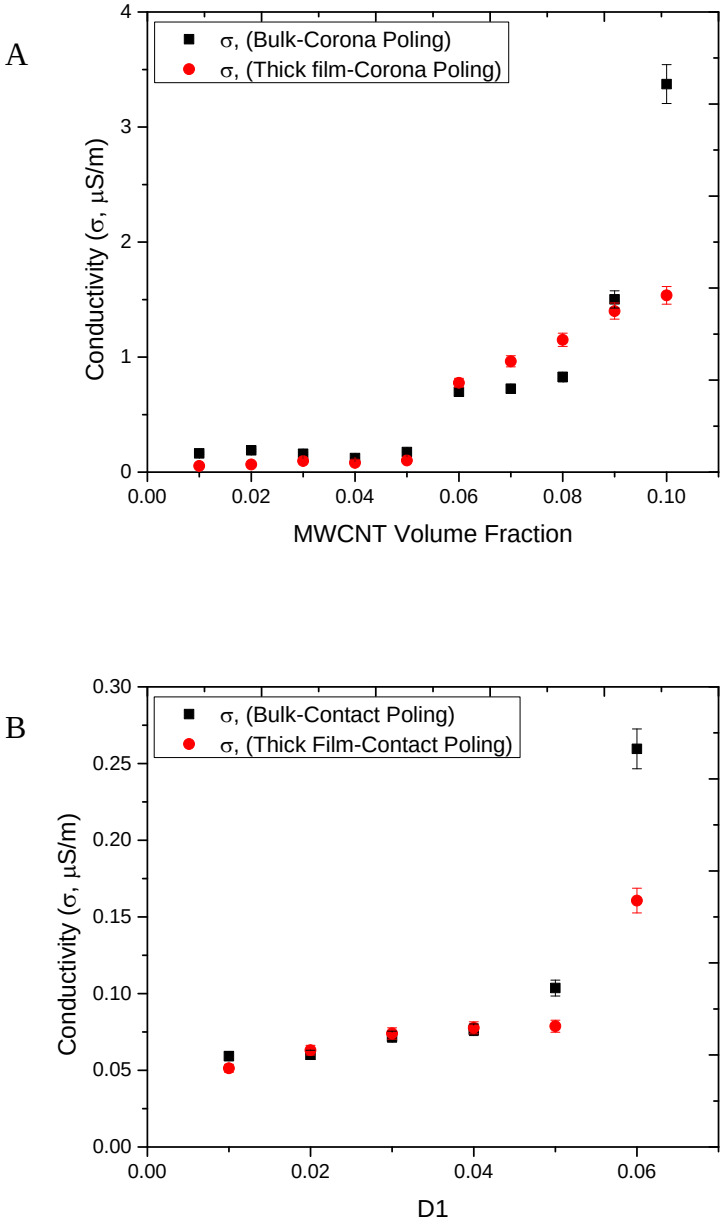

Figure 4.18 Conductivity measurements at 2 kHz for A) Corona poled and B) Contact poled bulk and thick film composites show a sharp rise in the values around a MWCNT volume fraction change from 5-6 % which is predicted to be the region of percolation threshold from the previous piezoelectric and dielectric characteristics of the composites.

A similar increase in the conductivity values are also seen for the contact poled composites. For a change in the MWCNT volume fraction from 5-6% the conductivity

changes from 0.10 – 0.25 μS/m and 0.0.07-0.16 μS/m for the bulk and thick film composites, as shown in Figure 4.18. This sharp rise in the conductivity values indicates that both the bulk and thick film composites reach the percolation threshold around a MWCNT volume fraction of 5-6%.

The bulk and thick film PZT-Epoxy-MWCNT composites show an increase in the dielectric constant and the piezoelectric strain coefficients with an increase in the volume fraction of the MWCNT inclusions below the percolation limit. In the region of the percolation threshold a sharp increase in the dielectric constant and the dielectric loss is observed due the formation of percolation pathways in the composites. Also, the conductivity of the composites rise sharply around the percolation threshold. A comparison of piezoelectric and dielectric properties based on corona and contact poling show that the corona discharge poling is more efficient than the contact poling method. The next chapter discusses the dielectric and impedance spectroscopy of the bulk and thick film composites to investigate the performance of these composites at variable frequencies.

Chapter 5

Impedance and dielectric spectroscopy of the three phase PZT-Epoxy-MWCNT thick films

Impedance spectroscopy is a powerful non-destructive technique to study the relationship between the microstructure and the electrical properties of the material. In a heterogeneous system like the PZT-Epoxy-MWCNT composites, impedance and dielectric spectroscopy can help us understand the performance of the composites over a frequency range and the mechanisms of electron transport, variation in resistance and the conductivity as a function of the volume fraction of the MWCNTs. This section investigates the conductive and dielectric properties of the PZT-Epoxy-MWCNT composites that have been poling using the corona or contact poling method. The electrical and dialectic properties are represented by the complex impedance and the complex permittivity (the dielectric constant, ε' and tan (δ)) of the three phase composites.

5.1 Impedance spectroscopy of three phase PZT-Epoxy-MWCNT bulk composites characterized by corona and contact poling methods

The impedance characteristics of the bulk composites with a variation in the MWCNT volume fraction from 1% to 10% and as a function of the frequency from 100Hz to 20 MHz is shown in Figure 5.1 A. The nominal sample thickness is 6mm. The plot shows higher values of impedance at lower frequencies. The value of impedance decreases with an increase in frequency indicating the increasing influence of the conductive MWCNT inclusions at higher frequencies. This is caused by an increase in

mobility of the conductive species at higher frequencies. Also, for the three phase PZT-Epoxy-MWCNT composites the impedance values decrease with an increase in the amount of MWCNTs; due the increase in the volume fraction of the conductive species in the composite. Figure 5.1 B shows the same impedance plot over a region of frequency varying from 2.5 – 20 MHz. The plot shows a sharp drop in the impedance values when the MWCNT volume fraction in the composite changes from 5% to 6%, indicating a sharp rise in conductivity of the composite. This trend is seen over the entire range of the frequencies. For example at a frequency of 2.5 kHz the impedance drops from ~ 1852 kΩ to 1631 kΩ for a change in the MWCNT volume fraction from 5% to 6% as compared to a drop of ~ 1990 kΩ to 1852 kΩ for a MWCNT volume fraction change of 4% to 5%. This phenomenon is consistent with the sharp drop in the piezoelectric strain coefficients and the sharp increase in the dielectric constants of the PZT-Epoxy-MWCNT bulk composites in Chapter 4 at the percolation threshold. The impedance values give us further evidence that the percolation threshold is present around this region in the case of three phase bulk composites.

Figure 5.2 and 5.3 show the impedance and phase plots of the corona poled PZT-Epoxy-MWCNT bulk composites with a varying MWCNT volume fraction from 1% to 10% and a frequency range of 100Hz-20MHz. The phase plots indicate multiple resonant modes formed due to the geometry and the microstructure of the three phase composite. For a MWCNT volume fraction of 4%, these resonant modes occur around 75 kHz, 3.2 MHz, 6.5 MHz, 7.7 MHz and 12.3 MHz.

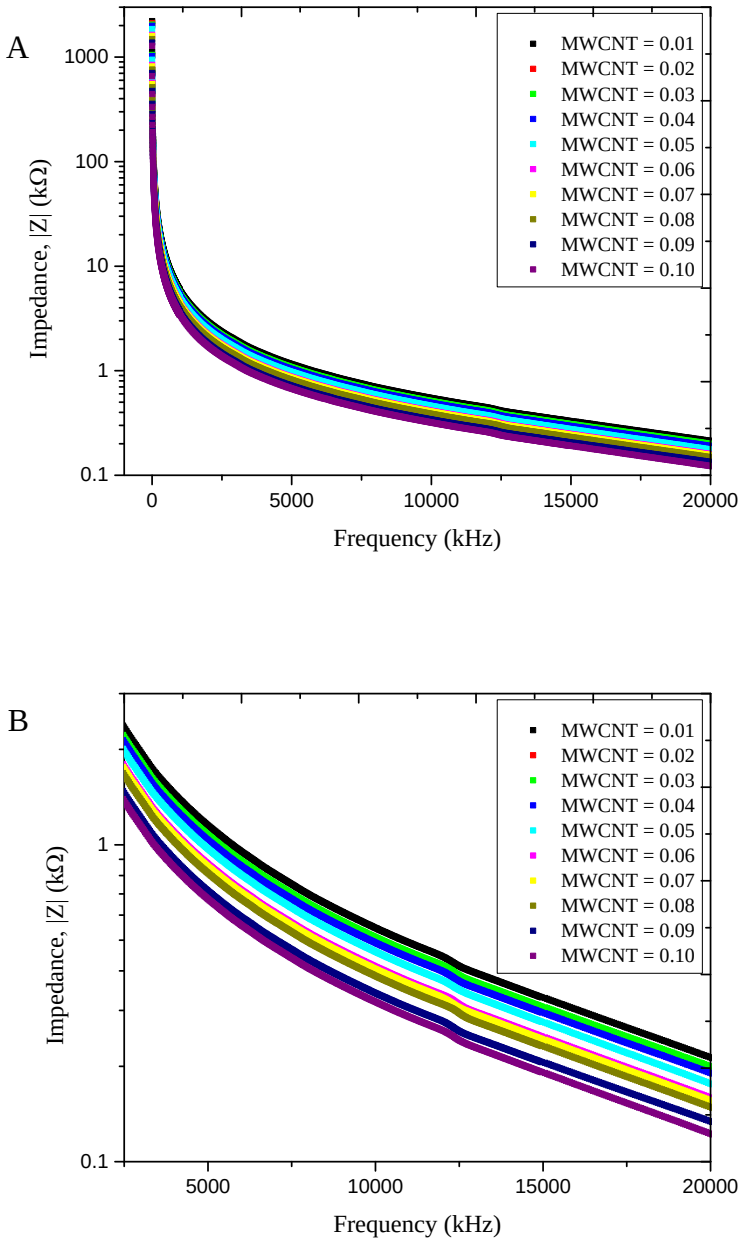

Figure 5.1 A) Impedance characteristics of the corona poled bulk PZT-Epoxy-MWCNT composites with a variation the MWCNT volume fraction from 1% to 10% and as a function of the frequency (100Hz – 20 MHz). The plot shows a decrease in the impedance with increase in MWCNT volume fraction and an increase in the frequency. B) The previous plot is shown over a frequency range of 2.5 MHz to 20 MHz. It shows a sharp drop of the impedance with a change in MWCNT volume fraction from 5% to 6%.

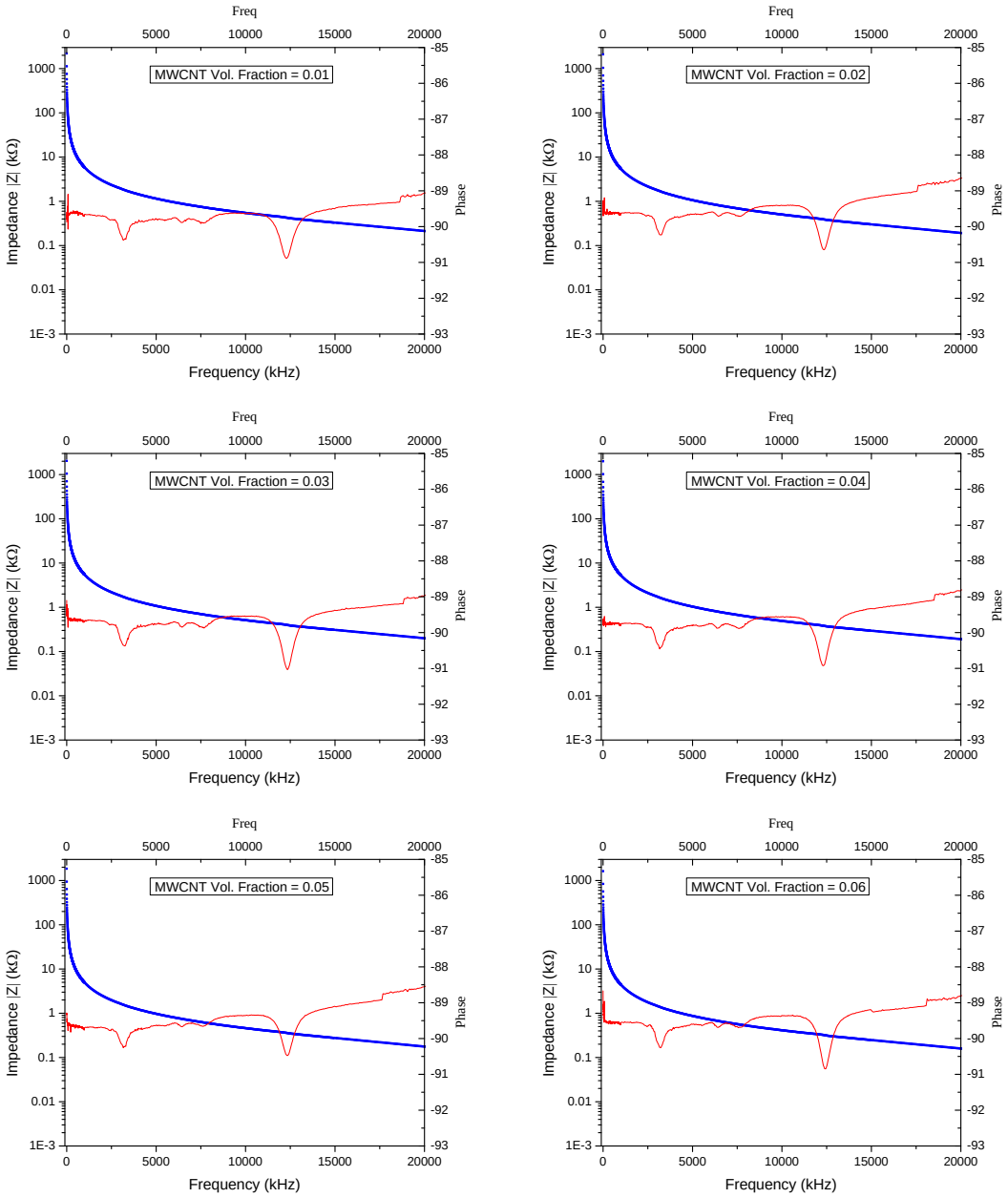

Figure 5.2 Impedance and phase diagrams of corona poled PZT-Epoxy-MWCNT bulk composites in the frequency range of 100 Hz-20MHz. The MWCNT volume fraction is varied from 0.01 (1%) – 0.06 (6%) as shown in the figures. The phase plots indicate the presence of distinct resonant modes formed due to the geometry and the microstructure of the composites.

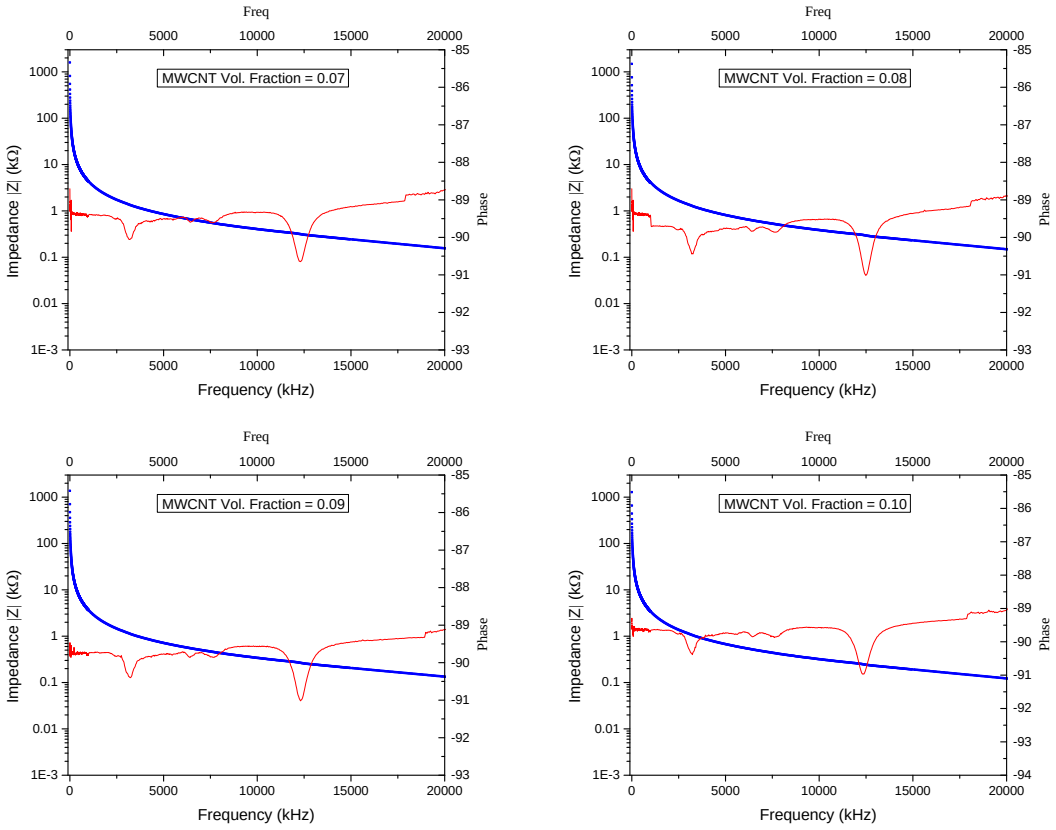

Figure 5.3 Impedance and phase plots of bulk PZT-Epoxy-MWCNT composites with corona poling and with varying MWCNT volume fraction from 0.07 (7%) – 0.10 (10%). The phase plots show distinct resonant modes similar to Figure 5.2, due to the bulk geometry and the composite microstructure of the material.

The possible sources for these modes are the resonance from the thickness of the cylindrical bulk composite, the radial mode of resonance along the surface of the composite and the resonance modes for the different phases of the composite [114, 115]. The resonant and anti-resonant peaks for the high frequency resonance mode around 12.3 MHz can also be seen in the impedance plot in Figure 5.1 B.

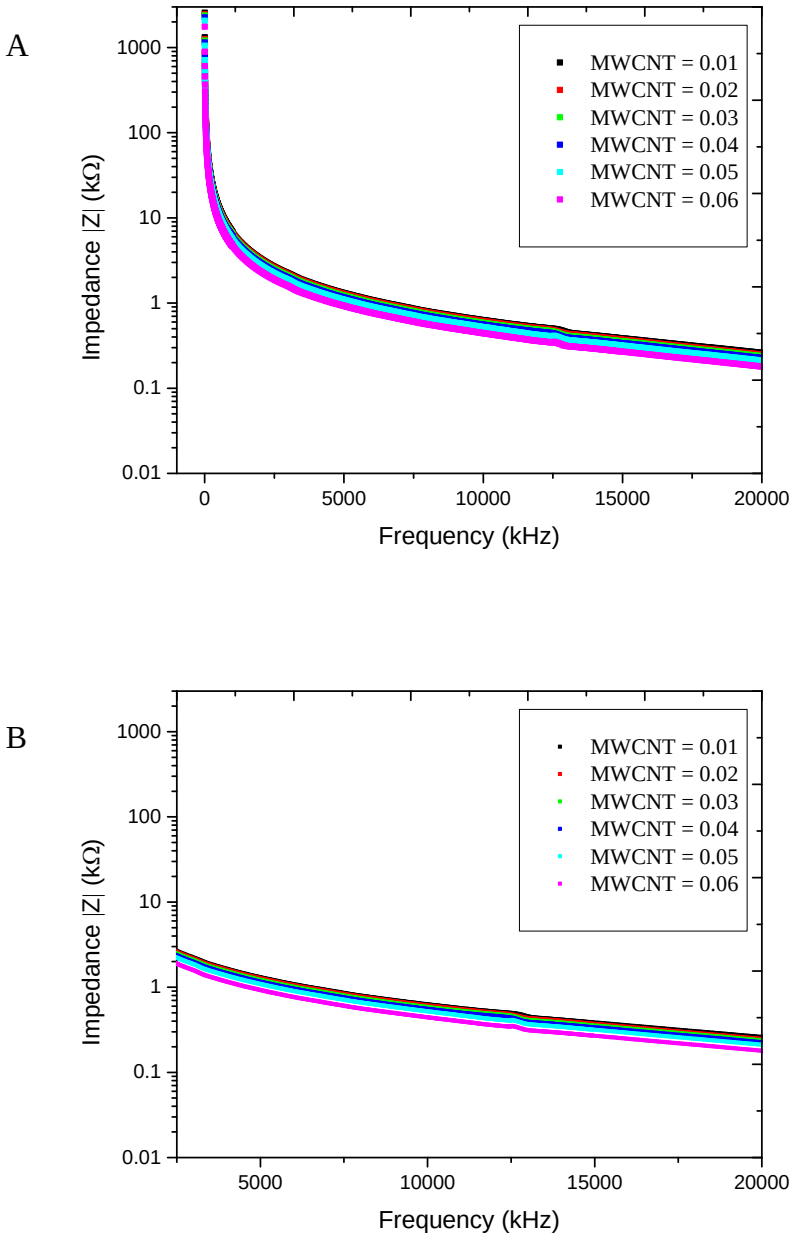

Figure 5.4 A) Impedance characteristics of the contact poled bulk PZT-Epoxy-MWCNT composite with a variation the MWCNT volume fraction from 0.01 (1%) to 0.06 (6%) as a function of the frequency (from 100Hz – 20 MHz). The impedance decreases with an increase in MWCNT volume fraction and an increase in the frequency. B) The impedance plot is shown over a frequency region of 2.5 MHz to 20 MHz. It shows a sharp drop of the impedance with a change in MWCNT volume fraction from 5% to 6%.

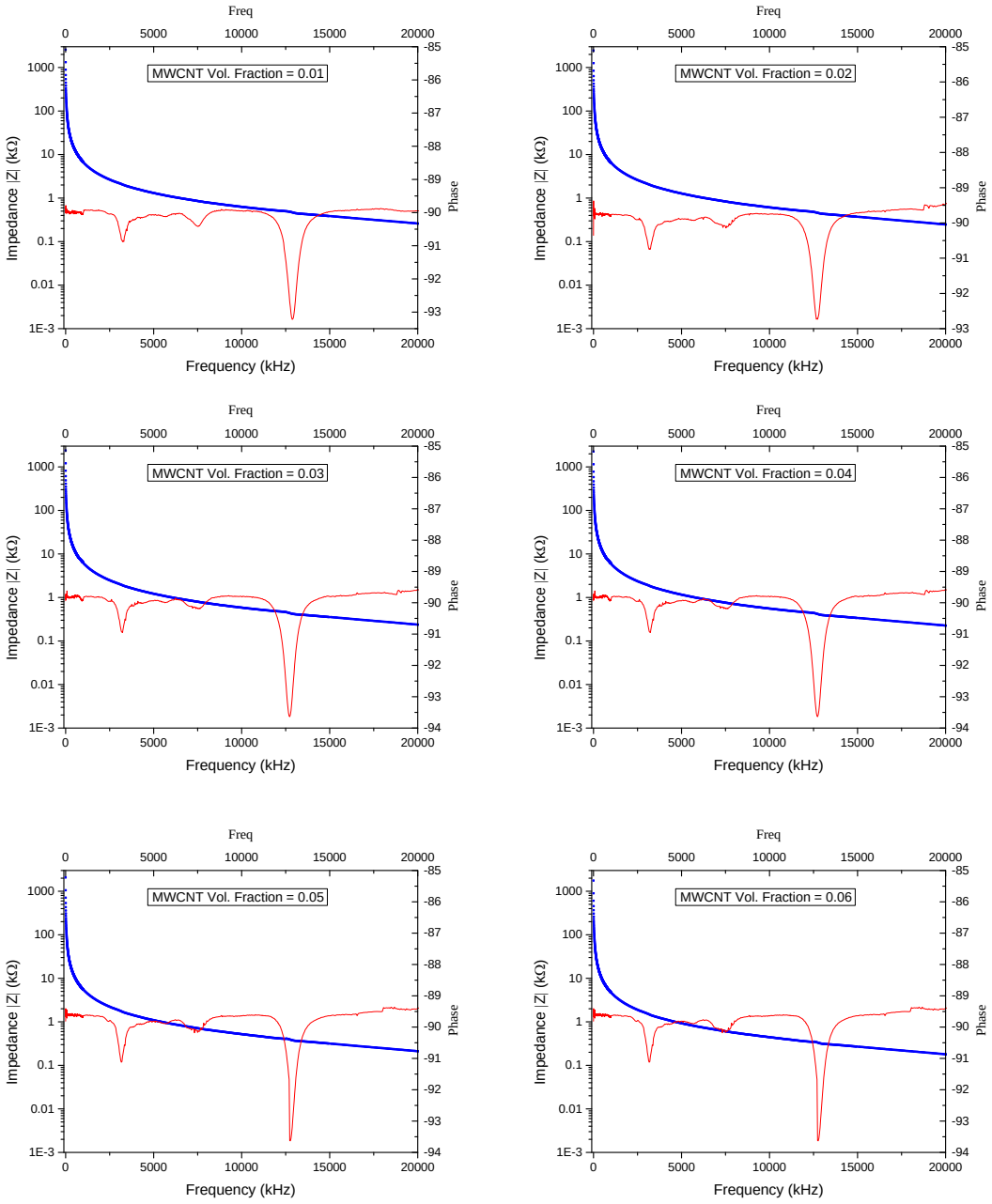

Figure 5.5 Impedance and phase plots of bulk PZT-Epoxy-MWCNT composites characterized by contact poling with varying MWCNT volume fraction from 0.01 (1%) – 0.06 (6%). The phase plots show distinct resonant modes similar to Figures 5.2 and 5.3, due to the geometry of the composite and the microstructure.

The impedance characteristics of contact poled PZT-Epoxy-MWCNT composites with variable MWCNT volume fraction (from 1% to 6%) is plotted as a function of

frequency (varying from 100 Hz-20MHz) and is shown in Figure 5.4 A. The nominal sample thickness is 6mm. Similar to the corona poled bulk composites the impedance is higher at a lower frequency and decreases with an increase in the frequency. This is due to the increased mobility of the conductive species in the composite. Also, the impedance decreases with an increase in the MWCNT volume fraction which indicates a decrease in resistance of the composite due to higher volume fraction of MWCNTs.

Figure 5.4 B shows the same plot at a frequency range of 2.5-20MHz. It shows a sharp drop in the impedance for a MWCNT volume fraction change from 5% - 6%. For example, at a frequency of 2 kHz the impedance changes from ~ 2070 -1759 kΩ with an increase in MWCNT volume fraction from 5% to 6%. The impedance and phase plots for the individual volume fractions of MWCNTs in the contact poled composites are shown in Figure 5.5. The figure show similar resonance modes as observed in the corona poled composites. For example, for a MWCNT volume fraction of 4%, these resonant modes occur around 72 kHz, 3.1 MHz, 6.7 MHz, 7.5 MHz and 12.5 MHz. The high frequency resonant and the anti-resonant peaks can also be seen around 12.5 MHz in the impedance plot in Figure 5.4 B.

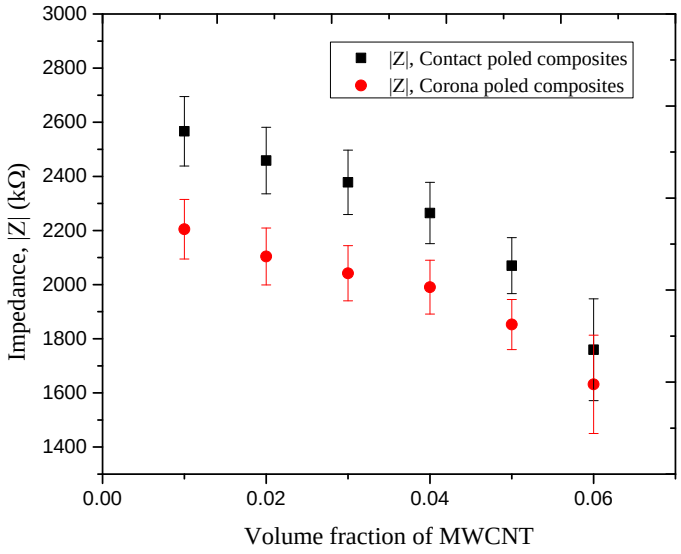

Figure 5.6 Figure showing the change in impedance for the corona and contact poled composites at a frequency of 2 kHz. The contact poled composites show a higher impedance as compared to the corona poled composites for all MWCNT volume fractions of the composite.

The impedance values for the contact poled three phase bulk PZT-Epoxy-MWCNT composites are higher than that of the corona poled composites. For example for a MWCNT volume fraction of 3% and a frequency of 2kHz the contact poled composite shows an impedance value of ~ 2377 kΩ as compared to ~ 2042 kΩ for the corona poled composite. This trend is followed for all volume fractions of the composite as shown in Figure 5.6. This difference in impedance indicates the higher resistance of contact poled composites. This can be due to a larger number of dipoles being aligned along the poling direction by the corona poling method as compared to the contact poling method i.e. due to the higher polarization density in the corona poling technique. In the contact poling technique the electrons flow through the path of least resistance (through hopping and electron tunneling) from one surface to another while in the corona poling

technique the polarized ions are distributed over the entire cross-sectional area of the sample geometry and flows from the top to the bottom surface. This causes high polarization density in the corona poling technique as opposed to the contact poling method. This is also demonstrated by the higher piezoelectric strain coefficients of the corona poled samples as shown in Chapter 4.

5.2 Dielectric spectroscopy of three phase PZT-Epoxy-MWCNT bulk composites characterized by corona and contact poling methods

Figures 5.7 A and B show the dielectric spectrum of the corona and contact poled composites respectively. The frequency range is varied from 100Hz-20MHz. For the corona poled composites the volume fraction is varied from 1-10%, and from 1-6% for the contact poled composites. Both the plots show an increase in the dielectric constant with an increase in the MWCNT volume fraction and also indicate the transition of the composites to the percolation threshold with a jump in the dielectric constant above a MWCNT volume fraction of 5%. For example below the percolation threshold, and for a MWCNT volume fraction change from 3%-4% the dielectric constant changes from ~ 88-98 for the corona poled composites and ~ 32-37 for the contact poled composites at a frequency of 2kHz. But when the volume fraction changes from 5-6% the dielectric constant jumps from ~ 124-241 and ~ 48-67 for corona and contact poling respectively. This increase in the dielectric constant is coupled with the decrease in the impedance as seen in Figures 5.1 and 5.4 and indicates the location of the percolation threshold in this region for the bulk composites. This occurs due to a sharp rise in electron hopping and

tunneling around the percolation threshold causing a rise in the conductivity of the composite.

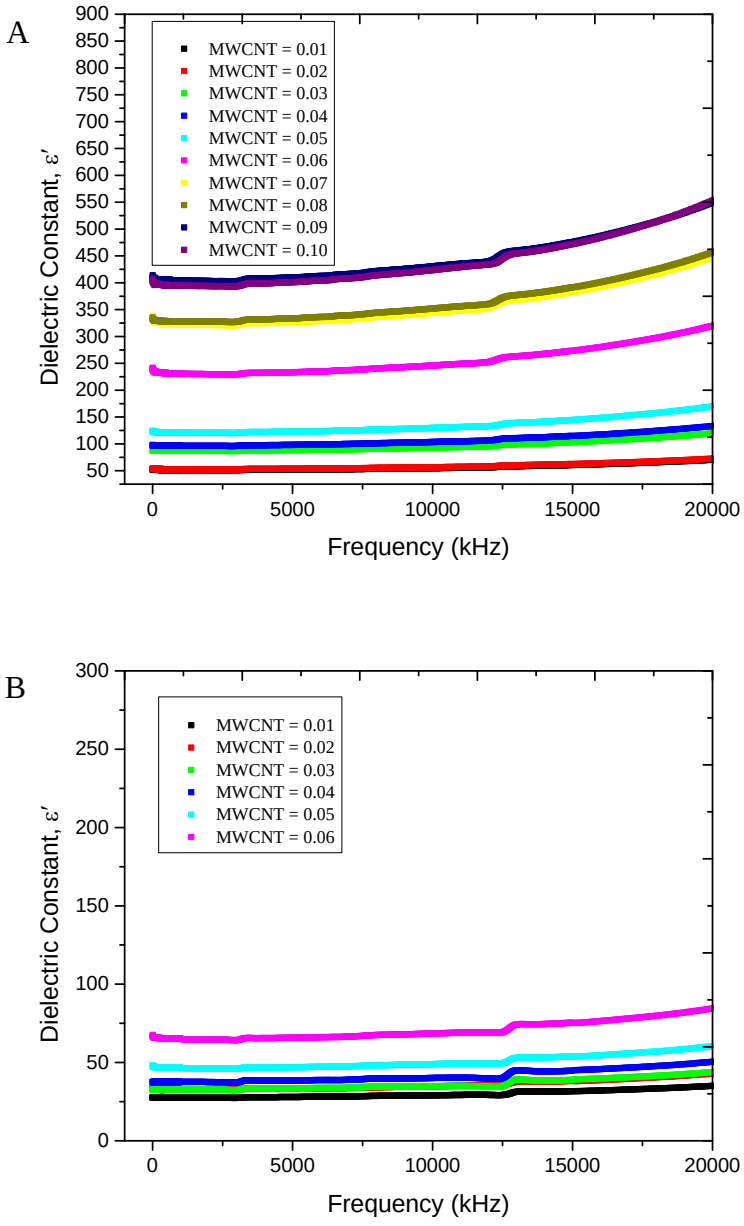

Figure 5.7 A) Dielectric spectrum of PZT-Epoxy-MWCNT bulk composites with corona discharge poling in the frequency range of 100Hz-20MHz and variable MWCNT volume fraction of 1-10%. B) Dielectric spectrum of contact poled PZT-Epoxy-MWCNT composites with a variation in MWCNT volume fraction from 1-6%. Both the plots show an increase in the dielectric constant with a variation in the MWCNT volume fraction.

The composites also show a consistent dielectric performance below 15 MHz for lower volume fractions of the composite.

For lower volume fractions of the composite below the percolation threshold (below 6% of MWCNTs), the dielectric performance of the composites show very little frequency dependence below 15 MHz. Above 15 MHz the dielectric constant values increase with increasing frequency indicating a frequency dependence due to the presence of the MWCNT inclusions which causes an increase in the mobility of the conductive species at higher frequencies. In the case of the composite with MWCNT volume fractions greater than or equal to 6%, the frequency dependence is observed over the entire range of frequencies from 100Hz-20MHz indicating a system with percolation, similar to the results shown by Yao et al and Dang et al [11, 34]. This phenomenon is also observed in Figures 5.8, 5.9 and 5.10 where the dielectric constant and tan (δ) is plotted for corona and contact poled composites with varying MWCNT volume fractions.

As observed in Figures 5.7 A and B, the dielectric constant of the contact poled composites are lower than that of the corona poled composites for all volume fractions of the MWCNTs. For example, below the percolation threshold and at MWCNT volume fractions of 1% and 3% and at a frequency of 2kHz the dielectric constant for the contact/corona poled composites are ~ 52/27 and 88/33 respectively. The lower values of the dielectric constant are also coupled with the lower values of the impedance as seen in the Figures 5.1 and 5.4. This is due to the higher poling efficiency (also indicated by the higher values of the piezoelectric strain coefficients for corona poling in Chapter4) obtained by the corona poling method with comparison to the contact poling method.

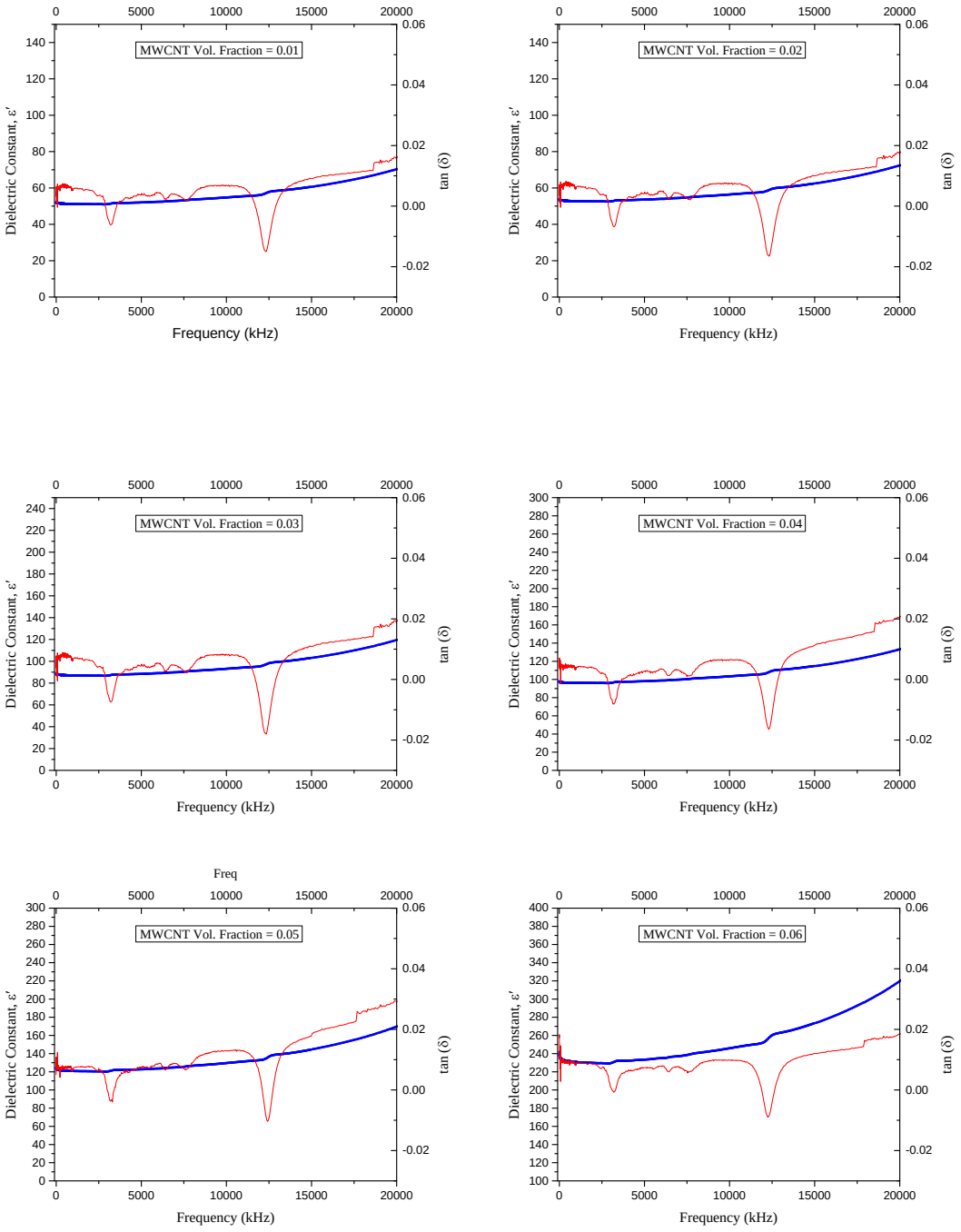

Figure 5.8 Dielectric constant, ε', and tan (δ) plots of corona poled PZT-Epoxy-MWCNT bulk composites in the frequency range of 100 Hz-20MHz. The MWCNT volume fraction is varied from 0.01 (1%) – 0.06 (6%). The tan (δ) plots indicate the presence of distinct resonant modes formed due to the geometry and the microstructure of the composites.

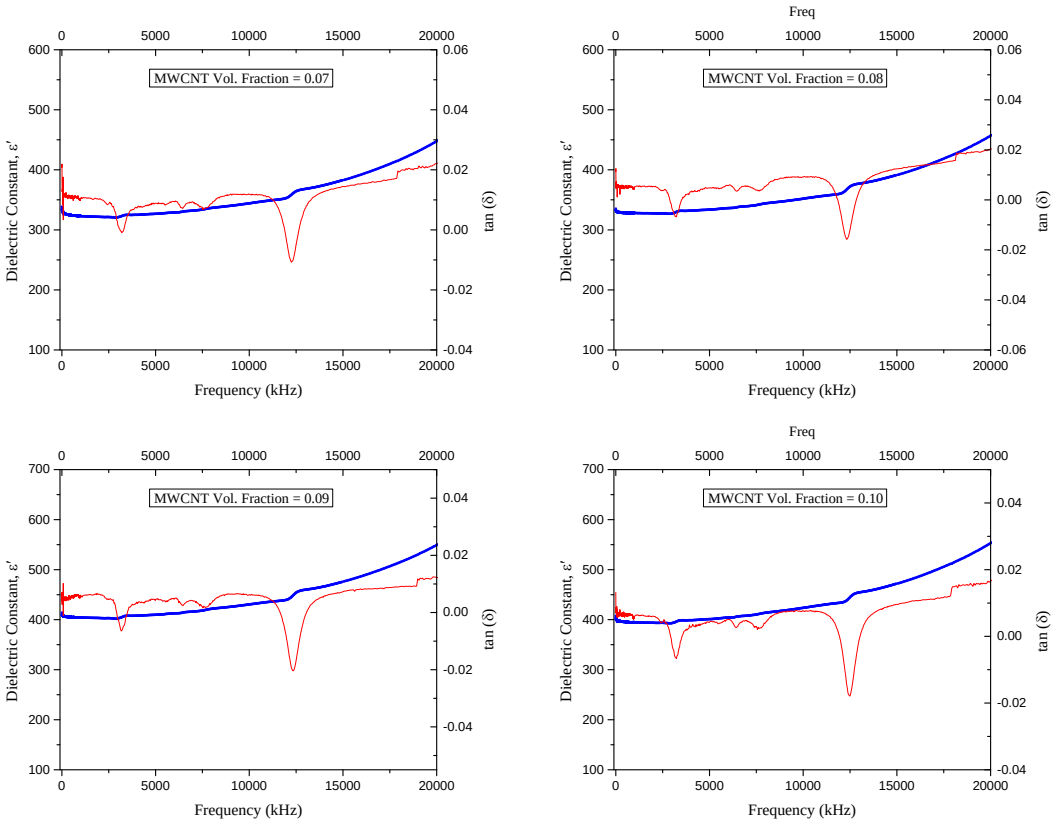

Figure 5.9 Dielectric constant, ε', and tan (δ) plots of bulk PZT-Epoxy-MWCNT composites characterized by corona poling, with varying MWCNT volume fractions from 0.07 (7%) – 0.10 (10%). The tan (δ) plots show distinct resonant modes similar to Figure 5.8, due to the bulk geometry and the composite microstructure of the material.

Figures 5.8, 5.9 and 5.10 show the dielectric constant ε' and the tangent of the loss angle, tan (δ), plotted as a function of variable frequency from 100 Hz-20MHz. The volume fraction of the composites are varied from 1-10% for the corona poled composites (as seen in Figures 5.8 and 5.9), and 1-6% for the contact poled ones. Similar to the phase plots in Figures 5.3, 5.3 and 5.5 the tan (δ) values show the presence of the resonant frequencies for the composites. In the case of the corona poled composites the resonant frequencies are around 75 kHz, 3.2 MHz, 6.5 MHz, 7.7 MHz and 12.3 MHz.

The ones for contact poling occurs around 72 kHz, 3.1 MHz, 6.7 MHz, 7.5 MHz and 12.5 MHz.

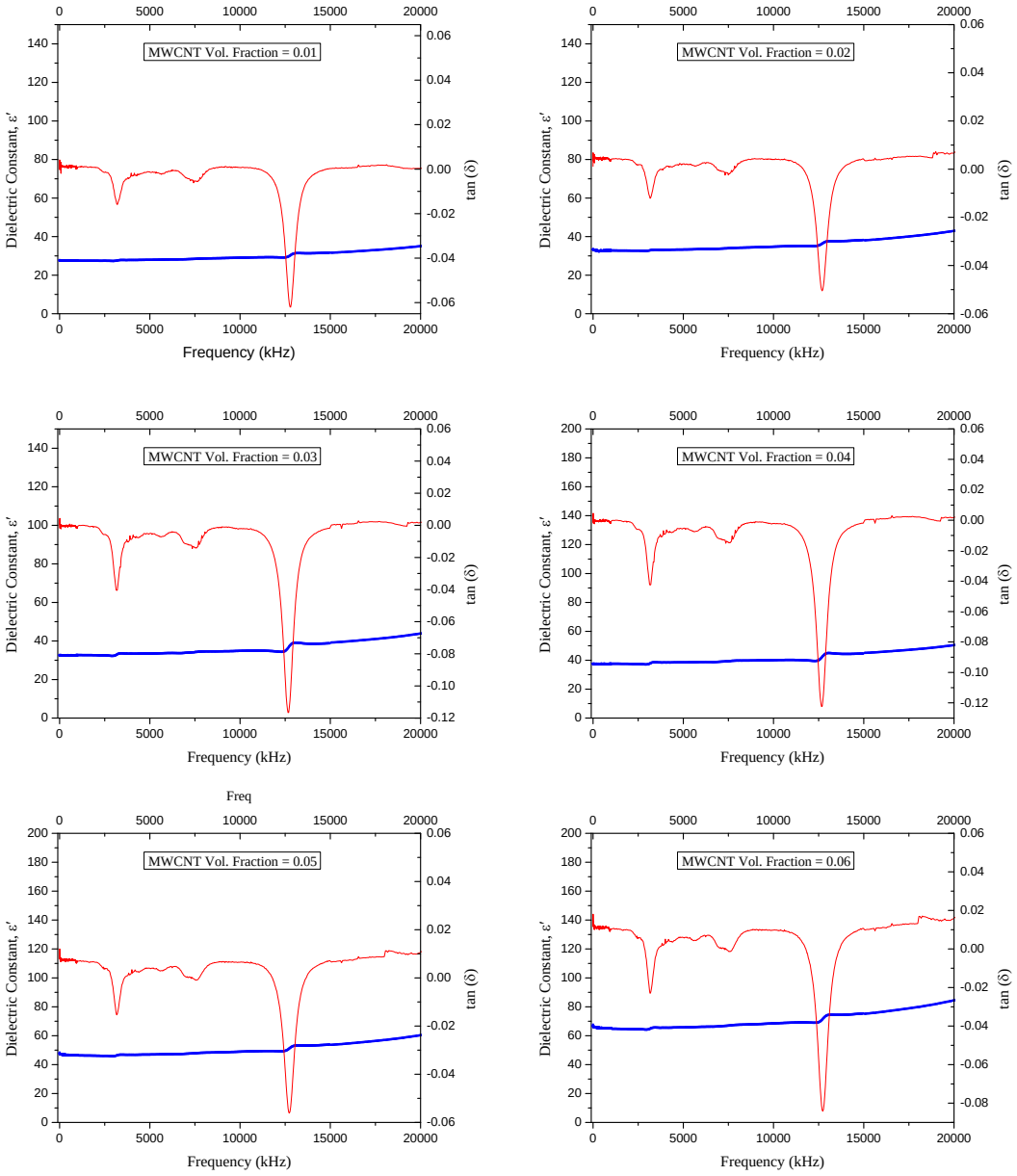

Figure 5.10 Dielectric constant, ε', and tan (δ) plots of bulk PZT-Epoxy-MWCNT composites with contact poling and with varying MWCNT volume fraction from 0.01 (1%) – 0.06 (6%). The phase plots show distinct resonant modes similar to Figures 5.8 and 5.9, due to the geometry of the composite and its microstructure.

5.3 Impedance spectroscopy of PZT-Epoxy-MWCNT flexible thick film composites characterized by corona and contact poling methods

The impedance characteristics of the PZT-Epoxy-MWCNT flexible thick film composites with a variation in the MWCNT volume fraction from 1% to 10% and plotted as a function of the frequency from 100Hz to 20 MHz is shown in Figure 5.11 A. 150 μm was the nominal sample thickness. Higher values of impedance are observed at lower frequencies. Similar to the bulk composites the impedance values decrease with an increase in frequency indicating the increasing influence of the conductive MWCNT inclusions at higher frequencies. At higher frequencies the mobility of the conductive species increases causing a drop in the resistance of the material which in turn decreases the impedance. The impedance values also decrease with an increasing MWCNT volume fraction due the increase in the number of the conductive species in the composite. Figure 5.11 B shows the impedance plots of the contact poled composites in the same frequency range. A similar trend of decreasing impedance with increasing frequency and increasing MWCNT volume fraction is also observed for the contact poled composites. A sharp drop in the impedance is also observed when the MWCNT volume fraction in the composite changes from 5% to 6% for both the corona and contact poled composites. This indicates a sharp rise in conductivity of the composite after the MWCNT volume fraction increases beyond 5%. For example at a frequency of 2.5 kHz the impedance for the corona poled composites drop from ~ 1845 kΩ to 1576 kΩ with a change in the MWCNT volume fraction from 5% to 6%; as compared to a drop of ~ 2224 kΩ to 2100 kΩ for a MWCNT volume fraction change of 3% to 4%. In the case of the contact poled composites the impedance drops from ~ 2213 kΩ to 1989 kΩ for a change in the

MWCNT volume fraction from 5% to 6% as compared to a drop of 2457 kΩ to 2344 kΩ for a MWCNT volume fraction change of 3% to 4% This is consistent with the sharp drop in the piezoelectric coefficients and the sharp rise increase of the dielectric constants of the PZT-Epoxy-MWCNT thick film composites around the percolation threshold discussed in Chapter 4 in sections 4.3.1 and 4.3.2.

As shown in Figure 5.12 the impedance for the contact poled thick film composites are higher than that of the corona poled composites for all volume fractions of MWCNT inclusions. For example for a MWCNT volume fraction of 3% and a frequency of 2kHz the contact poled composite shows an impedance value of ~ 2566 kΩ as compared to ~ 2224 kΩ for the corona poled composite. This trend is similar to the bulk composites and indicates higher resistance in contact poled composites due to a larger number of aligned dipoles formed during the corona poling method as compared to the contact poling method.

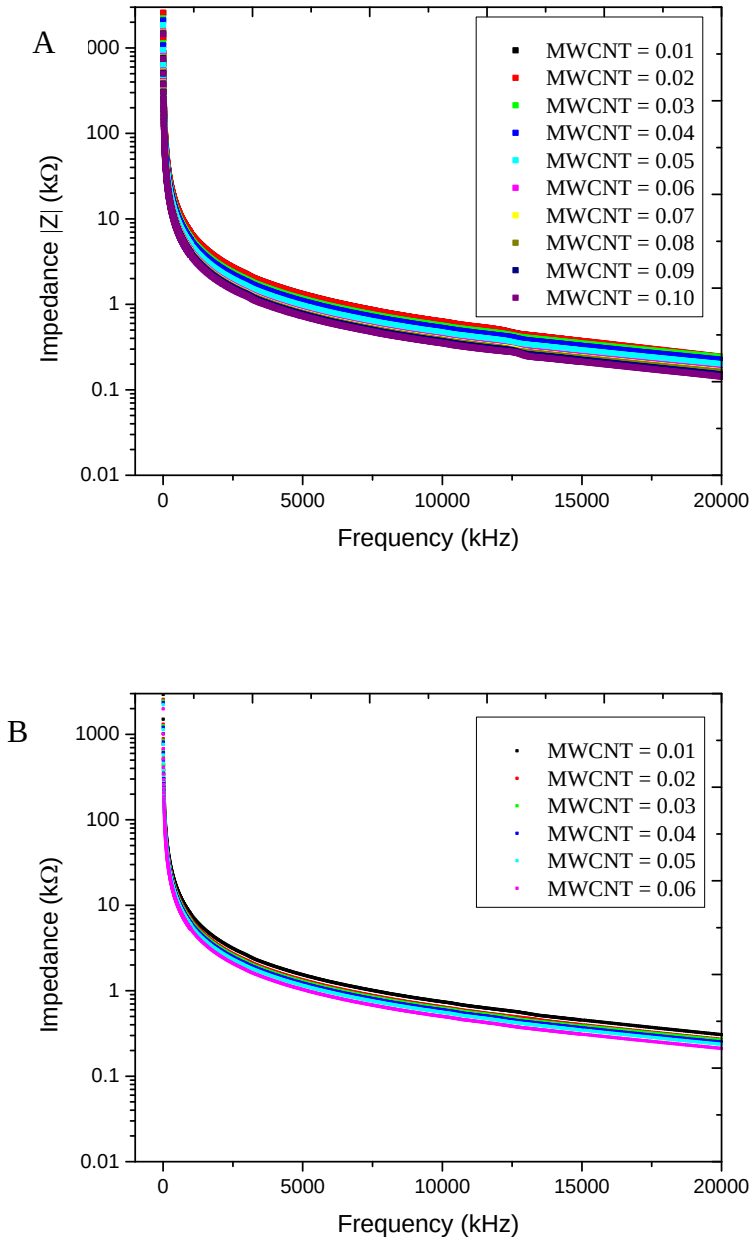

Figure 5.11 A) Impedance characteristics of the corona poled thick film composite with a variation the MWCNT volume fraction from 1% to 10% as a function of the frequency (from 100Hz – 20 MHz).. B) Impedance characteristics of the contact poled thick film composite PZT-Epoxy-MWCNT with a variation the MWCNT volume fraction from 0.01 (1%) to 0.06 (6%) as a function of the frequency (from 100Hz – 20 MHz). In both the cases the plots show a decrease in the impedance with increase in MWCNT volume fraction and an increase in the frequency.

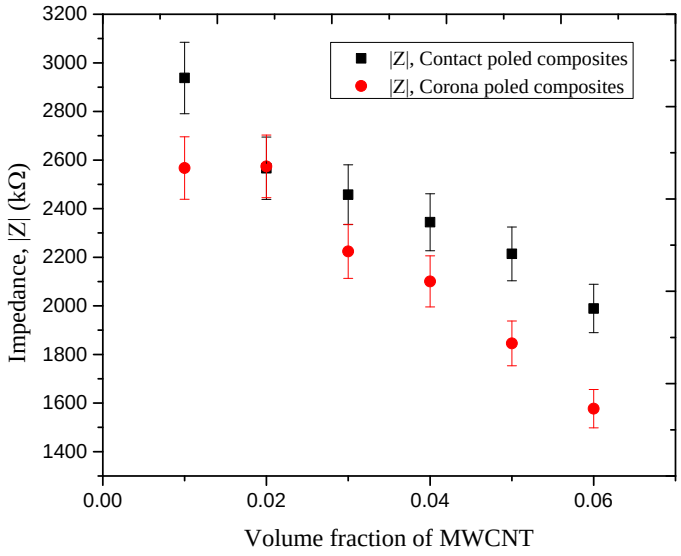

Figure 5.12 Change in the impedance for the corona and contact poled composites at a frequency of 2 kHz for PZT-Epoxy-MWCNT flexible thick films. The contact poled composites show a higher impedance as compared to the corona poled composites for all MWCNT volume fractions of the composite.

Figures 5.13, 5.14 and 5.15 show the impedance and phase plots of the corona and contact poled thick film composites. The MWCNT volume fraction for the corona poled composites is varied from 1% to 10% and that of the contact poled composites is varied from 1% to 6%. The frequency range if varied from 100Hz-20MHz. Similar to the bulk composites the phase plots indicate multiple resonant modes formed due to the microstructure and the geometry of the composite. For the corona poled composites the resonant modes occur around 76 kHz, 3.3 MHz, 6.5 MHz, 9.8 MHz and 12.3 MHz MWCNT volume fraction of 3%. For a similar volume fraction of MWCNT the resonant modes for the contact poled samples are around 75 kHz, 3.4 MHz, 6.7 MHz, 9.7 MHz and 12.4 MHz. The possible sources for these modes are the radial mode of resonance along the surface of the composite, the thickness of the thick film composite and the

resonance modes for the different phases of the composite [114, 115]. The resonant and anti-resonant peaks for the high frequency resonance mode around 12.3 MHz can also visible in the impedance plot in Figure 5.11 A.

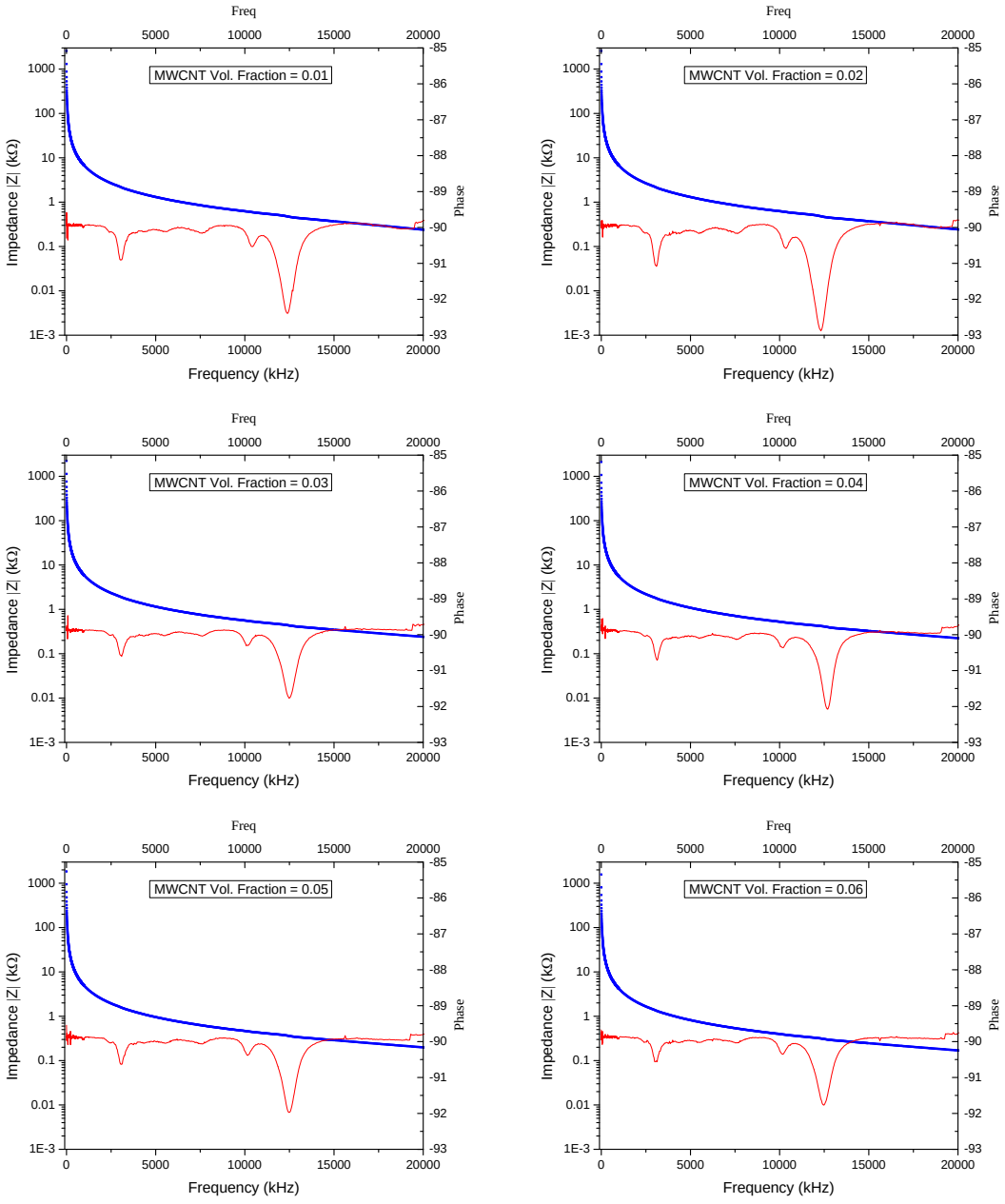

Figure 5.13 Impedance and phase diagrams of corona poled PZT-Epoxy-MWCNT thick film composites in the frequency range of 100 Hz-20MHz. The MWCNT volume fraction is varied from 0.01 (1%) – 0.06 (6%) as shown in the figures. The phase plots

indicate the presence of resonant modes formed due to the geometry and the microstructure of the composites.

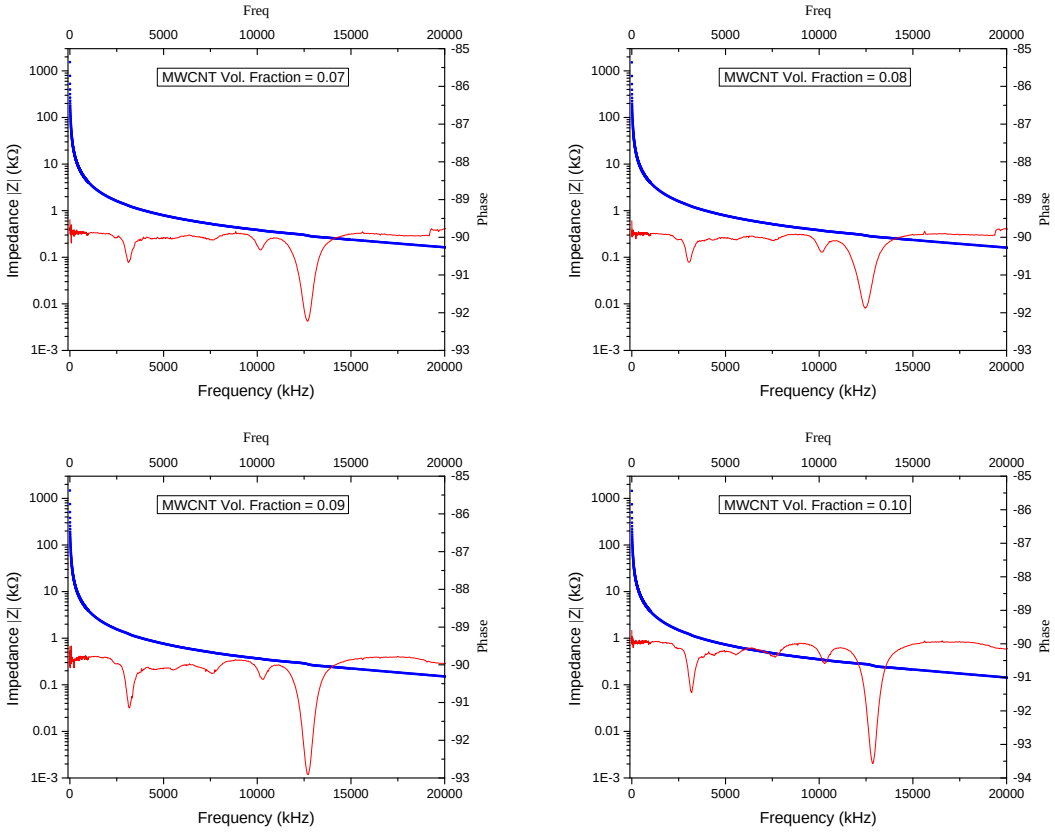

Figure 5.14 Impedance and phase plots of thick film PZT-Epoxy-MWCNT composites with corona poling and with varying MWCNT volume fraction from 0.07 (7%) – 0.10 (10%). These phase plots also show distinct resonant modes due to the bulk geometry and the composite microstructure of the material.

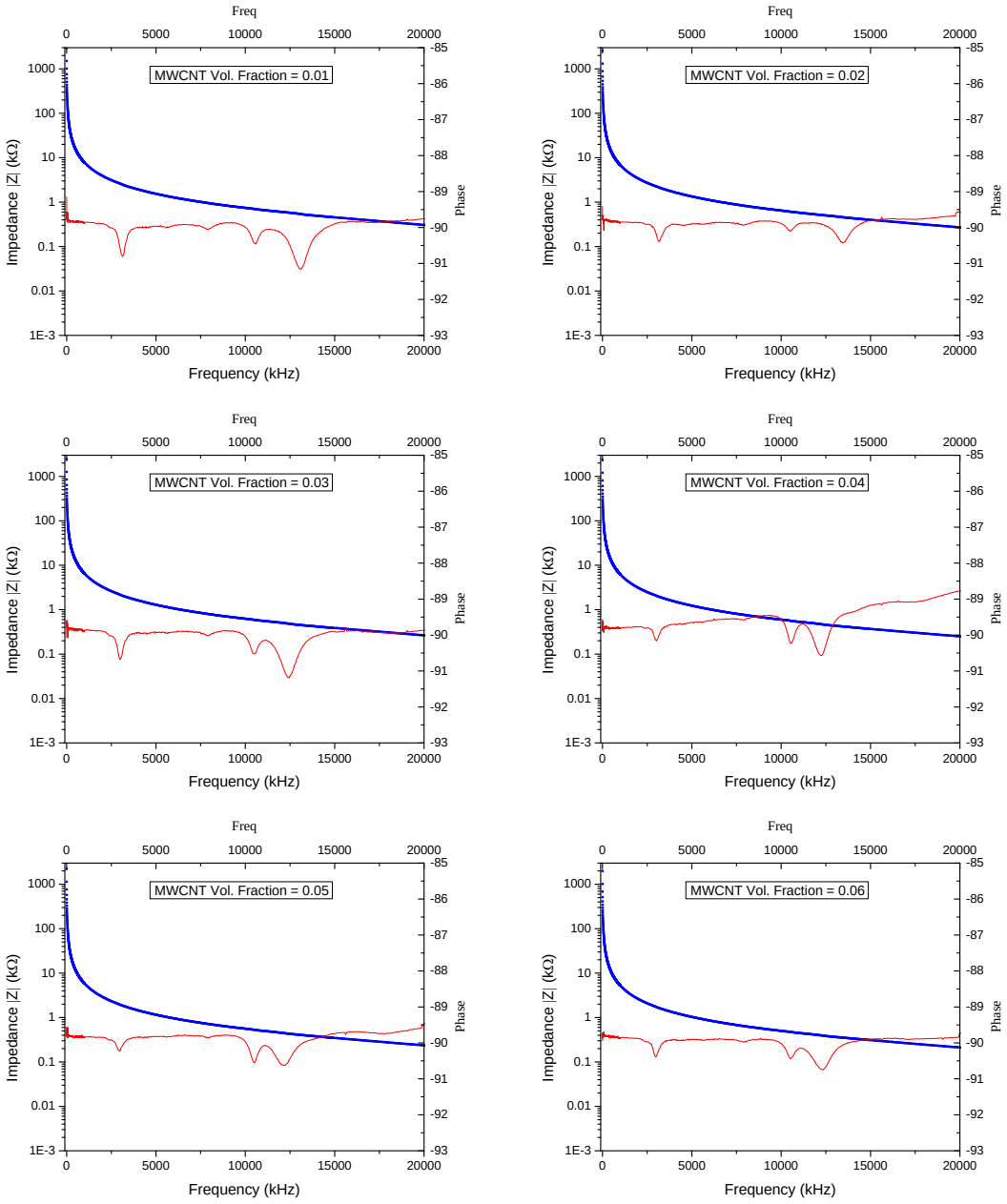

Figure 5.15 Impedance and phase plots of thick film PZT-Epoxy-MWCNT composites characterized by contact poling with varying MWCNT volume fraction from 0.01 (1%) – 0.06 (6%). The phase plots show resonant modes similar to Figures 5.13 and 5.14.

5.4 Dielectric spectroscopy of PZT-Epoxy-MWCNT flexible thick film composites characterized by corona and contact poling methods

The dielectric spectrum of the corona and contact poled composites is shown in Figures 5.16 A and B respectively. The frequency range is varied from 100Hz-20MHz. The volume fraction is varied from 1-10% for the corona poled composites and from 1-6% for the contact pole composites. An increase in the dielectric constant with an increase in the MWCNT volume fraction is observed in both the plots. The plots also indicate the transition of the composites to the percolation threshold with a jump in the dielectric constant after a MWCNT volume fraction of 5%. For example, below the percolation threshold, and for a MWCNT volume fraction change of 3%-4% the dielectric constant changes from ~ 79-96 for the corona poled composites and ~ 33-38 for the contact poled composites at a frequency of 2kHz. But when the volume fraction changes from 5-6% the dielectric constant jumps from ~ 102-176 and ~ 41-58 for corona and contact poling respectively. Similar to the bulk composites, this increase in the dielectric is coupled with the decrease in the impedance as seen in Figures 5.11 and indicates the location of the percolation threshold.

Below the percolation threshold (below 6% of MWCNTs) the dielectric performances of the composites show very little frequency dependence till a frequency of 15 MHz. The dielectric constant values increase with increasing frequency above 15 MHz, indicating frequency dependence due to the increase in the mobility of the conductive species (high rate of electron transport from MWCNTs) at higher frequencies. Above a MWCNT volume fraction of 5%, the frequency dependence is observed over

the entire range of frequencies from 100Hz-20MHz indicating a percolation system [11, 34]. The region of this percolation behavior is similar to that of the bulk composites.

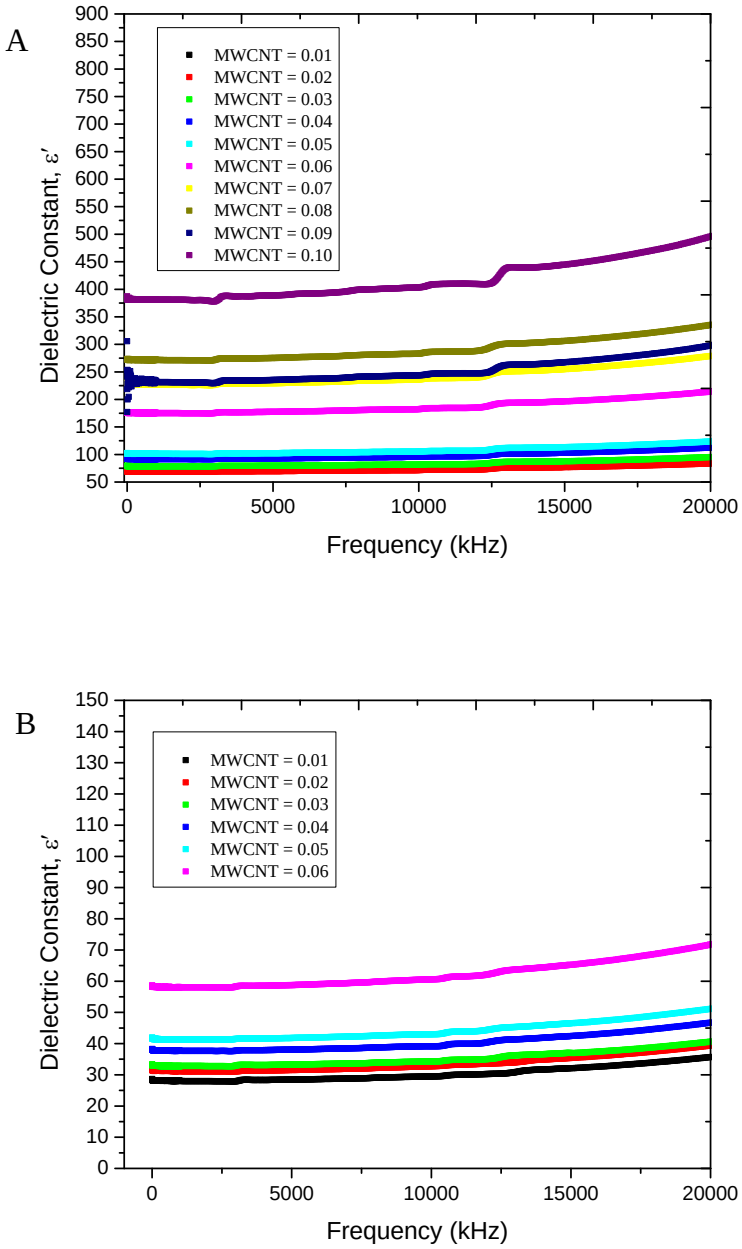

Figure 5.16 A) Dielectric spectrum of PZT-Epoxy-MWCNT thick film composites with corona discharge poling in the frequency range of 100Hz-20MHz and variable MWCNT volume fraction of 1-10%. B) Dielectric spectrum of contact poled PZT-Epoxy-MWCNT thick film composites with a variation in MWCNT volume fraction from 1-6%. Both the

plots show an increase in the dielectric constant with a variation in the MWCNT volume fraction.

As observed in Figures 5.16 A and B, the dielectric constant values for the contact poled composites are lower than that of the corona poled ones. This phenomenon is observed for all volume fractions of the MWCNTs. For example, at MWCNT volume fractions of 1% and 3% and at a frequency of 2kHz the dielectric constant for the contact/corona poled composites are ~ 68/28 and 79/33 respectively. The lower values of the dielectric constant are also coupled with the lower values of the impedance as can be observed in Figures 5.11 A and B. This is due to the higher poling efficiency obtained by the corona poling method in comparison to the contact poling method.

Figures 5.17, 5.18 and 5.19 shows the variation in the dielectric constant ε' and tan (δ) for corona and contact poled composites with varying MWCNT volume fractions plotted as a function of variable frequency from 100 Hz-20MHz. The plots show variation in MWCNT volume fraction from 1-10% for the corona poled composites and 1-6% for the contact poled composites. Similar to the previous phase plots for the bulk and thick films and the tan (δ) plots for the bulk composites; the tan (δ) plots in Figures 5.17, 5.18 and 5.19 show the presence of the resonant frequencies for the composites. In the case of the corona poled composites the resonant frequencies are around 76 kHz, 3.3 MHz, 6.5 MHz, 9.8 MHz and 12.3 MHz. For contact poling they occur around 75 kHz, 3.4 MHz, 6.7 MHz, 9.7 MHz and 12.4 MHz.

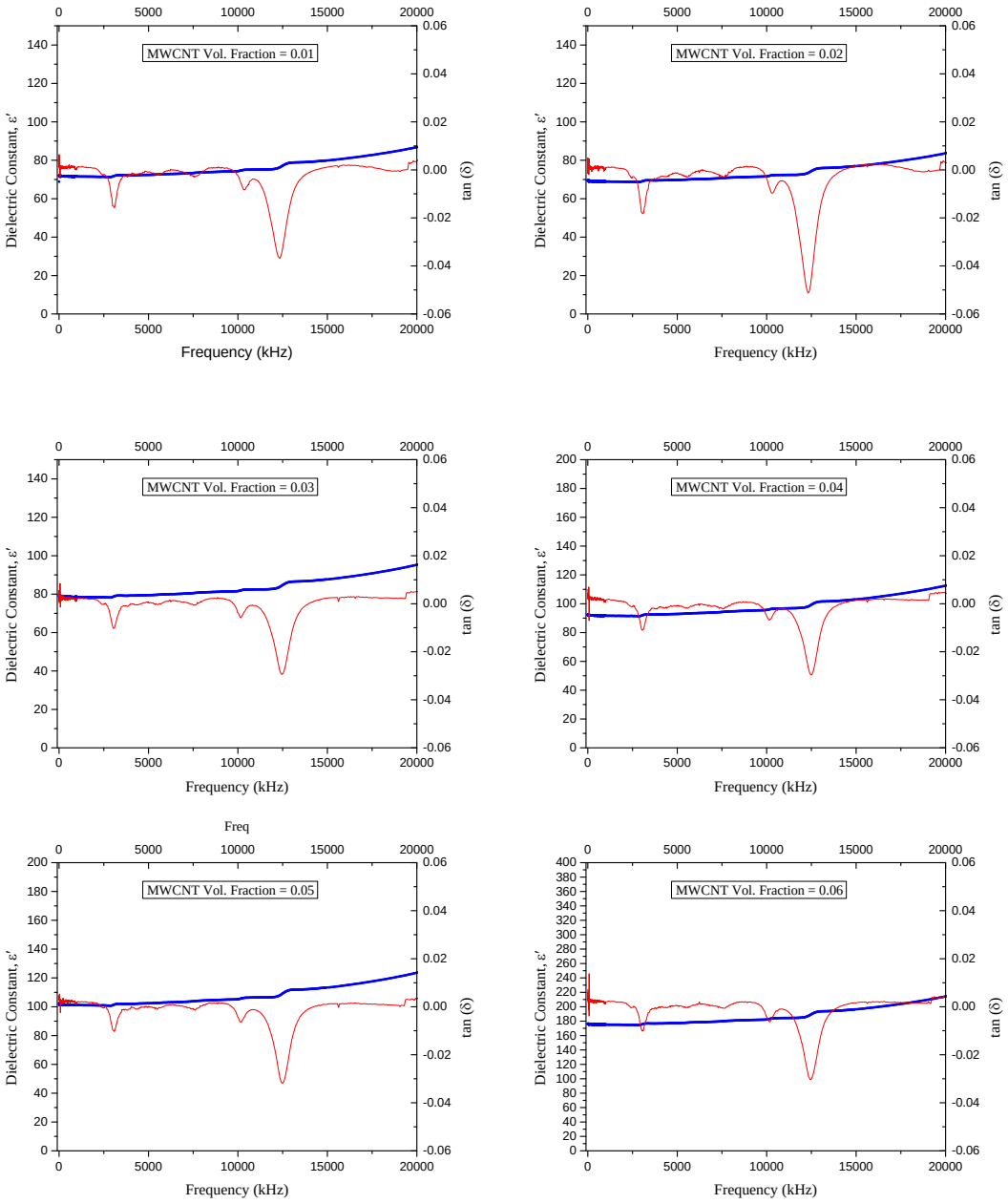

Figure 5.17 Dielectric constant, ε', and tan (δ) plots of corona poled thick film PZT-Epoxy-MWCNT composites in the frequency range of 100 Hz-20MHz. The MWCNT volume fraction is varied from 0.01 (1%) – 0.06 (6%). The tan (δ) plots indicate the presence of resonant modes.

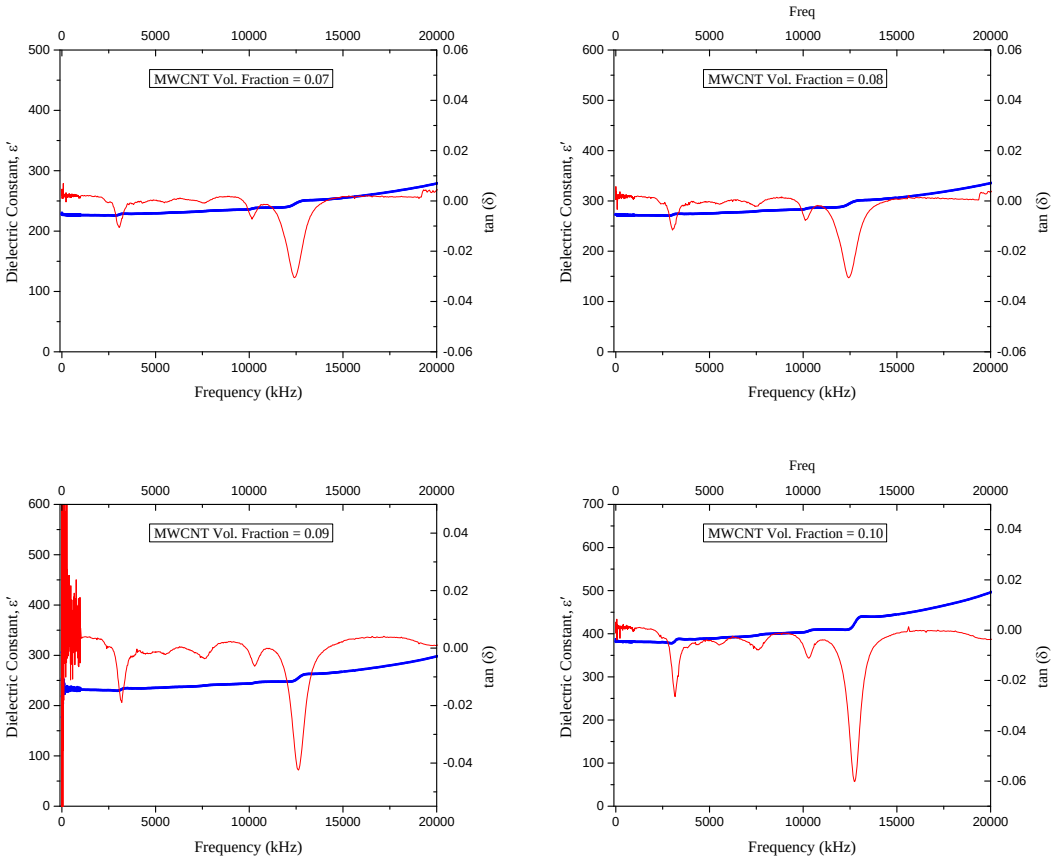

Figure 5.18 Dielectric constant, ε', and tan (δ) plots of PZT-Epoxy-MWCNT thick film composites characterized by corona poling, with varying MWCNT volume fraction from 0.07 (7%) – 0.10 (10%). The tan (δ) plots show resonant modes similar to Figure 5.17.

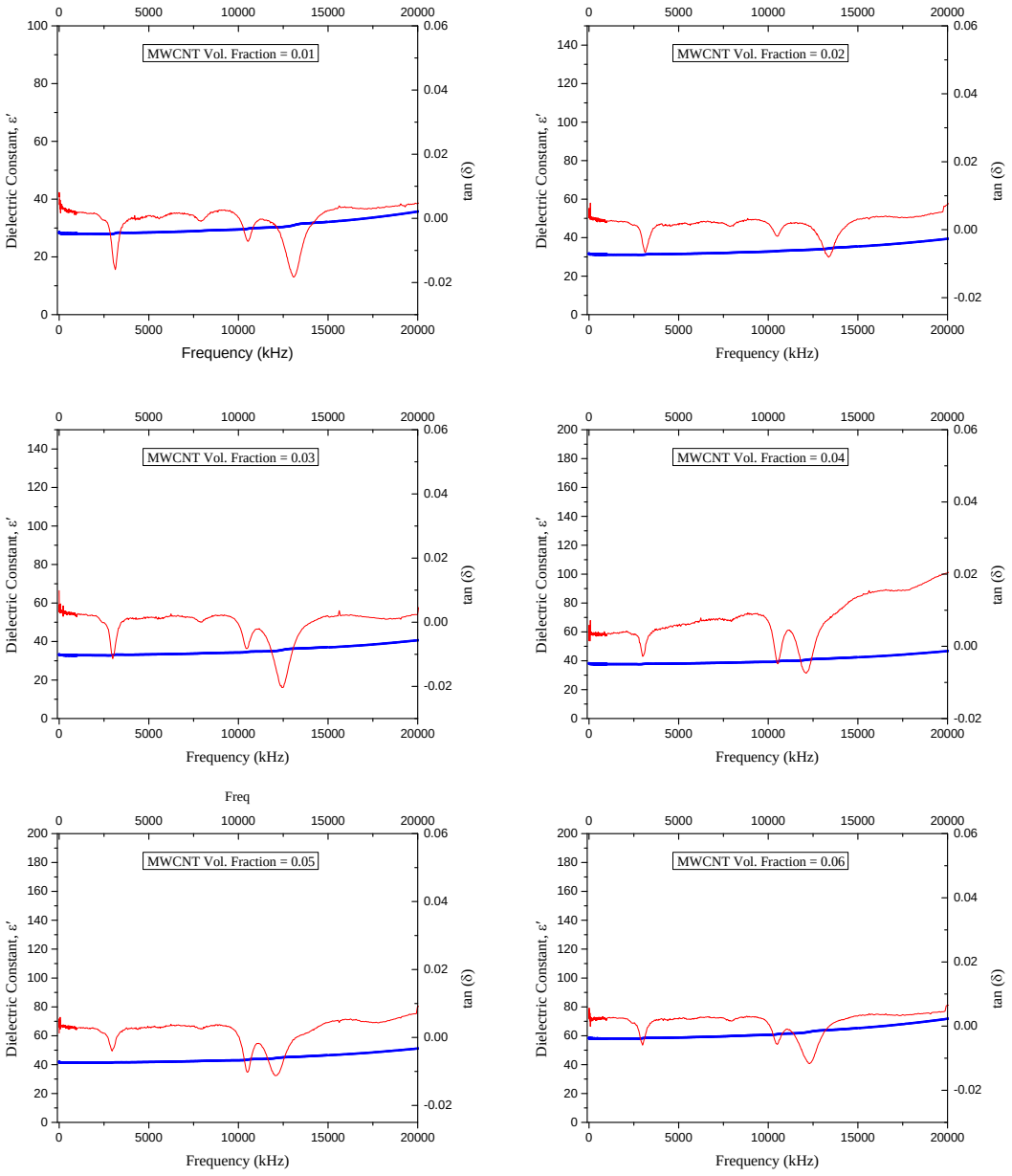

Figure 5.19 Dielectric constant, ε', and tan (δ) plots of thick film PZT-Epoxy-MWCNT composites with contact poling and with varying MWCNT volume fraction from 0.01 (1%) – 0.06 (6%). The phase plots show resonant modes similar to Figures 5.17 and 5.18.

5.5 Comparison of Impedance and dielectric spectroscopy of PZT-Epoxy-MWCNT bulk and flexible thick film composites characterized by corona and contact poling methods

The impedance and dielectric characteristics of the bulk and thick film PZT-Epoxy-MWCNT composites indicate that the composite reaches the percolation threshold above a MWCNT volume fraction of 5%. The impedance values and the dielectric constants of the bulk and thick film composites are summarized in Table 5.1 and 5.2 at a frequency of 2 kHz.

Table 5.1 Impedance and dielectric constant of PZT-Epoxy-MWCNT bulk composites with corona and contact poling at a frequency of 2 kHz and a variation of MWCNT volume fraction from 1-6%.

	MWCNT = 1%	MWCNT = 2%	MWCNT = 3%	MWCNT = 4%	MWCNT = 5%	MWCNT = 6%
Impedance (kΩ, Corona Poling)	2204.71	2104.21	2042.08	1990.77	1852.60	1631.86
Impedance (kΩ, Contact Poling)	2566.65	2458.52	2377.97	2264.74	2070.22	1759.68
Dielectric Constant (Corona Poling)	52.255	53.823	88.83	97.921	124.509	241.758
Dielectric Constant (Contact Poling)	27.80	33.42	32.74	37.65	48.28	67.60

The impedance and dielectric spectrum analysis in the previous sections and the summary of values in Tables 5.1 and 5.2 reveals that the corona poling technique is more effective than that of the contact poling method. This argument is also backed by the higher values of the piezoelectric strain coefficients for the corona poling method as

discussed in the previous chapter. The spectra analysis also shows the effect of the microstructure and the geometry of the material in determining the effective material properties of these composites.

Table 5.2 Impedance and dielectric constant of PZT-Epoxy-MWCNT thick films with corona and contact poling at a frequency of 2 kHz and a variation of MWCNT volume fraction from 1-6%.

	MWCNT = 1%	MWCNT = 2%	MWCNT = 3%	MWCNT = 4%	MWCNT = 5%	MWCNT = 6%
Impedance (kΩ, Corona Poling)	2567.25	2574.04	2224.29	2100.70	1845.7	1576.83
Impedance (kΩ, Contact Poling)	2937.75	2566.26	2457.39	2344.25	2213.92	1989.23
Dielectric Constant (Corona Poling)	68.83	69.71	79.42	92.65	102.56	176.65
Dielectric Constant (Contact Poling)	28.37	31.85	33.36	38.30	41.99	58.30

The next chapter deals with the variation in the piezoelectric and dielectric properties with the change in key poling parameters for both the corona and contact poling methods. The poling parameters that would be varied are the poling voltage and the poling temperature to determine the effect of these parameters on the effective properties of the bulk and thick film composites.

Chapter 6

Investigation of the variation in poling parameters on the piezoelectric and dielectric properties of three phase PZT-Epoxy-MWCNT bulk and thick films

The process of poling is one of the important steps in characterization of the piezoelectric composite materials. In this process a high potential is applied across the desired poling direction at a high temperature to align the dipoles of the polycrystalline piezoelectric phase in the composite. The poling method (contact or corona discharge poling) and parameters such as poling voltage, temperature and poling time determines the effective piezoelectric and dielectric properties of the composites. The following chapter investigates the effect of the variation in poling voltage and temperature on the piezoelectric and dielectric properties of the three phase PZT-Epoxy-MWCNT bulk and thick film composites based on the poling method, namely the corona discharge and contact poling techniques.

6.1 Variation of poling voltage in corona and contact poled bulk PZT-Epoxy-MWCNT composites

The variation in the piezoelectric strain coefficient, d33 in the bulk PZT-Epoxy-MWCNT composites with decreasing poling voltage for the corona and contact poling methods are shown in Figures 6.1 A and B respectively. The poling voltage is varied between 2.2-0.7 kV/mm and the MWCNT volume fraction is varied from 1% to 6%. The poling temperature is kept constant at 75^0 C.

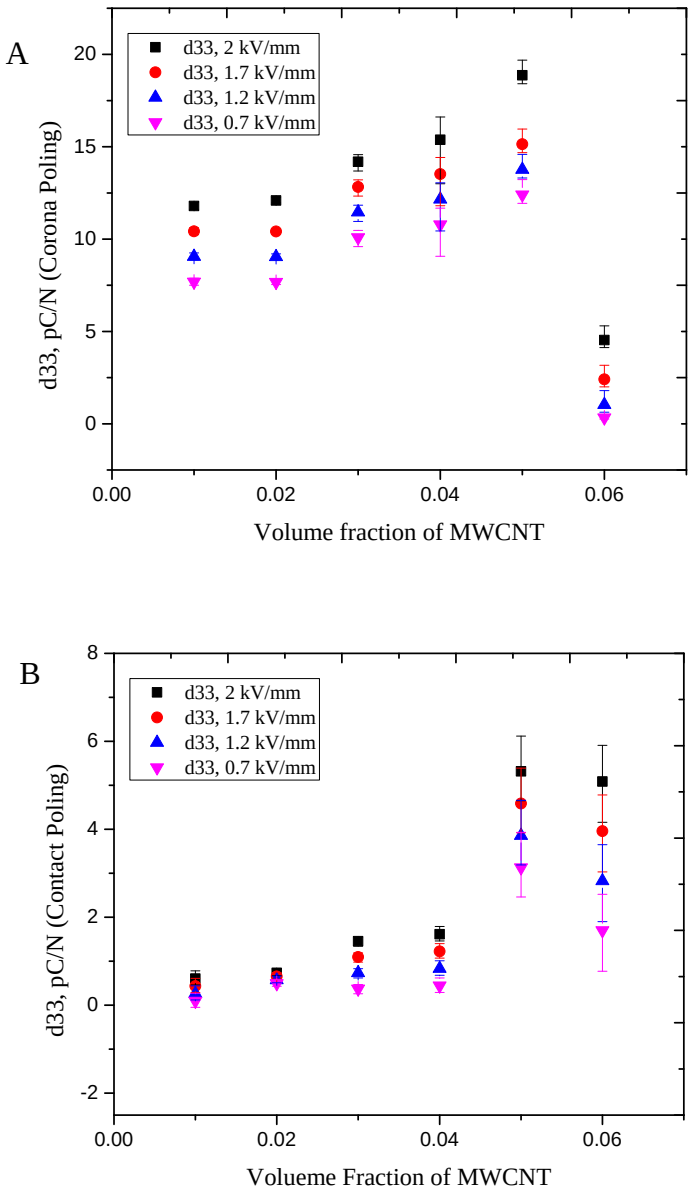

Figure 6.1 Variation in the piezoelectric strain coefficient, d33 for bulk PZT-Epoxy-MWCNT composites with increasing poling voltage from 0.7 – 2.2 kV/mm; for A) Corona poling and B) Contact poling methods. Both the figures show an increase in d33 with an increase in the poling voltage.

It was observed that the maximum poling voltage that could be reached for the composite with a MWCNT volume fraction of 6% was 2.2 kV/mm. For lower MWCNT

volume fractions the maximum poling voltage was higher as compared to the one at a volume fraction of 6%. This might to due to the increase in the number of conductive pathways in the composite with the increase in the MWCNT volume fraction and causes dielectric breakdown of the composite at higher voltages. To maintain a uniform maximum poling voltage over all MWCNT volume fractions, 2.2 kV/mm was chosen as the maximum poling voltage. The composites are poled for a time of 60 minutes.

It is observed that an increase in the poling voltage increases the d33. For example at a MWCNT volume fraction of 4% the d33 values for poling voltages of 0.7, 1.2, 1.7 and 2.2 kV/mm for the corona poling method are ~ 10.7, 12.15, 13.5 and 15.38 pC/N respectively. In the case of the contact poling method and for the same MWCNT volume fraction the d33 values are ~ 0.44, 0.83, 1.22 and 1.61 pC/N for the contact poling method with poling voltages of 0.7, 1.2, 1.7 and 2.2 kV/mm respectively. This trend is visible for all volume fractions of the MWCNTs. The increase in poling voltage (or poling strength) aligns more number of dipoles in the poling direction. This increases the polarization of the composite and leads to higher d33 values.

A similar trend is also observed in the dielectric constant, ε′, values for the three phase composites. Figures 6.2 A and B show the variation of the ε′ values with a varying poling voltage from 0.7-2.2 kV/mm. The dielectric constant is higher at higher poling voltage values for all volume fractions of MWCNTs. For example, in the case of corona poling and for a MWCNT volume fraction of 3% the ε′ values for poling voltages of 0.7, 1.2, 1.7 and 2.2 kV/mm are ~ 64, 74, 80 and 90 respectively. For the same volume fraction of MWCNT in the case of the contact poled samples the ε′ are ~ 25, 27, 36 and 38 for poling voltages of 0.7, 1.2, 1.7 and 2.2 kV/mm respectively. The orientation of the

dipoles and the effective polarization caused by them in the composite contributes to the values of dielectric constant in addition to the electronic and ionic polarization in the composite [50]. With an increase in the poling field the dipole polarization increases in the poling direction due to more number of dipoles being aligned. This causes an increase in the dielectric constant as seen Figure 6.2 for both corona and contact poling methods.

In addition to the ε′ values in the composite the tan (δ) values also increase with an increase in the poling voltage as seen in Figures 6.3 A and B. For example the tan (δ) values for the corona poled composites with poling fields of 0.7, 1.2, 1.7 and 2.2 kV/mm and a MWCNT volume fraction of 4% are ~ 0.0093, 0.011, 0.013 and 0.016 respectively at a frequency of 110 Hz. The higher values of tan (δ) with increased poling voltages can be attributed to the increased number of defects or localized regions of dielectric breakdown in the composites caused by high voltage polarization. This trend is also seen for most volume fractions of the contact poled composites. Also a sharp increase in the tan (δ) values are observed at a MWCNT volume fraction of 6% which indicates a sharp rise in the dielectric loss. This is due the sharp rise in conductivity of the composite around the percolation threshold.

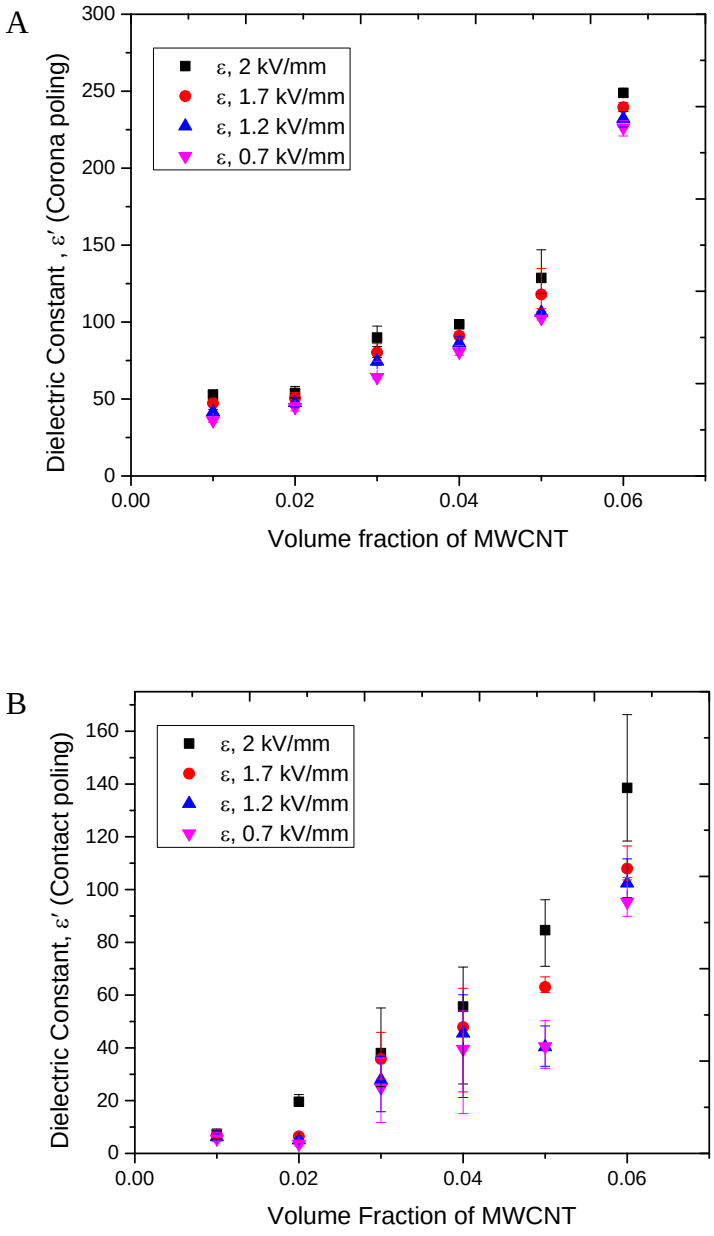

Figure 6.2 Variation in the dielectric constant, ε′, with variation in the poling voltage from 0.7-2.2 kV/mm in A) Corona poling and B) Contact poling techniques. The dielectric constant increases with an increase in the poling voltage.

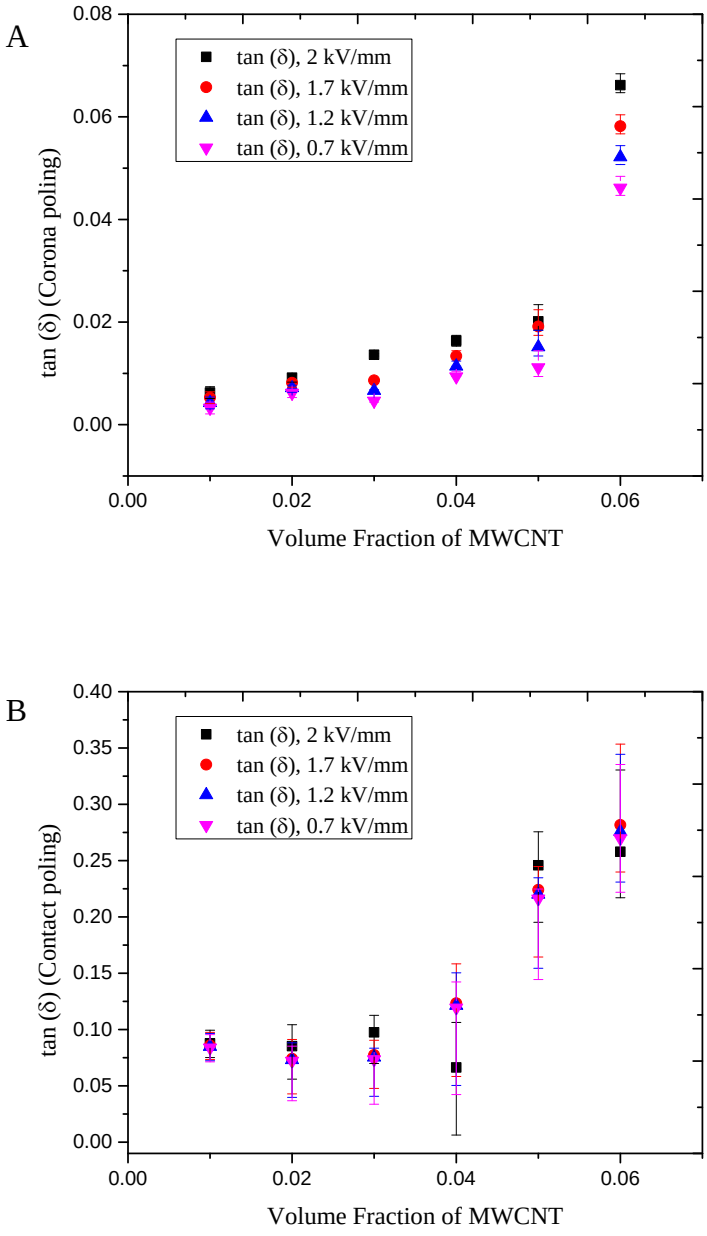

Figure 6.3 Variation in the tangent of the loss angle, tan (δ), with variation in the poling voltage from 0.7-2.2 kV/mm in A) Corona poling and B) Contact poling techniques. The tan (δ) increases with an increase in the poling voltage.

6.2 Variation of poling temperature in corona and contact poled bulk PZT-Epoxy-MWCNT composites

The variation in the piezoelectric strain coefficient, d33 in bulk PZT-Epoxy-MWCNT composites with decreasing poling temperature for both the corona and contact poling methods are shown in Figures 6.4 A and B respectively. The poling temperature is varied from $45^0 – 75^0$ C and the MWCNT volume fraction is varied from 1% to 6%. The poling temperature is not increased beyond the glass transition temperature of the epoxy matrix, which is 75^0 C. Beyond this temperature the epoxy matrix undergoes structural changes which is beyond the scope of this dissertation. The poling voltage is kept constant at 2.2 kV/mm. The composites are poled for a time of 60 minutes.

It can be seen that the d33increases with increase in the poling voltage. At a MWCNT volume fraction of 4% the d33 values for poling temperatures of 45^0, 55^0, 65^0 and 75^0 C for the corona poling method are ~ 10.45, 11.82, 13.19 and 15.38 pC/N respectively. In the case of the contact poling method and for the same MWCNT volume fraction the d33 values are 0.54, 0.63, 1.01 and 1.61 pC/N for the contact poling method with poling voltages of 0.7, 1.2, 1.7 and 2.2 kV/mm respectively. This trend is seen for all volume fractions of the MWCNTs. The increase in the temperature increases the mobility of the crystal lattice structures of the polycrystalline piezoelectric phase, PZT, to align along the poling direction [50, 74] and more number of dipoles can be aligned for the given poling voltage. This increases the polarization of the composite and leads to higher d33 values.

The ε′, values show a similar increase with the poling temperature for the three phase bulk composites. Figures 6.5 A and B show the change in ε′ values with the poling

temperature varying from 45^0- 75^0 C. For all volume fractions of MWCNTs the dielectric constant is higher at higher poling temperatures.

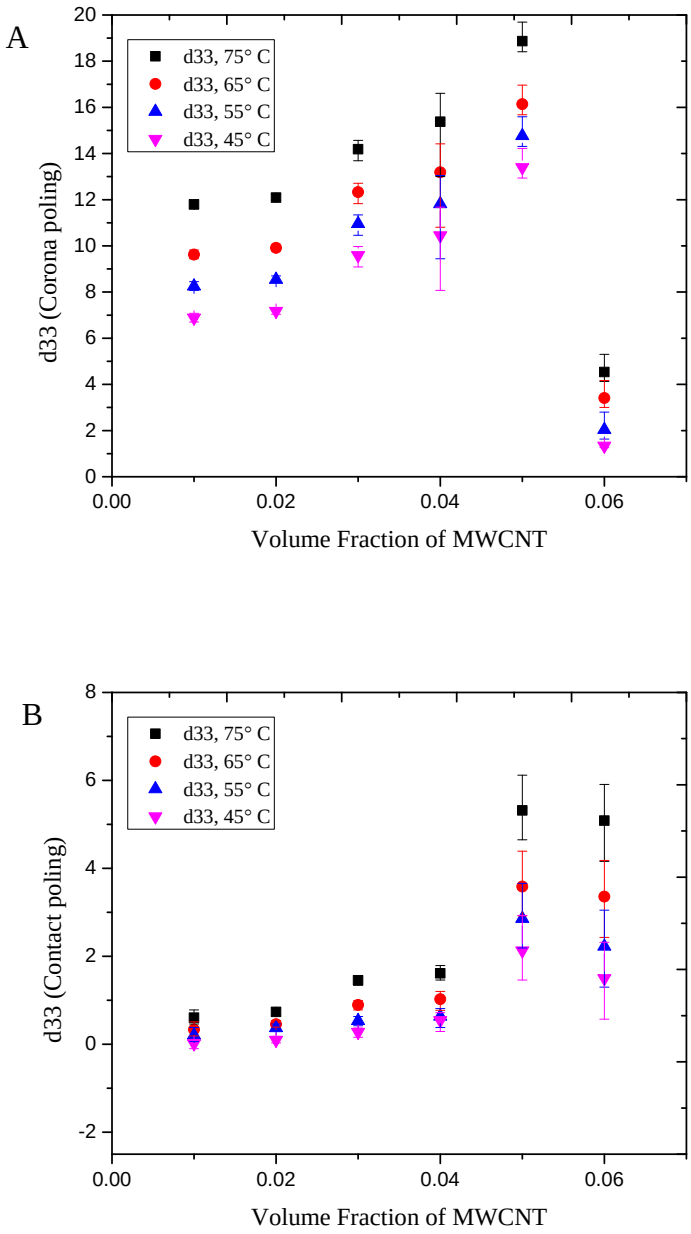

Figure 6.4 Variation in the piezoelectric strain coefficient, d33 for bulk PZT-Epoxy-MWCNT composites with increasing poling temperature from 45^0 – 65^0 C; for A) Corona poling and B) Contact poling methods. Both the figures show an increase in d33 with an increase in the poling temperature.

For example, in the case of corona poling and for a MWCNT volume fraction of 4% the ε′ values for poling temperatures of 45^0, 55^0, 65^0 and 75^0 C are ~ 83, 88, 93 and 98 respectively. For the same volume fraction of MWCNT in the case of the contact poled samples the ε′ is ~ 31, 38, 43 and 55 for poling temperatures of 45^0, 55^0, 65^0 and 75^0 C respectively. The dielectric constant is a combination of the effective polarization due to the dipoles and their orientation, in addition to the contributions of electronic and ionic polarizations in the composite. With an increase in the poling temperature the dipole polarization increases due to an increase in the number of dipoles being aligned in the poling direction. This causes an increase in ε′ as seen Figure 6.5 for both corona and contact poling methods.

The tan (δ) values of the bulk three phase composites are also measured as a function of the poling temperature in addition to the ε′ values. For both the corona poled and contact poled composites they increase by small amounts with an increase in the poling temperature and at volume fractions below the percolation threshold as seen in Figures 6.6 A and B. For example the tan (δ) values for the corona poled composites with poling temperatures of 45^0, 55^0, 65^0 and 75^0 C and a MWCNT volume fraction of 4% are ~ 0.01, 0.012, 0.014 and 0.016 respectively. Even for a MWCNT volume fraction of 6% the tan (δ) values are 0.05, 0.058, 0.064 and 0.066 for the same changes in temperature. This trend is consistent for the contact poled composites as seen in Figure 6.6 B. The small amount of increase in the tan (δ) values with increase in the poling temperature can be attributed to the higher chance of the formation of localized percolation pathways in the composites due to higher mobility of the ionic species in the composite at higher temperatures.

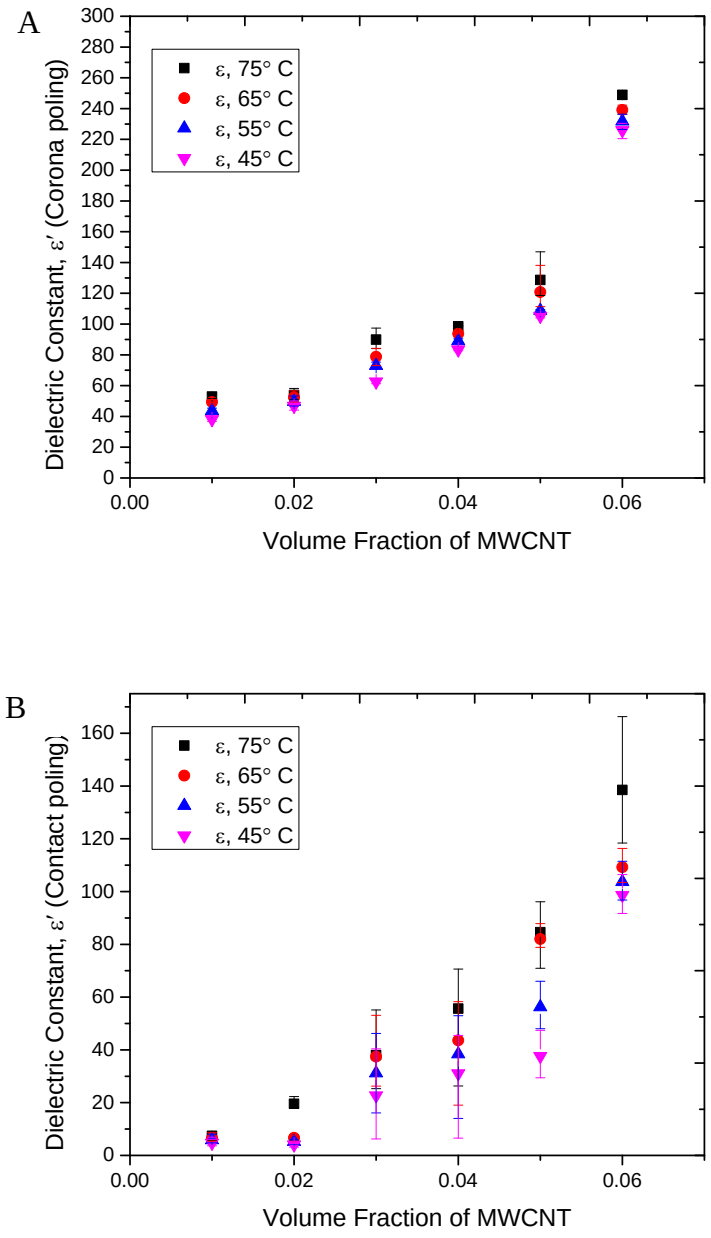

Figure 6.5 Variation in the dielectric constant, ε′, with variation in the poling temperature from 45^0 – 65^0 C in A) Corona poled and B) Contact poled composites. The dielectric constant increases with an increase in the poling temperature.

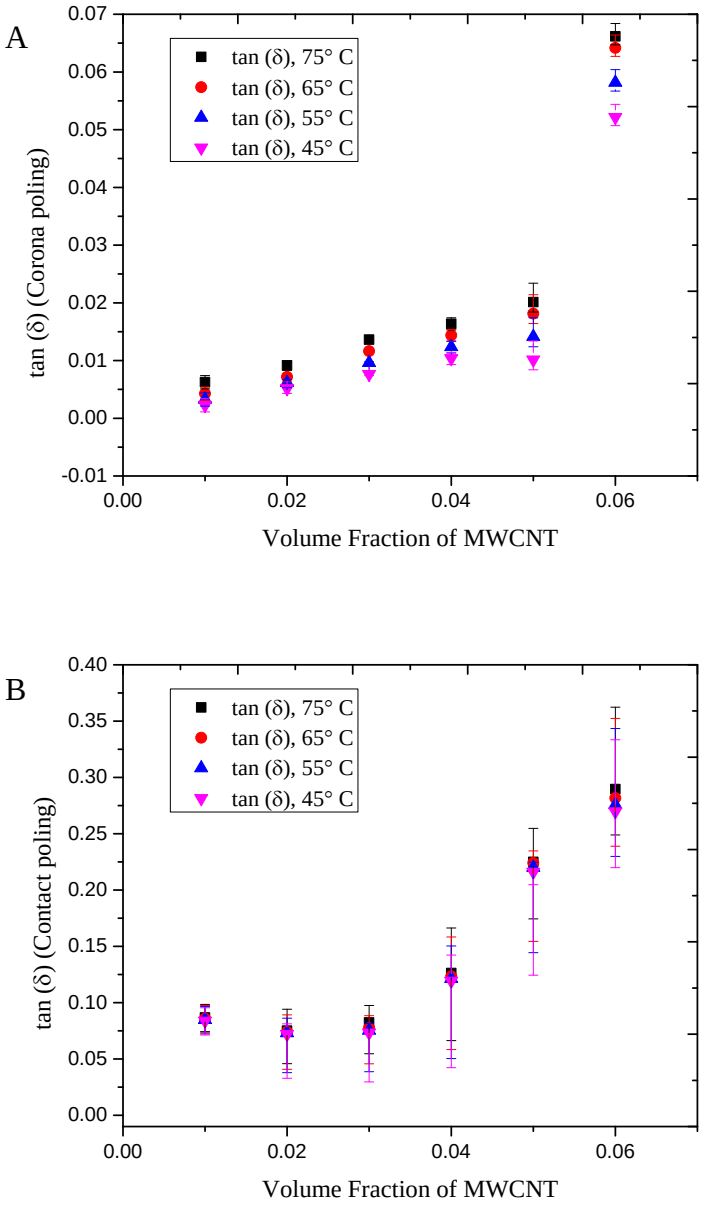

Figure 6.6 Variation in the tangent of the loss angle, tan (δ), with variation in the poling temperature from 45^0 – 65^0 C in A) Corona poling and B) Contact poling methods. The tan (δ) increases with an increase in the poling temperature.

6.3 Variation of poling voltage in corona and contact poled PZT-Epoxy-MWCNT thick films

The change in the piezoelectric strain coefficients, d33 and d31 in PZT-Epoxy-MWCNT thick film composites with decreasing poling voltage for the corona/contact poling methods are shown in Figures 6.7 A/B and 6.8 A/B respectively. The poling voltage is varied between 2.2-0.7 kV/mm and the MWCNT volume fraction is varied from 1% to 6%. The poling temperature is kept constant at 75^0 C.

It is seen that an increase in the poling voltage increases both the values of d33 and d31. For example at a MWCNT volume fraction of 4% the d33 values for poling voltages of 0.7, 1.2, 1.7 and 2.2 kV/mm for the corona poling method are ~ 5.66, 6.43, 7.62 and 8.45 pC/N respectively. For the same MWCNT volume fraction and poling voltages the d31 values are 3.86, 4.63, 6.86 and 8.71 pC/N. In the case of the contact poling method and for the same MWCNT volume fraction the d33 values are 0.04, 0.08, 0.17 and 0.27 pC/N for the contact poling method with poling voltages of 0.7, 1.2, 1.7 and 2.2 kV/mm respectively. The d31 values for the contact poled composites at a MWCNT volume fraction of 4% and for the same poling voltages are 0.24, 0.26, 0.3 and 0.32 respectively. The increase in the piezoelectric strain coefficients with increasing poling voltages are observed for all volume fractions of the MWCNTs. The increase in poling voltage aligns higher number of dipoles in the poling direction which increases the polarization of the composite and leads to higher d33 and d31 values in the thick film composites.

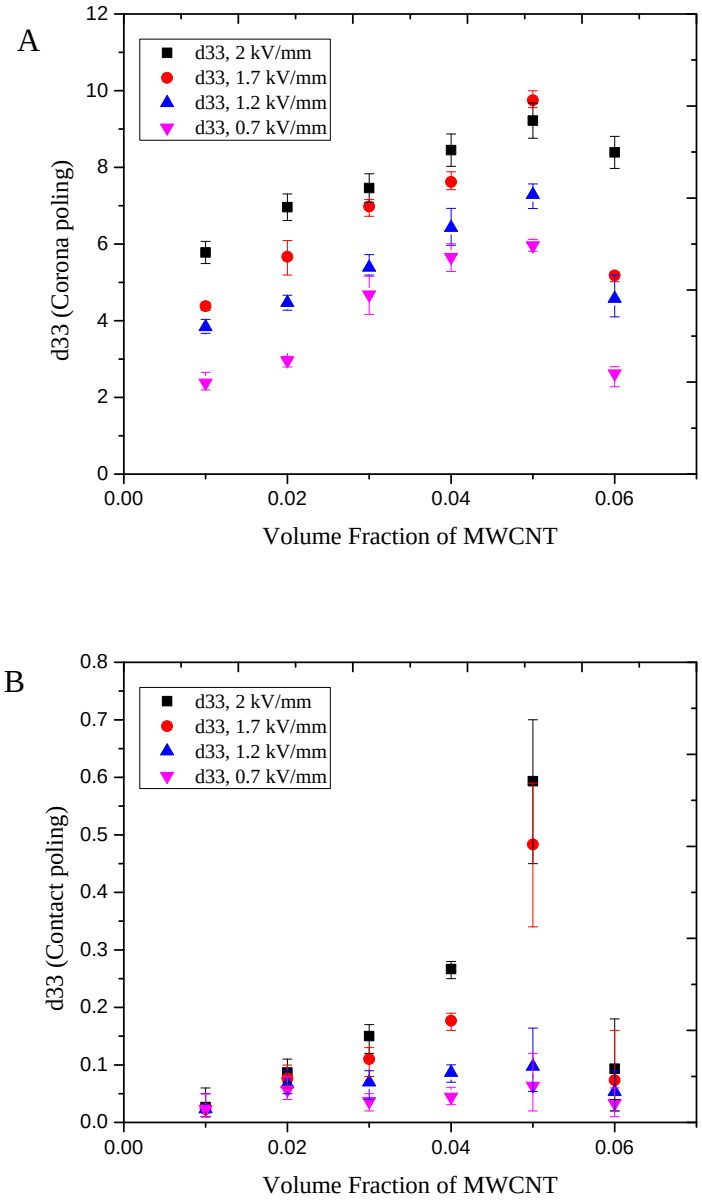

Figure 6.7 Variation in the piezoelectric strain coefficient, d33 for PZT-Epoxy-MWCNT thick film composites with increasing poling voltage from 0.7 – 2.2 kV/mm; for A) Corona poling and B) Contact poling methods. Both the figures show an increase in d33 with an increase in the poling voltage.

The dielectric constant, ε′, values for thick film composites show a similar change. Figures 6.9 A and B show the variation of the ε′ values with a varying poling

voltage from 0.7-2.2 kV/mm. The dielectric constant is higher at higher poling voltage values for all volume fractions of MWCNTs. For example, in the case of corona poling and for a MWCNT volume fraction of 3% the ε′ values for poling voltages of 0.7, 1.2, 1.7 and 2.2 kV/mm are ~ 60, 68, 79 and 81 respectively. For the same volume fraction of MWCNT in the case of the contact poled samples the ε′ are ~ 31, 36, 41 and 45 for poling voltages of 0.7, 1.2, 1.7 and 2.2 kV/mm respectively. Similar to the bulk composites, the polarization due to the orientation of the dipoles contributes to the values of dielectric constant. With an increase in the poling voltage more number of dipoles being aligned and the polarization due to the dipoles increase. This results in an increase in the dielectric constant for both corona and contact poling methods as seen in Figure 6.9.

The tan (δ) values also increase with an increase in the poling voltage as seen in Figures 6.10 A and B. For example the tan (δ) values for the contact poled composites with poling fields of 0.7, 1.2, 1.7 and 2.2 kV/mm and a MWCNT volume fraction of 4% are ~ 0.009, 0.01, 0.02 and 0.033 respectively. The higher values of tan (δ) with increased poling voltages can be attributed to the increased number of defects or localized regions of dielectric breakdown in the composites caused by high voltage polarization. The tan (δ) for the corona poled composites show very little change for all MWCNT volume fractions as seen in Figure 6.10 A indicating the effectiveness of the corona poling method (causes less poling defects) in thick films as compared to contact poling method [50].

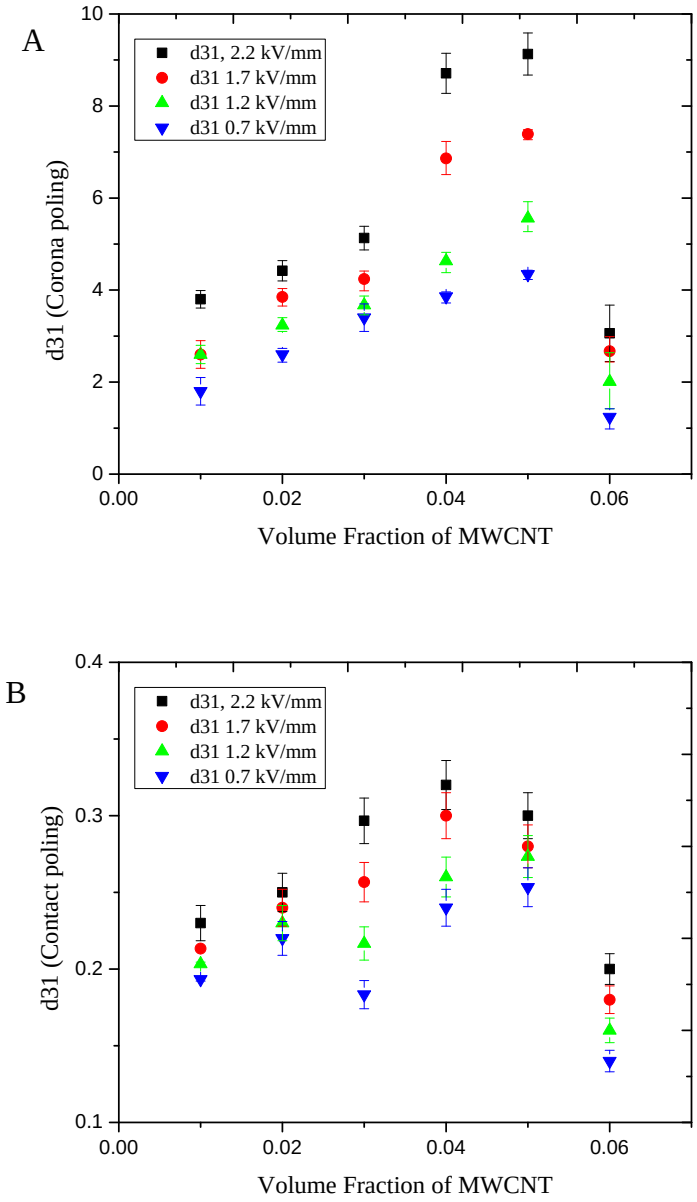

Figure 6.8 Variation in the piezoelectric strain coefficient, d31 for PZT-Epoxy-MWCNT thick film composites with increasing poling voltage from 0.7 – 2.2 kV/mm; for A) Corona poling and B) Contact poling methods. Both the figures show an increase in d31 with an increase in the poling voltage.

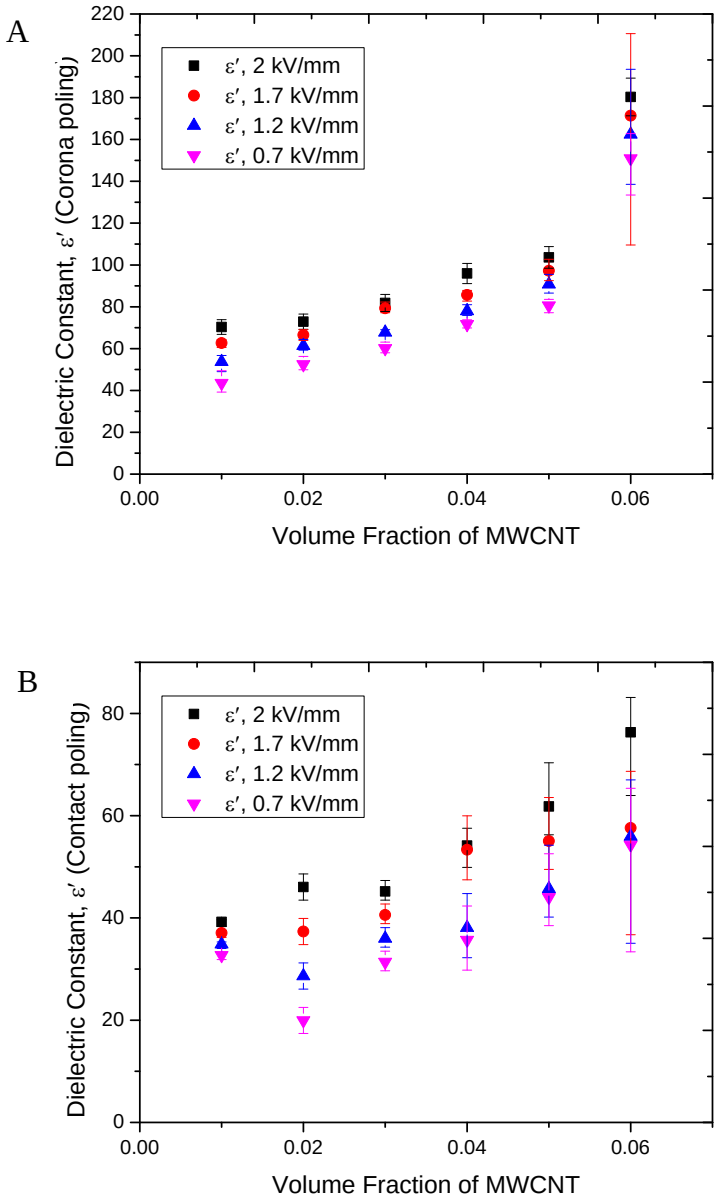

Figure 6.9 Variation in the dielectric constant, ε′, with variation in the poling voltage from 0.7-2.2 kV/mm in PZT-Epoxy-MWCNT thick films with A) Corona poling and B) Contact poling. The dielectric constant increases with an increase in the poling voltage for both the methods.

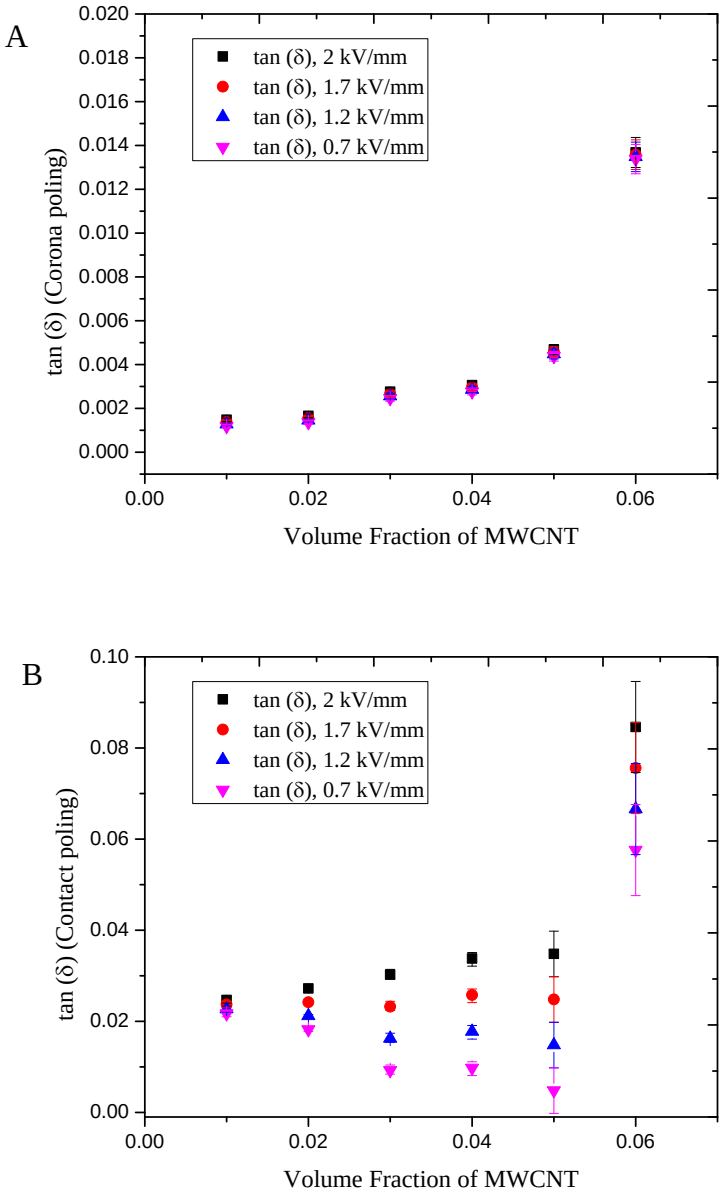

Figure 6.10 Variation in the tangent of the loss angle, tan (δ), with variation in the poling voltage from 0.7-2.2 kV/mm in A) Corona poling and B) Contact poled, thick films. The tan (δ) for the contact poled composites increase with an increase in the poling voltage. The tan (δ) for the corona poled composites remains almost constant for all MWCNT volume fractions.

6.4 Variation of poling temperature in corona and contact poled PZT-Epoxy-MWCNT thick films

The variation in the piezoelectric strain coefficient, d33 and d31 in PZT-Epoxy-MWCNT thick films with decreasing poling temperature both for the corona/contact poling methods are shown in Figures 6.11 A/B and 6.12 A/B respectively. The poling temperature is varied from 45^0 – 75^0 C and the MWCNT volume fraction is varied from 1% to 6%. The poling voltage is kept constant at 2.2 kV/mm.

It can be seen that both the d33 and d31 increases with an increase in the poling voltage. At a MWCNT volume fraction of 4% the d33 values for poling temperatures of 45^0, 55^0, 65^0 and 75^0 C for the corona poling method are ~ 4.3, 5.25, 6.84 and 8.45 pC/N respectively. For the same parameters the d31 values are ~ 4.23, 5.61, 6.2 and 8.71 pC/N. In the case of the contact poling method and for the same MWCNT volume fraction the d33 values are 0.086, 0.14, 0.20 and 0.26 pC/N for the contact poling method with poling voltages of 0.7, 1.2, 1.7 and 2.2 kV/mm respectively. The d31 values for the contact poling method with the same MWCNT volume fraction are ~ 0.2, 0.22, 0.26 and 0.32 for the same order of poling voltages. This trend is seen for all volume fractions of the MWCNTs. At high temperature more number of dipoles can be aligned for the given poling voltage due to the increase in the mobility of the dipoles. This increases the polarization of the composite and leads to higher d33 and d31 values.

The ε′, values show a similar increase with the poling temperature for the three phase thick film composites. Figures 6.13 A and B show the change in ε′ values with the poling

temperature varying from 45^0- 75^0 C. For all volume fractions of MWCNTs the dielectric constant is higher at higher poling temperatures.

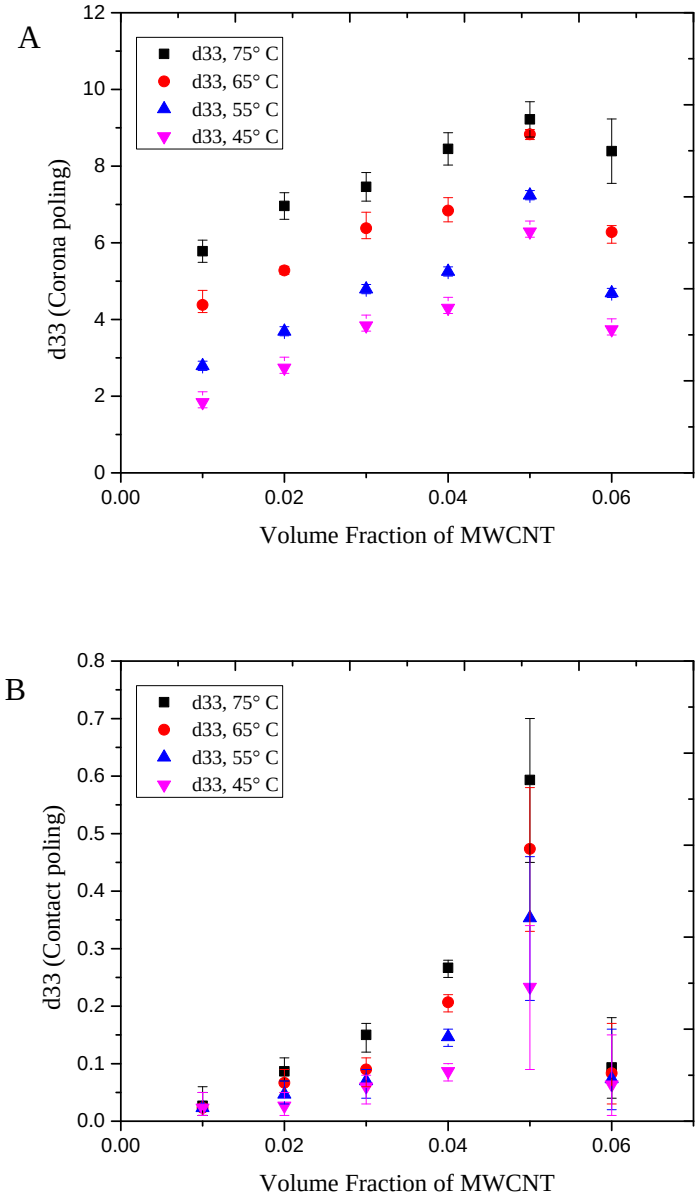

Figure 6.11 Variation in the piezoelectric strain coefficient, d33 for PZT-Epoxy-MWCNT thick films with increasing poling temperature from 45^0 – 65^0 C; for A) Corona poling and B) Contact poling methods. Both the figures show an increase in d33 with an increase in the poling temperature.

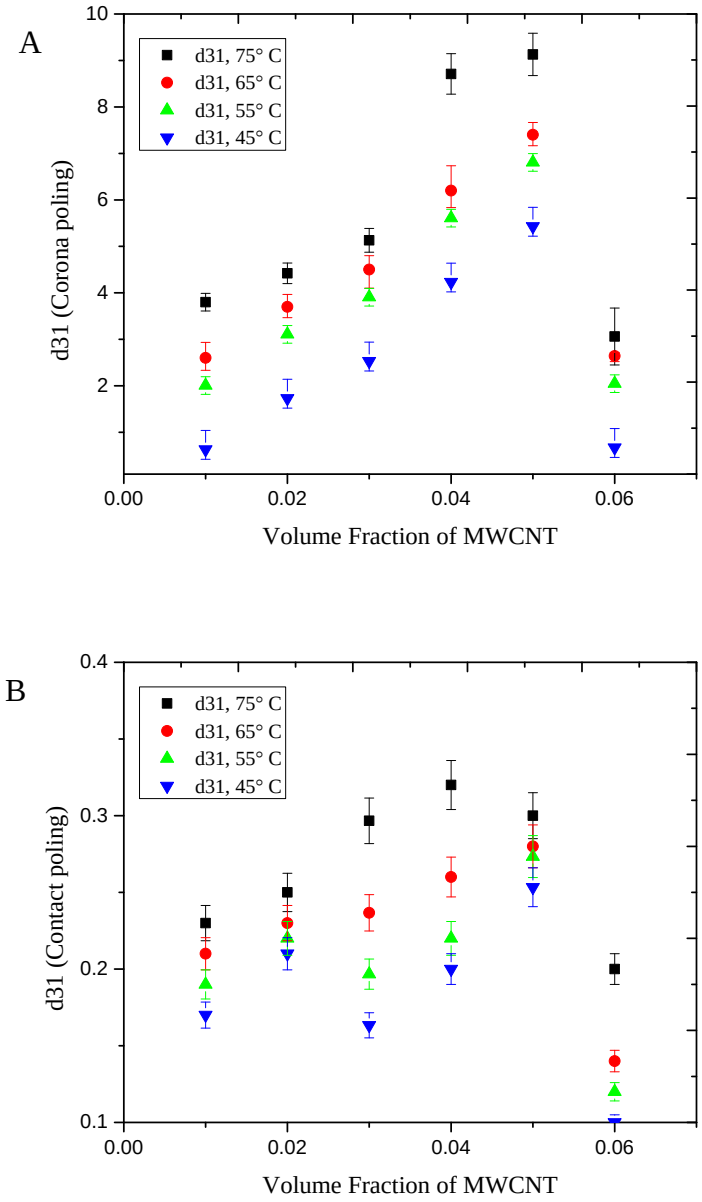

Figure 6.12 Variation in the piezoelectric strain coefficient, d31 for PZT-Epoxy-MWCNT thick films with increasing poling temperature from 45^0 – 65^0 C; for A) corona poling and B) contact poling methods. Both the figures show an increase in d31 with an increase in the poling temperature.

For example, in the case of corona poling and for a MWCNT volume fraction of 4% the ε′ values for poling temperatures of 45^0, 55^0, 65^0 and 75^0 C are ~ 57, 71, 81 and 95 respectively. For the same volume fraction of MWCNT in the case of the contact poled samples the ε′ is ~ 47, 50, 52 and 54 for poling temperatures of 45^0, 55^0, 65^0 and 75^0 C respectively. The dielectric constant of the composite increases with the increase in the effective dipole polarization which depends on the to the dipole orientation. With an increase in the poling temperature the dipole polarization increases due to an increase in the number of dipoles being aligned in the poling direction. This causes an increase in ε′ as seen Figure 6.13 for both the poling methods.

The tan (δ) values of the bulk three phase composites are also measured as a function of the poling temperature in addition to the ε′ values. For the contact poled composites they increase with an increase in the poling temperature and remains almost constant for the corona poling technique as seen in Figures 6 A and B. For example the tan (δ) values for the contact poled composites with poling temperatures of 45^0, 55^0, 65^0 and 75^0 C and a MWCNT volume fraction of 4% are ~ 0.02, 0.029, 0.031 and 0.033 respectively. This trend in followed for all MWCNT volume fractions of the thick film composites with contact poling. This increase in the tan (δ) values with increase in the poling temperature can be attributed to the higher chance of the formation of localized percolation pathways in the composites due to higher mobility of the ionic species in the composite at higher temperatures during contact poling of the thick films. These defects can also be coupled with the localized dielectric breakdown of the epoxy matrix material. In the case of the corona poling the probability of the formation of these defects are much lower and leads to almost constant tan (δ) values at different poling temperatures.

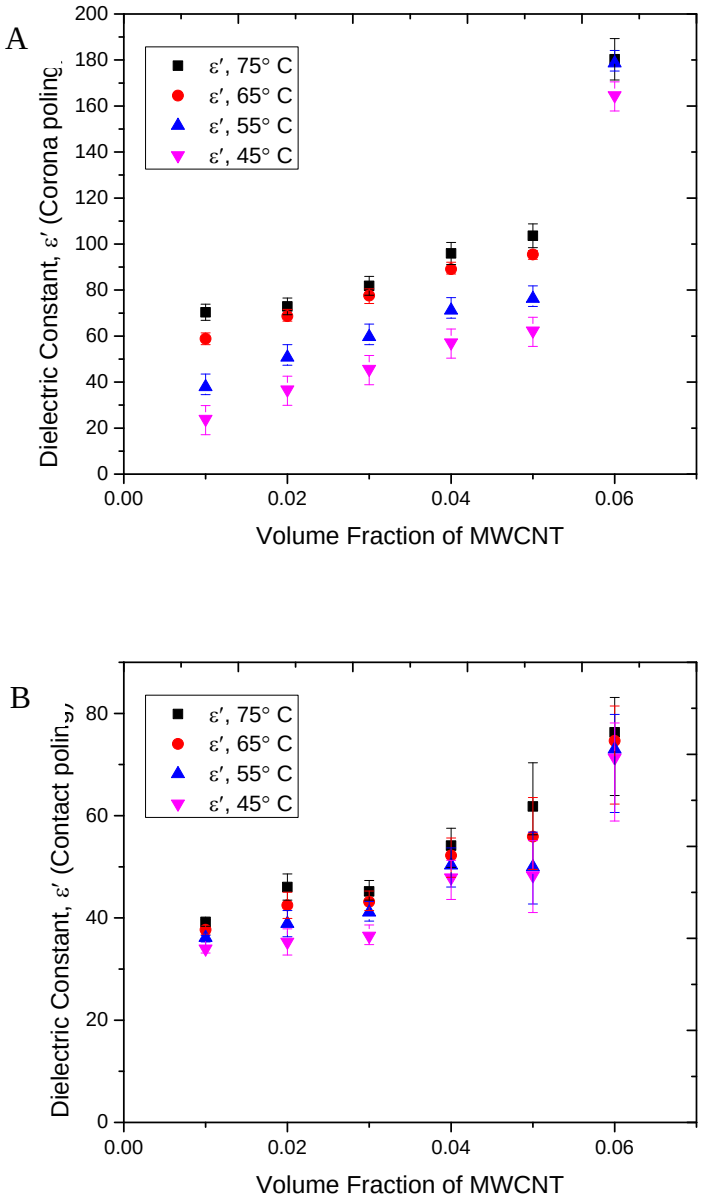

Figure 6.13 Variation in the dielectric constant, ε′, with variation in the poling temperature from 45^0 – 65^0 C for A) Corona poled and B) Contact poled thick film composites. The dielectric constant increases with an increase in the poling temperature.

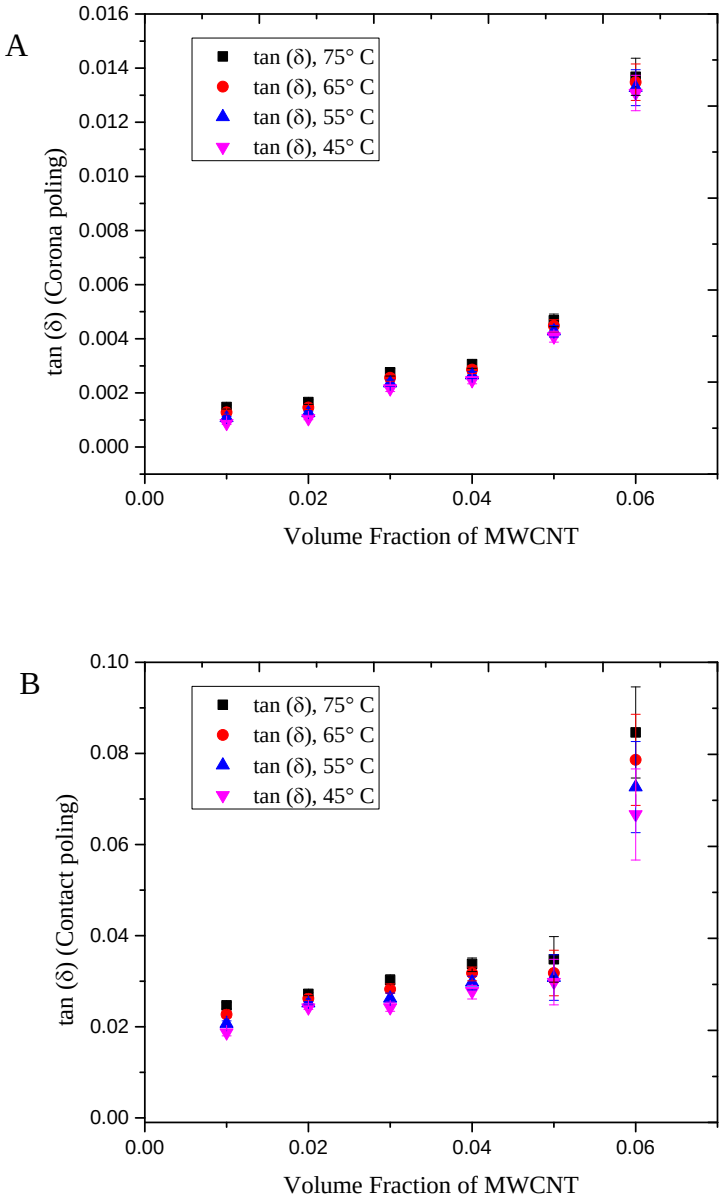

Figure 6.14 Variation in the tangent of the loss angle, tan (δ), with variation in the poling temperature from 45^0 – 65^0 C for composite thick films with A) Corona poling and B) Contact poling methods. The tan (δ) increases with an increase in the poling temperature.

6.5 Summary of the comparison of piezoelectric and dielectric characteristics of the three phase PZT-Epoxy-MWCNT bulk and composite thick films based on poling parameters

The piezoelectric and the dielectric properties of the PZT-Epoxy-MWCNT composite bulk and thick films have been studied in this chapter. The optimal values of the piezoelectric strain coefficients and the dielectric constant of the bulk composites and thick films with variation in poling voltage and poling temperature and at a MWCNT volume fraction of 5% are summarized in Tables 6.1 and 6.2 respectively.

Table 6.1 Optimal values of the piezoelectric strain coefficients and the dielectric constants (with variation in poling voltage) for PZT-Epoxy-MWCNT bulk composites and thick films at a MWCNT volume fraction of 5%.

	Poling Voltage = 2.2 kV/N	Poling Voltage = 1.7 kV/N	Poling Voltage = 1.2 kV/N	Poling Voltage = 0.7kV/N
Bulk composite (Corona poling)				
d33 (pC/N)	18.87	15.14	13.77	12.4
ε′	128.62	117.97	106.17	102.53
Bulk composite (Contact poling)				
d33 (pC/N)	5.31	4.58	3.85	3.12
ε′	84.60	60.08	40.35	40.51
Thick film composite (Corona poling)				
d33 (pC/N)	9.22	9.75	7.29	5.96
d31 (pC/N)	9.13	7.39	5.56	4.34
ε′	103.59	97.1	90.80	80.57
Thick film composite (Contact poling)				
d33 (pC/N)	0.59	0.48	0.09	0.06
d31 (pC/N)	0.3	0.28	0.27	0.25
ε′	61.81	55.03	45.69	44.03

The results indicate the enhancement of these properties with increasing poling voltage and temperature (It should be noted that the poling temperature has not been increased beyond 75^0 C which is the glass transition temperature of the epoxy matrix. Above this temperature the epoxy matrix undergoes softening and phase change which is out of the scope of this work).

Table 6.2 Optimal values of the piezoelectric strain coefficients and the dielectric constants (with variation in poling temperature) for PZT-Epoxy-MWCNT bulk composites and thick films at a MWCNT volume fraction of 5%.

	Poling Temp. = 75^0 C	Poling Temp. = 65^0 C	Poling Temp. = 55^0 C	Poling Temp. = 45^0 C
Bulk composite (Corona poling)				
d33 (pC/N)	18.87	16.14	14.77	13.4
ε′	126.62	120.82	108.82	105.1
Bulk composite (Contact poling)				
d33 (pC/N)	5.31	3.5	2.85	2.12
ε′	84.60	82.0	56.23	37.61
Thick film composite (Corona poling)				
d33 (pC/N)	9.22	8.83	7.24	6.29
d31 (pC/N)	9.13	7.4	6.81	5.43
ε′	103.59	95.49	76.30	62.28
Thick film composite (Corona poling)				
d33 (pC/N)	0.59	0.35	0.23	0.1
d31 (pC/N)	0.3	0.28	0.27	0.25
ε′	61.81	55.88	49.96	

Higher poling voltage increases the effective dipole moment in the direction of poling and enhances the effective properties. On the other hand an increase in the poling temperature will increase the mobility of the dipoles, which will allow more dipoles to orient themselves along the poling direction; effectively increasing the dipole moment and enhancing the piezoelectric and dielectric properties of the composites. Apart from the poling parameters the effective piezoelectric and dielectric characteristics of the composites also depend on the surface properties. The next chapter discusses the influence of a sputter coated metallic electrode layer in PZT-Epoxy-MWCNT thick films on the effective piezoelectric and dielectric properties of the composite.

Chapter 7

Influence of a sputter coated metallic layer on the surface transport properties of PZT-Epoxy-MWCNT thick film composites

The electron transport properties at the interface of the composite thick film surface and the device electrode are influenced by the surface characteristics, such as the surface morphology of the thick films, the contact resistance and the number of contact points connecting the thick film surface to the surface of the device electrode [15, 99]. In chapters 4, 5 and 6 the top surface of the thick film was in direct contact with the device electrode without any metallic coating on the top. For comparison of the dielectric performance with a metallic layer on the top surface the PZT-Epoxy-MWCNT thick films were coated with two different metallic electrodes, Gold (Au) and Chromium (Cr). The metallic nano particles are sputter coated on to the top surface of the thick films. The thicknesses of the electrodes are ~ 40 nm. The Au and Cr have different electrical properties (such as electrical resistivity and conductivity). Two different electrodes are used to study the effect of the variation of the electrical resistivity of the conductive layer on the effective composite properties. The following chapter investigates the influence of sputter coated metallic electrodes in reducing the contact resistance and enhancing the piezoelectric and dielectric properties of the corona poled thick film composites.

7.1 Influence of the metallic layer on the effective piezoelectric properties of the thick film composites

The variation of the piezoelectric strain coefficients, d33 and d31 of the three phase composite thick films are demonstrated in Figures 7.1 and 7.2 respectively. Both the

coefficients d33 and d31 are enhanced by the use of the metallic electrodes below the percolation threshold.

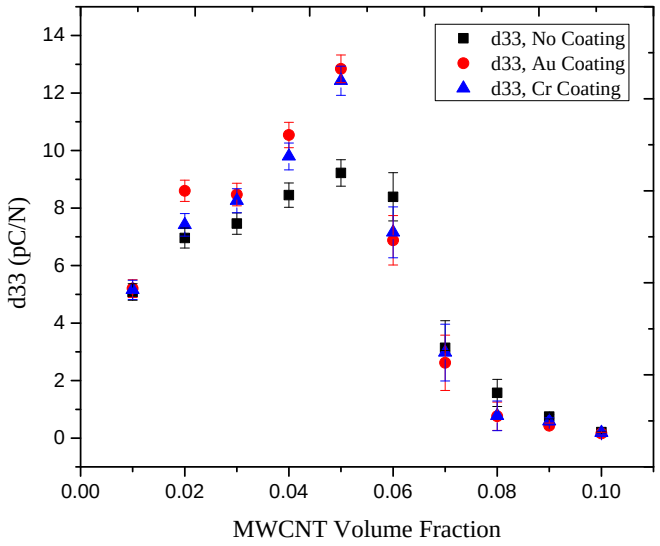

Figure 7.1 Plot of piezoelectric strain coefficient, d33, of thick film composites as a function of the MWCNT volume fraction from 1% to 10% with Au and Cr metallic coatings and thick films without any coating. The use of a nano sized metallic coating enhances the d33 coefficients in the thick film composites below the percolation threshold.

For example for a MWCNT volume fraction of 4% the d33 values for Au and Cr electrodes are ~ 10.54 and 9.8 pC/N as compared to a value of ~ 8.45 pC/N for the thick film without the sputtered metallic layer. A similar enhancement in the d33 is observed for a MWCNT volume fraction of 5%. The d33 values for Au and Cr electrodes are ~ 12.84 and 12.83 pC/N as compared to ~ 9.22 pC/N for the thick films without a metallic layer. A similar behavior is observed for the d31 values. For a MWCNT volume fraction of 4% the d31 values for Au and Cr electrodes are ~ 9.67 and 9.28 pC/N as compared to a

value of ~ 8.71 pC/N for the thick film without the sputtered coated metallic layer. The d31 values at a MWCNT volume fraction of 5% for Au and Cr electrodes are ~ 12.68 and 12.48 pC/N as compared to a value of ~ 9.13 pC/N for the thick films without a metallic layer. This enhancement in the d33 and d31 values is due to the decrease in the contact resistance and increase in the mobility of electrons between the thick film surface and the device electrode due to the presence of the sputter coated metallic layer.

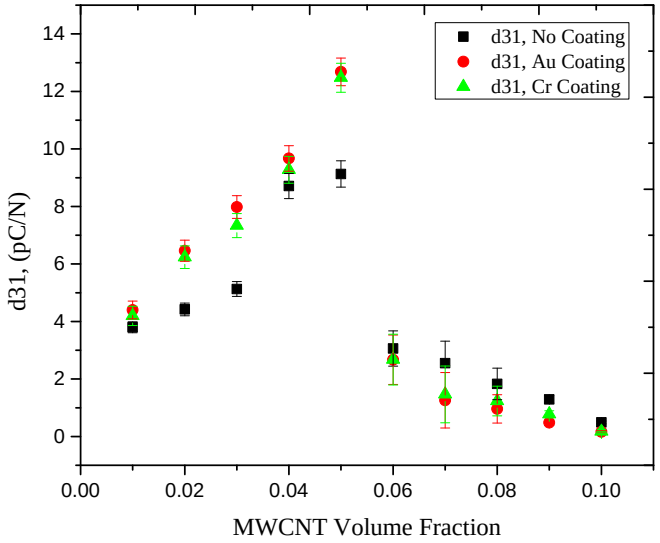

Figure 7.2 The piezoelectric strain coefficient, d31, of the thick film composites are plotted as a function of the MWCNT volume fraction from 1% to 10% with Au and Cr metallic coatings and thick films without a metallic coating. The use of metallic coating enhances the d33 coefficients in the thick film composites below the percolation threshold.

Above the percolation threshold the piezoelectric strain coefficients for the Au and Cr coated thick films are lower than the composites without an electrode. For a MWCNT volume fraction of 7% the d33 values for the composite with Au and Cr coatings are ~

2.62 and 2.98 pC/N respectively as compared to ~ 3.14 for the non coated thick film. For the same MWCNT volume fraction the d31 values of the composite thick films are ~ 1.26 and 1.47 pC/N with Au and Cr electrodes respectively; as compared to ~ 2.55 for the non coated composite. This trend can be due to the coupling of the decrease in the surface resistance of the composite due to the metallic layer and the formation of the percolation pathways along the thickness of the composite due to electron tunneling and direct contact between the percolation clusters.

The d33 and d31 values in the case of the Au coated composites are higher than that of the Cr coated thick films. For example for a MWCNT volume fraction of 3% the d33 values for the Au and Cr coated composites are ~ 8.47 and 8.26 pC/N respectively. The d31 values for the same MWCNT volume fraction are ~ 7.98 and 7.34 for the Au and Cr coated composites respectively. The electrical resistivity of Au is lower than that of Cr (Au ~ 22.14 nΩ·m, Cr ~ 125 nΩ·m) [116]. This increases the electron mobility and decreases the contact resistance in the case of the sputter coated Au layer as compared to a Cr coating; leading to lower values of piezoelectric strain coefficients.

7.2 Influence of the metallic layer on the effective dielectric properties of the thick film composites

Figures 7.3 and 7.4 show the variation of the Capacitance, C, and the dielectric constant, ε′, of the three phase PZT-Epoxy-MWCNT thick film composites with a electrode layer and without an electrode layer.

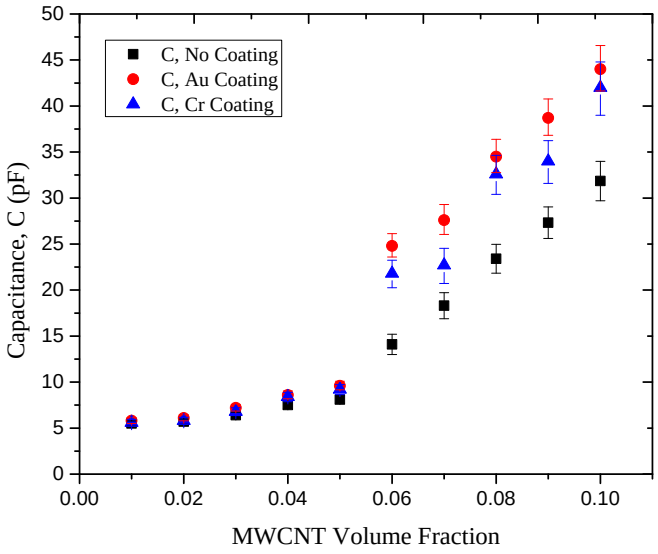

Figure 7.3 The Capacitance, C, of the thick film composites are plotted as a function of the MWCNT volume fraction from 1% to 10% with Au and Cr metallic coatings and thick films without a metallic coating. The use of metallic coating enhances the Capacitance values of the thick film composites.

Both the C and ε′ of the composite are enhanced by the use of the metallic electrodes. For example for a MWCNT volume fraction of 3% the ε′ values for Au and Cr electrodes are ~ 92 and 86.9 as compared to a value of ~ 81.8 for the thick film without the sputtered metallic layer. For the same volume fraction of MWCNTs the C values for Au and Cr electrodes are ~ 7.2 and 6.8 pF as compared to a value of ~ 6.4 pF for the thick film without the metallic layer. A similar enhancement in the C and ε′ are observed for all MWCNT volume fractions. This enhancement in the C and ε′ values is due to various factors such as electron hopping due to the presence of the metallic layer. Also, the conductive layer reduces the losses due to metal insulator transition and other interface defects as compared to the composite without a conductive layer. Another factor can be

the decrease in the contact resistance and increase in the mobility of electrons between the thick film surface and the device electrode due to the presence of the sputter coated metallic layer.

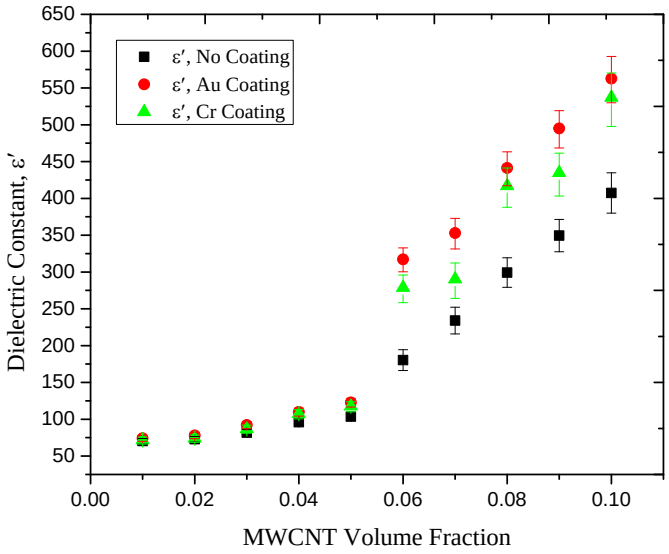

Figure 7.4 The dielectric constant, **ε′**, of the thick film composites are plotted as a function of the MWCNT volume fraction from 1% to 10% with Au and Cr metallic coatings and thick films without a metallic coating. The use of metallic coating enhances the **ε′** values of the thick film composites.

The C and ε′ values in the case of the Au coating are higher than that of the Cr coated thick films for all volume fractions. For example, at a MWCNT volume fraction of 4% the ε′ values for the Au and Cr coated composites are ~ 122.7 and 117.6 respectively. The C values for the same MWCNT volume fraction are ~ 9.4 and 9.4 pF for the Au and Cr coated composites respectively. This trend is seen for all MWCNT volume fractions of the composite. This can be due to the lower electrical resistivity of Au is as compared to that of Cr (Au ~ 22.14 nΩ·m, Cr ~ 125 nΩ·m) [116]. This causes a decrease in the contact resistance and an increase in the electron mobility in the case of

the sputter coated Au thick films as compared to the Cr coated ones; which increases the dielectric constant values.

The sputter coated metallic layers enhance the piezoelectric and dielectric properties of the thick film composites due to a decrease in the contact resistance between the thick film surface and the device electrode, the increase in electron mobility, increase in electron hopping and reduction in losses due to metal insulator transition and interfacial defects. The resistivity of the conductive layer also plays a role in determining the effective properties of the composite. Lower resistivity enhances electron mobility and leads to enhanced dielectric and piezoelectric characteristics in the thick film composites as have been demonstrated in the case of the gold and chromium electrodes. The next chapter concludes the work in this dissertation and also includes directions for future work in the PZT-Epoxy-MWCNT three phase composites.

Chapter 8

Conclusions and Future work

Three-phase PZT-Epoxy-MWCNT bulk composites and flexible composite thick films has been fabricated. The composites show an increase in the dielectric constant and the piezoelectric strain coefficients with an increase in the volume fraction of the MWCNT inclusions below the percolation limit. This increase is due to mechanisms such as electron hopping an increase in polarization of the composite with increase in MWCNT volume fraction. When the percolation threshold is reached, a sharp increase in the dielectric constant and the dielectric loss is observed. A sharp rise in the conductivity is also observed around the percolation threshold. This is accompanied by a sharp drop in the piezoelectric strain coefficients. These changes in properties are due the formation of percolation pathways which results in an increase in the conductivity of the composite through direct contact of the percolation clusters and by electron tunneling transport in the composite. Based on the variation in the piezoelectric and dielectric properties of the composite the percolation threshold is estimated to be in the region from 5-6% of the MWCNT volume fraction in the composite. The percolation threshold is higher than most volume fractions predicted in the literature for two and three phase composites due to the lower aspect ratio of the MWCNTs and the twisting and curling of the MWCNTs due to processing parameters which further reduces the effective aspect ratio. A comparison of piezoelectric and dielectric properties based on corona and contact poling has also been demonstrated. The results indicate that corona discharge poling is more effective than the contact poling method due to a higher polarization density in the corona discharge poling method.

A study of the dielectric and impedance characteristics of the bulk and thick film PZT-Epoxy-MWCNT composites also indicates that the composites reach the percolation threshold above a MWCNT volume fraction of 5%. Following the trend from the investigation into the piezoelectric and dielectric properties at a constant frequency, the impedance and dielectric spectrum analysis at variable frequency shows that the corona discharge poling technique is more effective than that of the contact poling method. The effect of the microstructure and the geometry of the material in determining the effective material properties of these composites are also established by the impedance and phase peaks at multiple locations of the spectra.

The poling conditions have also been established as key parameters in determining the effective material properties of the three phase composites. An increase in the poling voltage increases the effective dipole moment in the direction of poling and enhances the effective properties. On the other hand an increase in the poling temperature increases the mobility of the crystal lattices in the polycrystalline PZT inclusions, which allows them to orient themselves along the poling direction; effectively increasing the dipole moment and enhancing the piezoelectric and dielectric properties of the composites.

A study on the interfacial properties of the thick film composites with the addition of a sputter coated metallic layer shows an enhancement in the piezoelectric and dielectric properties. The addition of a conductive layer with thickness in the nano scale decreases the contact resistance between the thick film surface and the device electrode, increases the electron mobility and electron hopping, and reduces the losses due to metal insulator transition and interfacial defects. The electrical properties of the conductive

layer also play a role in determining the effective properties of the composite. Lower resistivity enhances electron mobility and leads to enhanced dielectric and piezoelectric characteristics in the thick film composites. This has been demonstrated by the use of gold and chromium coatings on the top surface of the thick films.

Future work on these materials might involve the study of the localized impedance and dielectric spectrum to determine the effects of the each of the microstructural and geometry based parameters in determining the effective properties of the composite and to calculate the electromechanical coupling coefficients towards applications as transducers, energy harvesters and sensing devices. In this work all the properties has been measures at room temperature. The piezoelectric and dielectric performance of these composites at elevated temperatures would also be of significance if these materials are used in real life applications. A study on the variation in the aspect ratio of the MWCNT inclusions can also give us insight into the piezoelectric and dielectric performance of these materials and the tailoring of the region of the percolation threshold based on application requirements. The surface characterization of the thick film composites with an addition of a conductive layer on the top surface has been shown in this work. The variation in the composite properties by means of variation of the thickness of the conductive layer and its effects on the percolation threshold can also be investigated.

References

[1] E. P. Scala, "A brief history of composites in the U.S.—The dream and the success," *JOM,* vol. 48, pp. 45-48, 1996/02/01 1996.

[2] G. H. Haertling, "Ferroelectric Ceramics: History and Technology," *Journal of the American Ceramic Society,* vol. 82, pp. 797-818, 1999.

[3] S. Banerjee and K. A. Cook-Chennault, "Influence of Al Particle Size and Lead Zirconate Titanate (PZT) Volume Fraction on the Dielectric Properties of PZT-Epoxy-Aluminum Composites," *Journal of Engineering Materials and Technology,* vol. 133, pp. 041016-041016, 2011.

[4] M. Lethiecq, F. Levassort, D. Certon, and L. Tran-Huu-Hue, "Piezoelectric Transducer Design for Medical Diagnosis and NDE," in *Piezoelectric and Acoustic Materials for Transducer Applications*, A. Safari and E. K. Akdoğan, Eds., ed: Springer US, 2008, pp. 191-215.

[5] M. Li, J. Yuan, D. Guan, and W. Chen, "Application of piezoelectric fiber composite actuator to aircraft wing for aerodynamic performance improvement," *Science China Technological Sciences,* vol. 54, pp. 395-402, 2011/02/01 2011.

[6] S. Chalasani and J. M. Conrad, "A survey of energy harvesting sources for embedded systems," in *Southeastcon, 2008. IEEE*, 2008, pp. 442-447.

[7] O. Guillon, F. Thiebaud, and D. Perreux, "Tensile fracture of soft and hard PZT," *International Journal of Fracture,* vol. 117, pp. 235-246, 2002/10/01 2002.

[8] S. Banerjee, W. Du, L. Wang, and K. A. Cook-Chennault, "Fabrication of dome-shaped PZT-epoxy actuator using modified solvent and spin coating technique," *Journal of Electroceramics,* pp. 1-11, 2013/07/09 2013.

[9] V. Pascariu, L. Padurariu, O. Avadanei, and L. Mitoseriu, "Dielectric properties of PZT–epoxy composite thick films," *Journal of Alloys and Compounds,* vol. 574, pp. 591-599, 2013.

[10] H.-W. Choi, H. Young-Woo, J.-H. Lee, J.-J. Kim, H.-Y. Lee, E.-T. Park, and Y.-K. Chung, "Effects of BaTiO3 on dielectric behavior of BaTiO3-Ni-polymethyl methacrylate composites," *Applied Physics Letters,* vol. 89, pp. 132910-132910-3, 2006.

[11] Z. M. Dang, L. Z. Fan, Y. Shen, and C. W. Nan, "Dielectric behavior of novel three-phase MWNTs/BaTiO3/PVDF composites," *Materials Science and Engineering: B,* vol. 103, pp. 140-144, 2003.

[12] Z. M. Dang, Y. Shen, and C. W. Nan, "Dielectric behavior of three-phase percolative Ni--BaTiO[sub 3]/polyvinylidene fluoride composites," *Applied Physics Letters,* vol. 81, pp. 4814-4816, 2002.

[13] Z.-M. Dang, S.-H. Yao, J.-K. Yuan, and J. Bai, "Tailored Dielectric Properties based on Microstructure Change in BaTiO3-Carbon Nanotube/Polyvinylidene Fluoride Three-Phase Nanocomposites," *The Journal of Physical Chemistry C,* vol. 114, pp. 13204-13209, 2010/08/12 2010.

[14] M. Dietze and M. Es-Souni, "Structural and functional properties of screen-printed PZT–PVDF-TrFE composites," *Sensors and Actuators A: Physical,* vol. 143, pp. 329-334, 2008.

[15] S. Banerjee, R. Kappera, M. Chhowalla, and K. A. Cook-Chennault, "Multi Walled Carbon Nanotube based Flexible Multi-morph Composite Thick Films with Graphene Electrodes," *Energy and Environmental Focus,* vol. In Press, 2013.

[16] O. T. L. Jordan and Z., "Piezoelectric ceramics characterization," Institute for Computer Applications in Science and Engineering (ICASE)2001.

[17] C.-H. Lin and A. Muliana, "Micromechanics models for the effective nonlinear electro-mechanical responses of piezoelectric composites," *Acta Mechanica,* vol. 224, pp. 1471-1492, 2013/07/01 2013.

[18] T. Rojac, A. Bencan, G. Drazic, M. Kosec, and D. Damjanovic, "Piezoelectric nonlinearity and frequency dispersion of the direct piezoelectric response of BiFeO3 ceramics," *Journal of Applied Physics,* vol. 112, pp. -, 2012.

[19] D. A. Berlincourt, C. Cmolik, and H. Jaffe, "Piezoelectric Properties of Polycrystalline Lead Titanate Zirconate Compositions," *Proceedings of the IRE,* vol. 48, pp. 220-229, 1960.

[20] E. Venkatragavaraj, B. Satish, P. R. Vinod, and M. S. Vijaya, "Piezoelectric properties of ferroelectric PZT-polymer composites," *Journal of Physics D: Applied Physics,* vol. 34, p. 487, 2001.

[21] S. Banerjee and K. A. Cook-Chennault, "An investigation into the influence of electrically conductive particle size on electromechanical coupling and effective dielectric strain coefficients in three phase composite piezoelectric polymers," *Composites Part A: Applied Science and Manufacturing,* vol. 43, pp. 1612-1619, 2012.

[22] T.-Y. Zhang, M. Zhao, and P. Tong, "Fracture of piezoelectric ceramics," in *Advances in Applied Mechanics*. vol. Volume 38, G. Erik van der and Y. W. Theodore, Eds., ed: Elsevier, 2002, pp. 147-289.

[23] N. Jaitanong, A. Chaipanich, and T. Tunkasiri, "Properties 0–3 PZT–Portland cement composites," *Ceramics International,* vol. 34, pp. 793-795, 2008.

[24] R. Rianyoi, R. Potong, N. Jaitanong, R. Yimnirun, and A. Chaipanich, "Dielectric, ferroelectric and piezoelectric properties of 0-3 barium titanate–Portland cement composites," *Applied Physics A,* vol. 104, pp. 661-666, 2011/08/01 2011.

[25] A. Chaipanich, N. Jaitanong, and R. Yimnirun, "Ferroelectric Hysteresis Behavior in 0-3 PZT-Cement Composites: Effects of Frequency and Electric Field," *Ferroelectrics Letters Section,* vol. 36, pp. 59-66, 2009/09/23 2009.

[26] S. Huang, J. Chang, R. Xu, F. Liu, L. Lu, Z. Ye, and X. Cheng, "Piezoelectric properties of 0-3 PZT/sulfoaluminate cement composites," *Smart Materials and Structures,* vol. 13, p. 270, 2004.

[27] Z. Li, D. Zhang, and K. Wu, "Cement-Based 0-3 Piezoelectric Composites," *Journal of the American Ceramic Society,* vol. 85, pp. 305-313, 2002.

[28] S. Banerjee and K. A. Cook-Chennault, "An Analytical Model for the Effective Dielectric Constant of a 0-3-0 Composite," *Journal of Engineering Materials and Technology,* vol. 133, pp. 041005-041005, 2011.

[29] S. Banerjee and K. A. Cook-Chennault. (2014, Influence of aluminium inclusions on dielectric properties of three-phase PZT–cement–aluminium composites. *Advances in Cement Research 26,* 63-76. Available: http://www.icevirtuallibrary.com/content/article/10.1680/adcr.12.00059

[30] K.-I. Park, S. Xu, Y. Liu, G.-T. Hwang, S.-J. L. Kang, Z. L. Wang, and K. J. Lee, "Piezoelectric BaTiO3 Thin Film Nanogenerator on Plastic Substrates," *Nano Letters,* vol. 10, pp. 4939-4943, 2010/12/08 2010.

[31] M. Akiyama, Y. Morofuji, T. Kamohara, K. Nishikubo, M. Tsubai, O. Fukuda, and N. Ueno, "Flexible piezoelectric pressure sensors using oriented aluminum nitride thin films prepared on polyethylene terephthalate films," *Journal of Applied Physics,* vol. 100, pp. 114318-5, 2006.

[32] **L. Qi, B. I. Lee, W. D. Samuels, G. J. Exarhos, and S. G. Parler, "Three-phase percolative silver–BaTiO3–epoxy nanocomposites with high dielectric constants," *Journal of Applied Polymer Science,* vol. 102, pp. 967-971, 2006.**

[33] **L.-y. Zhao, J.-g. Guan, H.-r. Ma, and Z.-g. Sun, "Mechanical properties and curing kinetics of epoxy resins cured by various amino-terminated polyethers," *Chinese Journal of Polymer Science,* vol. 28, pp. 961-969, 2010/11/01 2010.**

[34] **S.-H. Yao, Z.-M. Dang, M.-J. Jiang, and J. Bai, "BaTiO[sub 3]-carbon nanotube/polyvinylidene fluoride three-phase composites with high dielectric constant and low dielectric loss," *Applied Physics Letters,* vol. 93, pp. 182905-3, 2008.**

[35] **W. Zepu, J. K. Nelson, M. Jianjun, R. J. Linhardt, L. S. Schadler, H. Hillborg, and Z. Su, "Effect of high aspect ratio filler on dielectric properties of polymer composites: a study on barium titanate fibers and graphene platelets," *Dielectrics and Electrical Insulation, IEEE Transactions on,* vol. 19, pp. 960-967, 2012.**

[36] **W. S. Bao, S. A. Meguid, Z. H. Zhu, and G. J. Weng, "Tunneling resistance and its effect on the electrical conductivity of CNT nanocomposites," *Journal of Applied Physics,* vol. 111, p. 093726, 2012.**

[37] **W. Yang, Y. Pan, and A. A. Pelegri, "Multiscale modeling of matrix cracking coupled with interfacial debonding in random glass fiber composites based on volume elements," *Journal of Composite Materials,* vol. 47, pp. 3389-3399, December 1, 2013 2013.**

[38] **J. Fukushima, K. Kodaira, and T. Matsushita, "Preparation of ferroelectric PZT films by thermal decomposition of organometallic compounds," *Journal of Materials Science,* vol. 19, pp. 595-598, 1984/02/01 1984.**

[39] **C. K. Kwok and S. B. Desu, "Low temperature perovskite formation of lead zirconate titanate thin films by a seeding process," *Journal of Materials Research,* vol. 8, pp. 339-344, 1993.**

[40] **Richard E. Eitel, Clive A. Randall, Thomas R. Shrout, and S.-E. Park, "Preparation and Characterization of High Temperature Perovskite Ferroelectrics in the Solid-Solution (1- x)BiScO 3 – x PbTiO 3," *Japanese Journal of Applied Physics,* vol. 41, p. 2099, 2002.**

[41] **R. W. P. King, *Fundamental Electromagnetic Theory*: New York: Dover, 1963.**

[42] **H. Fröhlich, *Theory of dielectrics: dielectric constant and dielectric loss*: Clarendon Press, 1958.**

[43] **R. E. Newnham, D. P. Skinner, and L. E. Cross, "Connectivity and piezoelectric-pyroelectric composites," *Materials Research Bulletin,* vol. 13, pp. 525-536, 1978.**

[44] **L. F. Chen, Y. P. Hong, X. J. Chen, Q. L. Wu, Q. J. Huang, and X. T. Luo, "Preparation and properties of polymer matrix piezoelectric composites containing aligned BaTiO3 whiskers," *Journal of Materials Science,* vol. 39, pp. 2997-3001, 2004/05/01 2004.**

[45] **P. Muralt, "Ferroelectric thin films for micro-sensors and actuators: a review," *Journal of Micromechanics and Microengineering,* vol. 10, p. 136, 2000.**

[46] **S. C. Stein, C. Liang, and C. A. Rogers, "Power consumption of piezoelectric actuators driving a simply supported beam considering fluid coupling," *The Journal of the Acoustical Society of America,* vol. 96, pp. 1598-1604, 1994.**

[47] **V. H. Pham, T. T. Dang, S. H. Hur, E. J. Kim, and J. S. Chung, "Highly Conductive Poly(methyl methacrylate) (PMMA)-Reduced Graphene Oxide Composite Prepared by Self-Assembly of PMMA Latex and Graphene Oxide through Electrostatic Interaction," *ACS Applied Materials & Interfaces,* vol. 4, pp. 2630-2636, 2012/05/23 2012.**

[48] **R. K. Zheng, S. N. Dong, Y. Q. Wu, Q. X. Zhu, Y. Wang, H. L. W. Chan, X. M. Li, H. S. Luo, and X. G. Li, "Effects of electric-field-induced piezoelectric strain on the electronic transport properties of La0.9Ce0.1MnO3 thin films," *Thin Solid Films,* vol. 525, pp. 45-48, 2012.**

[49] **S. M. Pilgrim and R. E. Newnham, "3:0: A new composite connectivity," *Materials Research Bulletin,* vol. 21, pp. 1447-1454, 1986.**

[50] **K. Arlt and M. Wegener, "Piezoelectric PZT / PVDF-copolymer 0-3 composites: aspects on film preparation and electrical poling," *Dielectrics and Electrical Insulation, IEEE Transactions on,* vol. 17, pp. 1178-1184, 2010.**

[51] **D.-H. Kuo, C.-C. Chang, T.-Y. Su, W.-K. Wang, and B.-Y. Lin, "Dielectric behaviours of multi-doped BaTiO3/epoxy composites," *Journal of the European Ceramic Society,* vol. 21, pp. 1171-1177, 2001.**

[52] **W. T. Doyle and I. S. Jacobs, "The influence of particle shape on dielectric enhancement in metal‐insulator composites," *Journal of Applied Physics,* vol. 71, pp. 3926-3936, 1992.**

[53] **W. T. Doyle, "Particle clustering and dielectric enhancement in percolating metal–insulator composites," *Journal of Applied Physics,* vol. 78, pp. 6165-6169, 1995.**

[54] **Y. Bai, Z. Y. Cheng, V. Bharti, H. S. Xu, and Q. M. Zhang, "High-dielectric-constant ceramic-powder polymer composites," *Applied Physics Letters,* vol. 76, pp. 3804-3806, 2000.**

[55] **M. Ma and X. Wang, "Preparation, microstructure and properties of epoxy-based composites containing carbon nanotubes and PMN-PZT piezoceramics as rigid piezo-damping materials," *Materials Chemistry and Physics,* vol. 116, pp. 191-197, 2009.**

[56] **K. A. Cook-Chennault, N. Thambi, and A. M. Sastry, "Powering MEMS portable devices—a review of non-regenerative and regenerative power supply systems with special emphasis on piezoelectric energy harvesting systems," *Smart Materials and Structures,* vol. 17, p. 043001, 2008.**

[57] **C. Chen, R. Zhang, Z. Wang, and W. Cao, "Electromechanical coupling coefficient k31eff for arbitrary aspect ratio resonators made of [001] and [011] poled (1−x)Pb(Mg1/3Nb2/3)O3–xPbTiO3 single crystals," *Journal of Applied Physics,* vol. 105, pp. -, 2009.**

[58] **P. Zhao and J. Li, "Investigation of orientation effects on the electro-mechanical coupling behavior of 1–3 piezoelectric composites under compression," *Smart Materials and Structures,* vol. 18, p. 104011, 2009.**

[59] **H. Gong, Y. Zhang, J. Quan, and S. Che, "Preparation and properties of cement based piezoelectric composites modified by CNTs," *Current Applied Physics,* vol. 11, pp. 653-656, 2011.**

[60] **A. Seema, K. R. Dayas, and J. M. Varghese, "PVDF-PZT-5H composites prepared by hot press and tape casting techniques," *Journal of Applied Polymer Science,* vol. 106, pp. 146-151, 2007.**

[61] **R. Senthilkumar, K. Sridevi, J. Venkatesan, V. Annamalai, and M. S. Vijaya, "Investigations on Ferroelectric PZT-PVDF Composites of 0–3 Connectivity," *Ferroelectrics,* vol. 325, pp. 121-130, 2005/09/01 2005.**

[62] **B. Satish, K. Sridevi, and M. S. Vijaya, "Study of piezoelectric and dielectric properties of ferroelectric PZT-polymer composites prepared by hot-press technique," *Journal of Physics D: Applied Physics,* vol. 35, p. 2048, 2002.**

[63] **Y. Song, Z. Zhao, W. Yu, B. Li, and X. Chen, "Morphological structures of poly(vinylidene fluoride)/montmorillonite nanocomposites," *Science in China Series B: Chemistry,* vol. 50, pp. 790-796, 2007/12/01 2007.**

[64] **K. A. Cook-Chennault, N. Thambi, M. A. Bitetto, and E. B. Hameyie, "Piezoelectric Energy Harvesting: A Green and Clean Alternative for Sustained Power Production," *Bulletin of Science, Technology & Society,* vol. 28, pp. 496-509, December 1, 2008 2008.**

[65] **Y. Dan, Y. Lu, N. J. Kybert, Z. Luo, and A. T. C. Johnson, "Intrinsic Response of Graphene Vapor Sensors," *Nano Letters,* vol. 9, pp. 1472-1475, 2009/04/08 2009.**

[66] **Z. Li, B. Dong, and D. Zhang, "Influence of polarization on properties of 0–3 cement-based PZT composites," *Cement and Concrete Composites,* vol. 27, pp. 27-32, 2005.**

[67] **M. Thomas, K. Folliard, T. Drimalas, and T. Ramlochan, "Diagnosing delayed ettringite formation in concrete structures," *Cement and Concrete Research,* vol. 38, pp. 841-847, 2008.**

[68] **K. Yadav, C. W. Smelser, S. Jacob, C. Blanchetiere, C. L. Callender, and J. Albert, "Simultaneous corona poling of multiple glass layers for enhanced effective second-order optical nonlinearities," *Applied Physics Letters,* vol. 99, pp. -, 2011.**

[69] **W. S. Bao, S. A. Meguid, Z. H. Zhu, Y. Pan, and G. J. Weng, "A novel approach to predict the electrical conductivity of multifunctional nanocomposites," *Mechanics of Materials,* vol. 46, pp. 129-138, 2012.**

[70] **P. Blanas and K. Das-Gupta, "Composite Piezoelectric Materials for Health Monitoring of Composite Structures," in *MRS Proceedings*, 1999.**

[71] **S. Maiti, S. Suin, N. K. Shrivastava, and B. B. Khatua, "Low percolation threshold in melt-blended PC/MWCNT nanocomposites in the presence of styrene acrylonitrile (SAN) copolymer: Preparation and characterizations," *Synthetic Metals,* vol. 165, pp. 40-50, 2013.**

[72] **V. Nagarajan, C. S. Ganpule, B. Nagaraj, S. Aggarwal, S. P. Alpay, A. L. Roytburd, E. D. Williams, and R. Ramesh, "Effect of mechanical constraint on the dielectric and piezoelectric behavior of epitaxial Pb(Mg1/3Nb2/3)O3(90%)–PbTiO3(10%) relaxor thin films," *Applied Physics Letters,* vol. 75, pp. 4183-4185, 1999.**

[73] **S. L. Kok, N. M. White, and N. R. Harris, "Free-standing thick-film piezoelectric device," *Electronics Letters,* vol. 44, 2008.**

[74] **V. Sencadas, S. Lanceros-Mendez, R. G. Filho, D. L. Chinaglia, and A. S. Pouzada, "Influence of the processing conditions and corona poling on the morphology of β-PVDF," in *Electrets, 2005. ISE-12. 2005 12th International Symposium on*, 2005, pp. 161-164.**

[75] **Z. Ounaies, C. Park, J. Harrison, and P. Lillehei, "Evidence of Piezoelectricity in SWNT-Polyimide and SWNT-PZT-Polyimide Composites," *Journal of Thermoplastic Composite Materials,* vol. 21, pp. 393-409, 2008.**

[76] **R. H. Baughman, A. A. Zakhidov, and W. A. de Heer, "Carbon Nanotubes--the Route Toward Applications," *Science,* vol. 297, pp. 787-792, August 2, 2002 2002.**

[77] **S. Frank, P. Poncharal, Z. L. Wang, and W. A. d. Heer, "Carbon Nanotube Quantum Resistors," *Science,* vol. 280, pp. 1744-1746, June 12, 1998 1998.**

[78] **W. Liang, M. Bockrath, D. Bozovic, J. H. Hafner, M. Tinkham, and H. Park, "Fabry - Perot interference in a nanotube electron waveguide," *Nature,* vol. 411, pp. 665-669, 2001.**

[79] G. Gao, T. Çagin, and W. A. G. III, "Energetics, structure, mechanical and vibrational properties of single-walled carbon nanotubes," *Nanotechnology,* vol. 9, p. 184, 1998.

[80] M. J. Biercuk, M. C. Llaguno, M. Radosavljevic, J. K. Hyun, A. T. Johnson, and J. E. Fischer, "Carbon nanotube composites for thermal management," *Applied Physics Letters,* vol. 80, pp. 2767-2769, 2002.

[81] S. Reich, C. Thomsen, and J. Maultzsch, *Carbon Nanotubes: Basic Concepts and Physical Properties*. Wiley-VCH, 2004.

[82] X. Zeng, X. Xu, P. M. Shenai, E. Kovalev, C. Baudot, N. Mathews, and Y. Zhao, "Characteristics of the Electrical Percolation in Carbon Nanotubes/Polymer Nanocomposites," *The Journal of Physical Chemistry C,* vol. 115, pp. 21685-21690, 2011/11/10 2011.

[83] H. Chen, H. Muthuraman, P. Stokes, J. Zou, X. Liu, J. Wang, Q. Huo, S. I. Khondaker, and L. Zhai, "Dispersion of carbon nanotubes and polymer nanocomposite fabrication using trifluoroacetic acid as a co-solvent," *Nanotechnology,* vol. 18, p. 415606, 2007.

[84] R. H. Schmidt, I. A. Kinloch, A. N. Burgess, and A. H. Windle, "The Effect of Aggregation on the Electrical Conductivity of Spin-Coated Polymer/Carbon Nanotube Composite Films," *Langmuir,* vol. 23, pp. 5707-5712, 2007/05/01 2007.

[85] V. Leon, R. Parret, R. Almairac, L. Alvarez, M. R. Babaa, B. P. Doyle, P. Ienny, P. Parent, A. Zahab, and J. L. Bantignies, "Spectroscopic study of double-walled carbon nanotube functionalization for preparation of carbon nanotube / epoxy composites," *Carbon,* vol. 50, pp. 4987-4994, 2012.

[86] W. Bauhofer and J. Z. Kovacs, "A review and analysis of electrical percolation in carbon nanotube polymer composites," *Composites Science and Technology,* vol. 69, pp. 1486-1498, 2009.

[87] S. Tian and X. Wang, "Fabrication and performances of epoxy/multi-walled carbon nanotubes/piezoelectric ceramic composites as rigid piezo-damping materials," *Journal of Materials Science,* vol. 43, pp. 4979-4987, 2008/07/01 2008.

[88] W. S. Bao, S. A. Meguid, Z. H. Zhu, and G. J. Weng, "A novel approach to predict the electrical conductivity of multifunctional nanocomposites," *Mechanics of Materials,* vol. 46, 2012.

[89] M. Heimann, M. Wirts-Ruetters, B. Boehme, and K. J. Wolter, "Investigations of carbon nanotubes epoxy composites for electronics packaging," in *Electronic Components and Technology Conference, 2008. ECTC 2008. 58th*, 2008, pp. 1731-1736.

[90] L.-H. Sun, Z. Ounaies, X.-L. Gao, C. A. Whalen, and Z.-G. Yang, "Preparation, characterization, and modeling of carbon nanofiber/epoxy nanocomposites," *J. Nanomaterials,* vol. 2011, pp. 1-8, 2011.

[91] M. C. Hermant, "Manipulating the percolation threshold of carbon nanotubes in polymeric composites," Doctor of Philosophy, Technische Universiteit Eindhoven, Technische Universiteit Eindhoven, 2009.

[92] J. A. Arsecularatne and L. C. Zhang, "Carbon Nanotube Reinforced Ceramic Composites and their Performance," *Recent Patents on Nanotechnology,* vol. 1, pp. 176-185, 2007.

[93] E. M. McKenna, A. S. Lin, A. R. Mickelson, R. Dinu, and D. Jin, "Comparison of r33 values for AJ404 films prepared with parallel plate and corona poling," *Journal of the Optical Society of America B,* vol. 24, pp. 2888-2892, 2007/11/01 2007.

[94] M. Wegener and K. Arlt, "PZT/P(VDF-HFP) 0–3 composites as solvent-cast thin films: preparation, structure and piezoelectric properties," *Journal of Physics D: Applied Physics,* vol. 41, p. 165409, 2008.

[95] **D. L. Corker, Q. Zhang, R. W. Whatmore, and C. Perrin, "PZT 'composite' ferroelectric thick films," *Journal of the European Ceramic Society,* vol. 22, pp. 383-390, 2002.**

[96] **C. T. Pan, Z. H. Liu, Y. C. Chen, and C. F. Liu, "Design and fabrication of flexible piezo-microgenerator by depositing ZnO thin films on PET substrates," *Sensors and Actuators A: Physical,* vol. 159, pp. 96-104, 2010.**

[97] **S. Y. Chung, S. Kim, J.-H. Lee, K. Kim, S.-W. Kim, C.-Y. Kang, S.-J. Yoon, and Y. S. Kim, "All-Solution-Processed Flexible Thin Film Piezoelectric Nanogenerator," *Advanced Materials,* vol. 24, pp. 6022-6027, 2012.**

[98] **S.-L. Kok, N. M. White, and N. R. Harris, "Fabrication and characterization of free-standing thick-film piezoelectric cantilevers for energy harvesting," *Measurement Science and Technology,* vol. 20, p. 124010, 2009.**

[99] **T. Pedersen, C. C. Hindrichsen, E. V. Thomsen, K. Hansen, and R. Lou-Moller, "Investigation of Top/Bottom Electrode and Diffusion Barrier Layer for PZT Thick Film MEMS Sensors," in *Sensors, 2007 IEEE*, 2007, pp. 756-759.**

[100] **G. Eda, G. Fanchini, and M. Chhowalla, "Large-area ultrathin films of reduced graphene oxide as a transparent and flexible electronic material," *Nat Nano,* vol. 3, pp. 270-274, 2008.**

[101] **Y. Wang, R. Yang, Z. Shi, L. Zhang, D. Shi, E. Wang, and G. Zhang, "Super-Elastic Graphene Ripples for Flexible Strain Sensors," *ACS Nano,* vol. 5, pp. 3645-3650, 2011/05/24 2011.**

[102] **H. Gullapalli, V. S. M. Vemuru, A. Kumar, A. Botello-Mendez, R. Vajtai, M. Terrones, S. Nagarajaiah, and P. M. Ajayan, "Flexible Piezoelectric ZnO–Paper Nanocomposite Strain Sensor," *Small,* vol. 6, pp. 1641-1646, 2010.**

[103] **S. Huang, J. Luo, H.-L. Yip, A. Ayazi, X.-H. Zhou, M. Gould, A. Chen, T. Baehr-Jones, M. Hochberg, and A. K. Y. Jen, "Efficient Poling of Electro-Optic Polymers in Thin Films and Silicon Slot Waveguides by Detachable Pyroelectric Crystals," *Advanced Materials,* vol. 24, pp. OP42-OP47, 2012.**

[104] **C. W. Nan, L. Liu, N. Cai, J. Zhai, Y. Ye, Y. H. Lin, L. J. Dong, and C. X. Xiong, "A three-phase magnetoelectric composite of piezoelectric ceramics, rare-earth iron alloys, and polymer," *Applied Physics Letters,* vol. 81, pp. 3831-3833, 2002.**

[105] **B. Dong and Z. Li, "Cement-based piezoelectric ceramic smart composites," *Composites Science and Technology,* vol. 65, pp. 1363-1371, 2005.**

[106] **S. Huang, J. Chang, L. Lu, F. Liu, Z. Ye, and X. Cheng, "Preparation and polarization of 0–3 cement based piezoelectric composites," *Materials Research Bulletin,* vol. 41, pp. 291-297, 2006.**

[107] **Y. Shen, Y. Guan, Y. Hu, Y. Lei, Y. Song, Y. Lin, and C.-W. Nan, "Dielectric behavior of graphene/BaTiO[sub 3]/polyvinylidene fluoride nanocomposite under high electric field," *Applied Physics Letters,* vol. 103, pp. 072906-4, 2013.**

[108] **H. Park, P. R. Brown, V. Bulović, and J. Kong, "Graphene As Transparent Conducting Electrodes in Organic Photovoltaics: Studies in Graphene Morphology, Hole Transporting Layers, and Counter Electrodes," *Nano Letters,* vol. 12, pp. 133-140, 2012/01/11 2011.**

[109] **F. Oliveira, Y. Leterrier, J.-A. Månson, O. Sereda, A. Neels, A. Dommann, and D. Damjanovic, "Process influences on the structure, piezoelectric, and gas-barrier properties of PVDF-TrFE copolymer," *Journal of Polymer Science Part B: Polymer Physics,* vol. 52, pp. 496-506, 2014.**

[110] **H. Hammami, M. Arous, M. Lagache, and A. Kallel, "Experimental study of relaxations in unidirectional piezoelectric composites," *Composites Part A: Applied Science and Manufacturing,* vol. 37, pp. 1-8, 2006.**

[111] **J. H. Sandoval, K. F. Soto, L. E. Murr, and R. B. Wicker, "Nanotailoring photocrosslinkable epoxy resins with multi-walled carbon nanotubes for stereolithography layered manufacturing," *Journal of Materials Science,* vol. 42, pp. 156-165, 2007/01/01 2007.**

[112] **J. H. Sandoval and R. B. Wicker, "Functionalizing stereolithography resins: effects of dispersed multi-walled carbon nanotubes on physical properties," *Rapid Prototyping Journal,* vol. 12, pp. 292-303, 2006.**

[113] **S. Reem, A. Yick, and W. H. Steier, "Conductivity-dependency-free in-plane poling for Mach-Zehnder modulator with highly conductive electro-optic polymer," *Applied Physics Letters,* vol. 90, pp. 191103-191103-3, 2007.**

[114] **Y. Zhang, Z. Wang, J. David, and N. Cheeke, "Resonant Spectrum Method to Characterize Piezoelectric Films in Composite Resonators," *Transactions on ultrasonics, ferroelectrics, and frequency control,* vol. 50, 2003.**

[115] **C. P. Chong, H. L. W. Chan, M. H. Chan, and P. C. K. Liu, "Analysis of the resonance modes of PZT/epoxy 1-3 composite rings," in *Applications of Ferroelectrics, 2002. ISAF 2002. Proceedings of the 13th IEEE International Symposium on*, 2002, pp. 295-298.**

[116] **P. L. Rossiter, *The Electrical Resistivity of Metals and Alloys*. Cambridge University Press: Cambridge University Press, 1991.**